

ENERGY

SAN-1229-1

DEVELOPMENT OF AMMONIATED SALTS

Thermochemical Energy Storage Systems. Phase IB

Final Report, February–September 1977

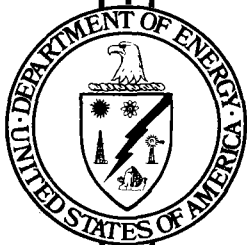
By
F. A. Jaeger
M. T. Howerton
S. E. Podlaseck
J. E. Myers
D. G. Beshore
W. R. Haas

DO NOT RETURN TO
TECHNICAL LIBRARY

May 1978
Date Published

Work Performed Under Contract No. EY-76-C-03-1229

Martin Marietta Corporation
Denver, Colorado



U. S. DEPARTMENT OF ENERGY

Division of Energy Storage Systems

NOV 1978

NOTICE

This report was prepared as an account of work sponsored by the United States Government. Neither the United States nor the United States Department of Energy, nor any of their employees, nor any of their contractors, subcontractors, or their employees, makes any warranty, express or implied, or assumes any legal liability or responsibility for the accuracy, completeness or usefulness of any information, apparatus, product or process disclosed, or represents that its use would not infringe privately owned rights.

This report has been reproduced directly from the best available copy.

Available from the National Technical Information Service, U. S. Department of Commerce, Springfield, Virginia 22161.

Price: Paper Copy \$8.00
Microfiche \$3.00

DEVELOPMENT OF AMMONIATED SALTS
THERMOCHEMICAL ENERGY STORAGE
SYSTEMS

Phase IB

FINAL REPORT FOR THE
PERIOD FEBRUARY-SEPTEMBER 1977

F. A. Jaeger
M. T. Howerton
S. E. Podlaseck
J. E. Myers
D. G. Beshore
W. R. Haas

MARTIN MARIETTA CORPORATION
DENVER DIVISION
DENVER, COLORADO

Date Published May 1978

PREPARED FOR THE
DEPARTMENT OF ENERGY

Division of Energy Storage Systems
Work Performed Under Contract No. EY-76-C-03-1229

CONTENTS

	<u>Page</u>
I. SUMMARY	I-1 thru I-4
II. INTRODUCTION	II-1 and II-2
III. ANALYSIS (TASK 1)	III-1
A. Description of the Model	III-1
B. Comparison of Test Data	III-9
C. Conclusions	III-13 thru III-15
IV. CHEMICAL AND PHYSICAL PROPERTIES	IV-1
A. Dissociation/Recombination Cycling (Task 3)	IV-2
B. Bulk Density (Task 3)	IV-7
C. Theoretical Density (Task 3)	IV-9
D. Surface Area (Task 3)	IV-11
E. Particle Size Distribution (Task 3)	IV-13
F. Effects of Moisture on Salt Reaction Rates (Task 4).	IV-13
G. Nonaqueous Impurities (Task 10)	IV-18
H. Heats of Reaction Verification (Task 9)	IV-19 thru IV-23
V. SUBSCALE TESTING (TASK 2)	V-1
A. Objectives	V-1
B. Basis for Coupled Reaction Process	V-1
C. Experimental Test Equipment and Operation	V-7
D. Results	V-13
E. Conclusions	V-21
VI. SYSTEM DESIGN AND ECONOMIC ANALYSIS	VI-1
A. Economic Analysis of Power Plant Storage	VI-1
B. Alternative Bed Configuration-Fluidization	VI-12
C. Alternative Reactor Designs	VI-27 thru VI-31

VII.	CONCLUSIONS	VII-1
A.	Computer Modeling	VII-1
B.	Chemical and Physical Properties Testing	VII-1
C.	Subscale Testing	VII-2
D.	System Design and Economics	VII-2

VIII.	RECOMMENDED FOLLOW-ON EFFORT	VIII-1
A.	Task 1 - Chemical Tests	VIII-2
B.	Task 2 - Laboratory Scale System Tests	VIII-2
C.	Task 3 - Computer Models	VIII-4
D.	Schedule	VIII-4

IX.	REFERENCES	IX-1 and IX-2
-----	----------------------	---------------------

APPENDIX A	STORAGE SYSTEM SIZING AND COST CALCULATIONS	A-1 thru A-35
------------	---	---------------------

APPENDIX B	ECONOMIC ANALYSIS OF ALTERNATIVE REACTOR DESIGNS	B-1 thru B-5
------------	--	--------------------

ABSTRACT

Thermal energy is usually stored in energy storage systems as sensible heat at temperatures well above the ambient temperature. Most energy storage systems of this type suffer from two drawbacks: (1) the thermal losses to the surroundings are large, and (2) the energy is only available for recovery at the bulk temperature of the storage material; therefore, the stored energy can only be partially recovered. If the energy could be stored at near ambient temperature and recovered at the desired use temperature, thermal losses can be minimized and a high degree of efficiency can be maintained.

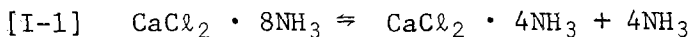
The purpose of this program is to develop an energy storage system that accepts thermal energy at high temperatures, stores that energy at ambient temperature, and recovers the energy at the original high temperature. The energy is stored as chemical energy. The concept consists of storage and subsequent extraction of the heat of reaction from a pair of ammoniated salts near equilibrium conditions. By shifting the equilibrium in the forward or reverse direction, the heat of reaction can be stored or recovered. The system can be used for many different applications (i.e., different temperature levels) by selecting the appropriate salt pair for the high and low temperature reactions. In this phase of the program, the technical feasibility of the concept was demonstrated using several ammoniated salt pairs.

I. SUMMARY

The objective of this contract is to develop an energy storage system that accepts thermal energy at high temperatures, stores the energy at ambient temperature, and recovers the energy at the original high temperature. The energy is stored as chemical energy.

The approach that has been used for the energy storage system is as follows. The reversible energy storage system operates by using the heat of reaction of ammoniated salts as a means of converting heat to a form of chemical energy that can be re-claimed. By coupling two reactions that take place at the same pressure but different temperatures, energy can be absorbed by the system at a temperature with one reaction and stored or released at a different temperature with another reaction. Ammonia gas is endothermically released at one temperature from one ammoniated salt and exothermically absorbed or stored at a different temperature by another ammoniated salt. The system can be reversed by adding heat to the reactor where the ammonia is stored causing the ammonia gas to flow to the other reactor where the ammonia is stored causing the ammonia gas to flow to the other reactor where the energy is again released.

For purposes of illustration, the vapor pressure data of several salts are presented in Figure I-1. These data can be used to select a pair of appropriate reactions for any application from ambient temperature to 600°F. It is apparent that an appropriate ambient-temperature reaction is



This reaction can be paired with any of the other reactions depending on the source temperature available.

A possible solar power plant application is shown in Figure I-2. In the charging mode, saturated steam from a solar boiler at 535°F is condensed in the heat exchanger of the high-temperature reactor. Allowing a 10F delta between the condensing steam and the salt bed, $\text{MgCl}_2 \cdot 4\text{NH}_3$ decomposes endothermically at 525°F to evolve ammonia gas at a pressure of 1 atm. The ammonia gas is transferred to the low-temperature reactor through a small pressure drop and reacts with $\text{CaCl}_2 \cdot 4\text{NH}_3$ to form $\text{CaCl}_2 \cdot 8\text{NH}_3$ exothermically at 90°F. In a power plant operation, the evolved thermal energy is not stored but is discarded at 80°F in cooling water.

Note: Refer to International Critical Tables Vol VII.

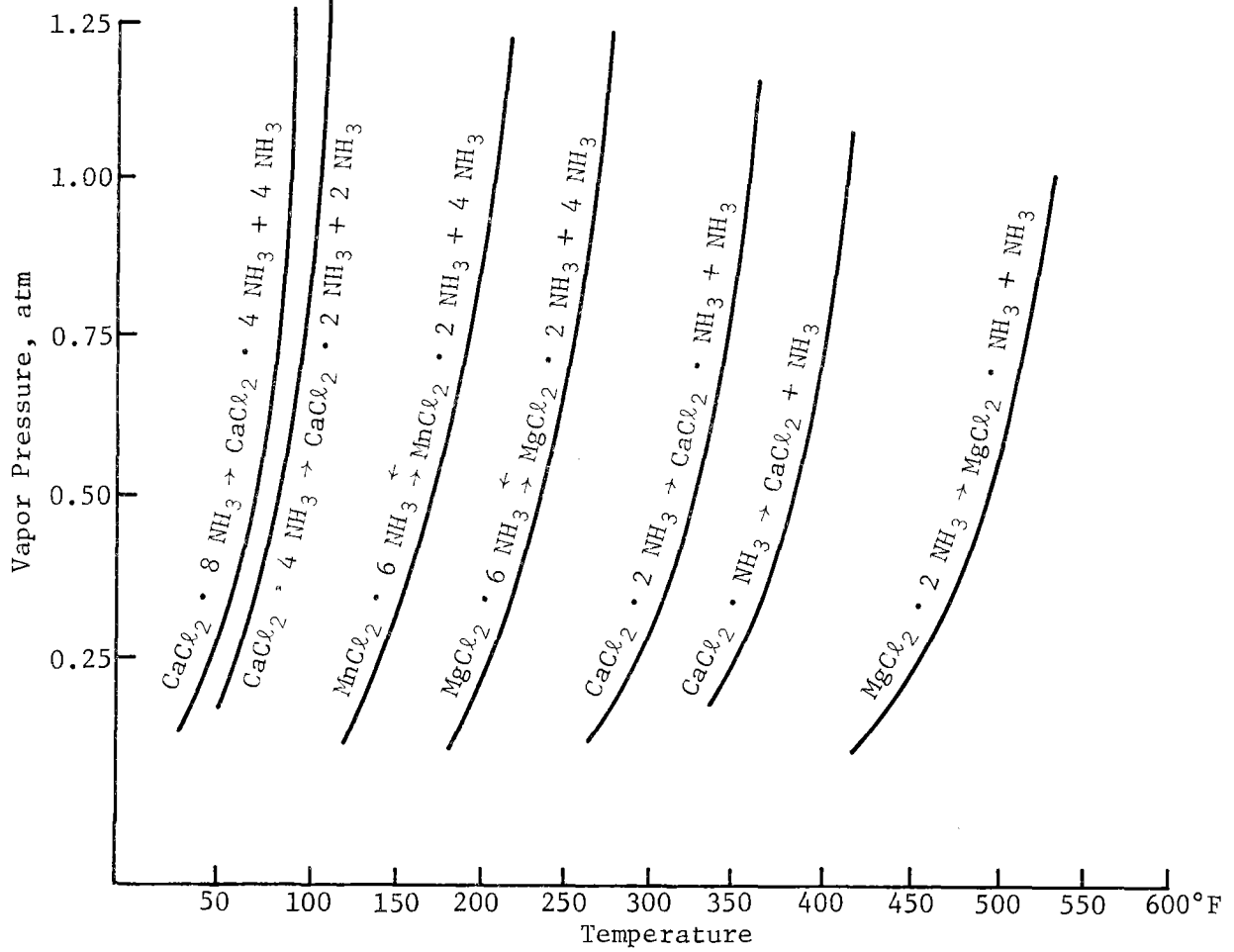


Figure I-1 Vapor Pressure Data for Ammoniated Salts

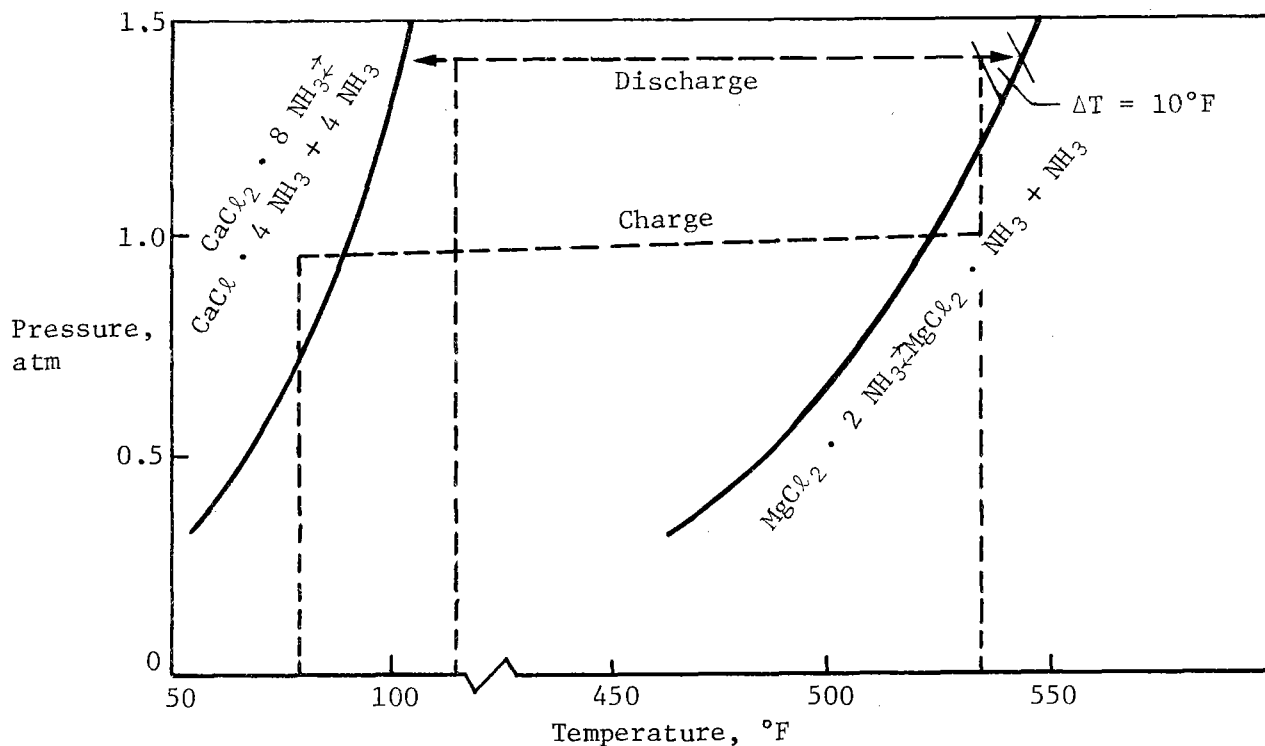


Figure I-2 Power System

On demand, water from the turbine condenser at 115°F is passed through the heat exchanger of the low-temperature reactor and raises the temperature of the salt bed to 105°F where the $\text{CaCl}_2 \cdot 8\text{NH}_3$ decomposes endothermically to $\text{CaCl}_2 \cdot 4\text{NH}_3$ and evolves ammonia at a pressure of 1.4 atmospheres. The evolved ammonia transfers back to the high-temperature cell through a slight pressure drop where it reacts with the $\text{MgCl}_2 \cdot \text{NH}_3$ to form $\text{MgCl}_2 \cdot 2\text{NH}_3$ at a temperature of 535°F . The heat of reaction is used to vaporize water in the cell heat exchanger to generate steam at near the original temperature of 535°F .

The system can also be used for home heating and cooling using solar energy if the high temperature salt is replaced with either $\text{MgCl}_2 \cdot 6\text{NH}_3$ or $\text{MnCl}_2 \cdot 6\text{NH}_3$.

In this phase of the program feasibility of the system was demonstrated by performing the following tasks:

- 1) Chemical and physical properties testing was conducted to determine:
 - The effect of ammoniation/deammoniation cycling on density, particle size, surface area, and the reversibility of the chemical reactions;
 - The effect of moisture on the reaction rates of two ammoniated salts;
 - The effect of nonaqueous impurities on the reaction rates of an ammoniated salt;
 - The heats of reaction for all of the CaCl_2 and MgCl_2 ammoniates.
- 2) Tests of a small scale reactor system were performed with various ammoniates in the high-temperature reactor to demonstrate that the ammoniated salt systems are chemically reversible and reproducible over a number of cycles.
- 3) A computer model was developed to analyze and predict the performance of fixed bed chemical reactors.
- 4) The use of this type of storage system for solar and conventional power plants was evaluated. Several alternative configurations were compared and a preliminary economic analysis was performed.

The results of the preceding tasks show that the process is feasible and not affected by repeated cycling up to 100 cycles. The use of chemical energy storage was found to be economically attractive when compared with high-temperature oil storage systems on relatively large power plants (i.e., 100 MWe for 24 hours).

This report describes the effort performed in Phase 1b of the program to develop ammoniated salts thermochemical energy storage systems. This is the second phase of a three-phase program. The first phase was completed in September of 1976 and is described in the Final Report, *Development of Ammoniated Salts Thermochemical Energy Storage Systems*, dated September 24, 1976. In the first phase four major tasks were accomplished. In the first task, candidate storage system concepts for use in power plant applications were compared from a technical and economic standpoint; the second task evaluated by test the thermal stability of ammonia at temperatures up to 650°F; in the third phase, the rates of reaction and heats of reaction for several ammoniates were determined, and finally a plan for the next phase was prepared.

The original program plan was for the first phase to be followed by a bench scale (115,000 Btu) system to obtain system performance for a power plant application. A third phase was to design, fabricate, and test a 13.6 million Btu storage system for a power plant application.

The results of the Phase 1 program were encouraging in that several of the candidate reactions were characterized, and the economic analysis looked promising. However, it was believed that further work was necessary to develop analytical tools, to determine the effects of cycling and impurities on the reaction kinetics, to refine the economic analysis, and to perform small scale system tests to demonstrate system feasibility before proceeding with the Phase 2 program of testing a bench scale system; therefore, Phase 1b of the program was formed.

The goal of Phase 1b of the contract was to demonstrate the technical feasibility of ammoniated salt storage systems. The program was divided in ten tasks, described as follows:

Task 1 - Analytical Modeling. Formulate a computerized mathematical model for predicting the performance of an ammoniated salt reactor.

Task 2 - Laboratory Scale System Tests. Design, fabricate, and test a laboratory scale thermal storage system to demonstrate the reversibility and reproducibility of the reactions over a number of cycles.

Task 3 - Cyclic Tests. Determine the effects of dissociation/recombination cycling on each of seven ammoniates in the free and constrained volume condition. Determine particle size distribution at 0, 1, 5, 10, 20, 50, and 100 cycles in the constrained volume test. Determine surface area after 0, 50, and 100 cycles.

Task 4 - Moisture Effects Evaluation. Determine the effect of from 1% to 6% moisture on the reaction kinetics of one ammoniate of $MgCl_2$ and $CaCl_2$.

Task 5 - Economics. Prepare a cost comparison of an ammoniated salt storage system with a sensible heat system using oil for two typical power plant sizes.

Task 6 - Alternate Bed Configuration - Fluidization. Analyze the effect of fluidization on performance of reversible thermal storage systems. Design and fabricate a small-scale reactor to determine gas velocity required to fluidize a salt bed. Calculate power requirements for fluidization.

Task 7 - Alternate Bed Configuration - Moving Salt and High Flow Fixed Bed. Prepare schematic flow diagrams, analyze performance, and investigate potential areas for application of these concepts.

Task 8 - Phase 2 Planning. Prepare proposed plan for the next phase of the program.

Task 9 - Heats of Reaction Verification. Measure the heats of reaction of various ammoniates determined previously to verify the result.

Task 10 - Effect of Nonaqueous Impurities. Determine probable impurities in commercial grades of $CaCl_2$ and $MgCl_2$; prepare samples; and determine the effect on the reaction kinetics of three ammoniates of $CaCl_2$ and $MgCl_2$.

All of the preceding effort has been completed and is reported in detail in the following sections.

III. ANALYSIS (TASK 1)

The objective of this task was to modify the Martin Marietta Interactive Thermal Analysis System, Version 2.0 (MITAS-II) computer program (Ref. III-A) to permit analyzing fixed-bed chemical reactors and to compare the results obtained from this analysis with the test results obtained in subscale testing, described in Section V.

A. DESCRIPTION OF THE MODEL

The MITAS II program is a general software system designed to solve, primarily, lumped parameter (resistance-capacitor) network representations of thermal systems. The major modification to the program added provisions for a chemical reaction rate. Specific features of the program that permit it to realistically describe the fixed-bed chemical reactor are as follows:

- 1) Chemical reaction rates as a function of temperature and pressure for various chemical reaction zones in the particle bed;
- 2) Temperature gradients between reaction zones to transfer heat in and out of the bed of the reactor;
- 3) Pressure gradients to transfer ammonia gas in and out of the reactor bed;
- 4) Temperature gradients within the heat transfer fluid flowing inside the conduits that traverse the reactor bed;
- 5) Conduction, convection, and mass flow paths to account for the transfer of energy and mass in and out of the reactor bed;
- 6) A source/sink term for both mass and energy generated or absorbed by the chemical reaction for each reaction node.

The modification of the MITAS II program to provide it with the preceding capabilities was conducted in three steps. Step 1 considered a steady state model of the reaction zone consisting of a particle bed contained between three adjacent tubes located at the corners of an equilateral triangle. Step 2 of the model was constructed as a transient model for a single, constant temperature heat transfer tube surrounded by five concentric

rings representing the reaction zones. Step 3 was a complete model of the experimental reactor. This model is a thermally-symmetrical quarter-section of the experimental reactor used in Tank 2 (Section V, Subscale Testing). The analytical model contains eight longitudinal, 12-in. long tubes, $\frac{1}{2}$ -in. OD, on 1-in. triangular centers as shown in Figure III-1. Each of the eight tubes is surrounded by five concentric rings of reacting solid as shown in Figure III-2. The reactor is divided longitudinally in six, 2-in. thick layers and numbered one through six from the top down. The ammonia flows in and out of the reactor at the top layer. The triangular, crosshatched space between the outer concentric reaction rings in Figure III-2 represents void space or zero-capacitance nodes. The model contains void space or zero-capacitance nodes. The model contains 240 reaction nodes (5 nodes per tube, 8 tubes, 6 layers), 48 heat transfer fluid nodes (1 node per tube, 8 tubes, 6 layers), 144 zero-capacitance nodes (24 nodes per layer, 6 layers), six gas nodes (1 per layer) for temperature calculations, six gas nodes for pressure calculations and four constant temperature (or pressure) boundary nodes for a total of 448 nodes. The six fluid nodes (in each of 8 tubes) were connected longitudinally by one-way enthalpy transfer paths representing fluid flow. The temperature for each of these nodes was calculated on the basis of input values of mass flowrate and heat capacity.

The gas pressure of each layer was calculated by the thermal analyzer network by assigning a mass source/sink to each gas node according to the calculated rate of ammonia gas generation (or absorption) associated with each gas node plus a particle bed permeability (analogous to a thermal conductance).

The computational time step has been a severe problem relative to the analysis of the reactors. It was found while analyzing the single tube model (step 2) that if the usual forward differencing approach is taken, the computer time becomes prohibitive. This is due to the requirement to take extremely small time steps in order to maintain numerical stability. This requirement is forced on the numerical solution due to the low thermal capacitance of the reacting nodes and large temperature-dependent reaction rates.

A method was developed for the single tube model that reduced computer time. The method controlled the computational time step, making it dependent on the reaction rates. However, this approach did not reduce computer run times to a practical value for the complete reaction model (step 3). Therefore, another method of calculating the temperature of each reaction node was developed.

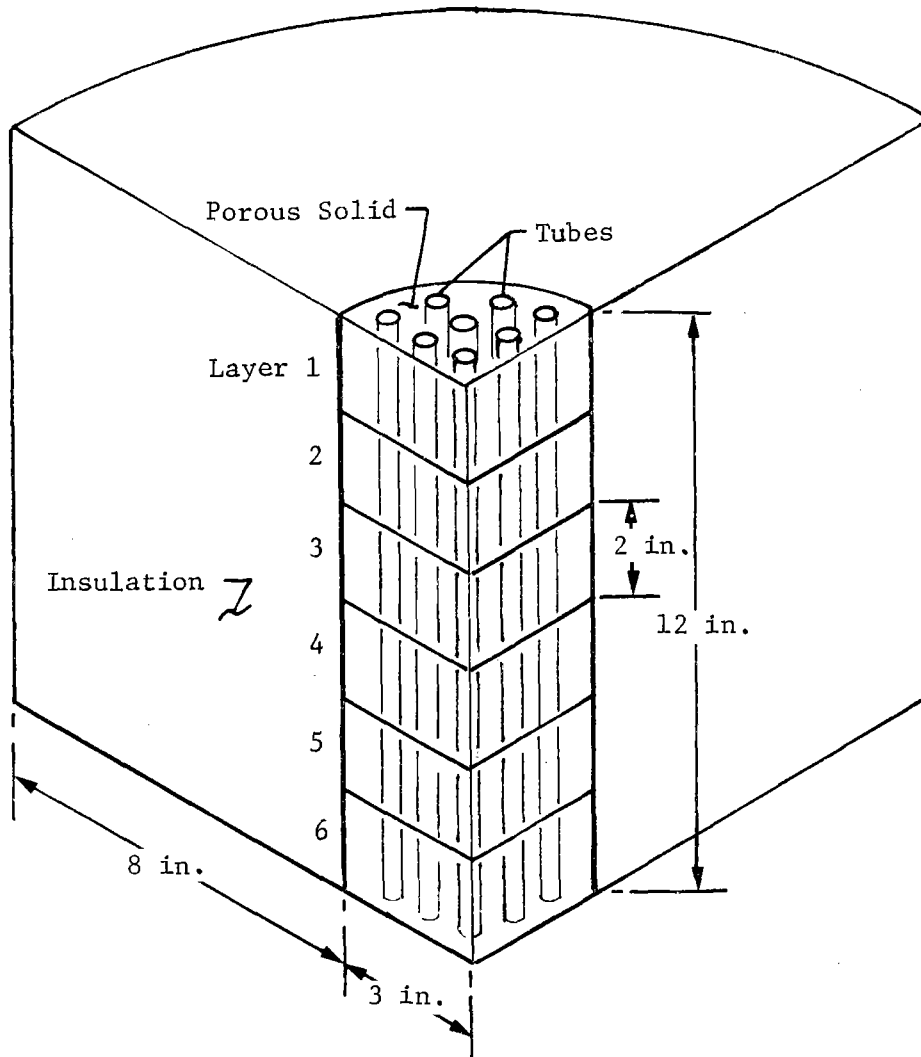
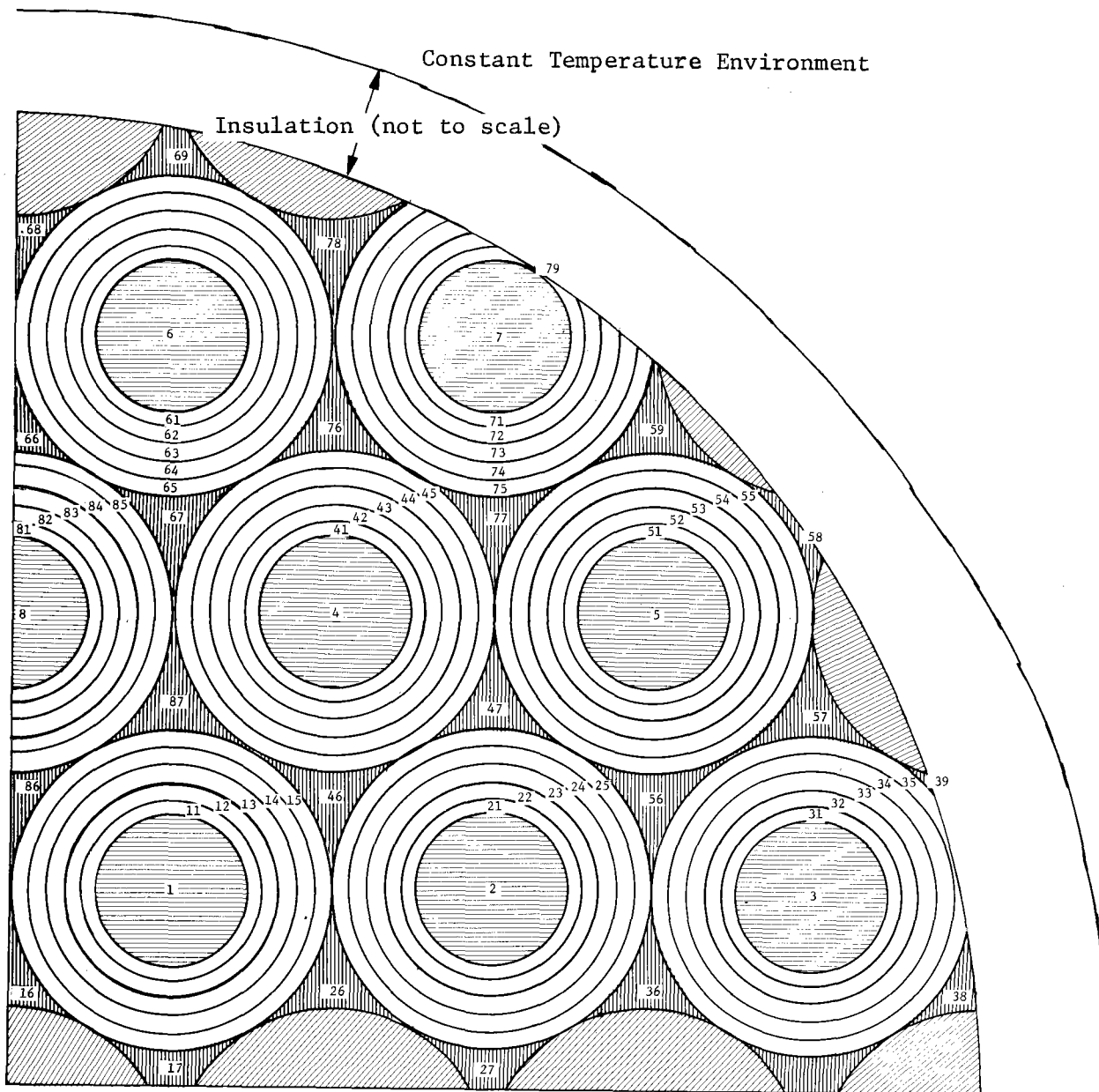


Figure III-1 Overall Dimensions of Reactor Model







Legend		
	Solid Reactant	(40 nodes/layer)
	Fluid	(8 nodes/layer)
	Zero Capacitance	(24 nodes/layer)
	Void Space	

Figure III-2 Node Definitions in Top Layer

The method adopted was derived from the conservation of energy relation and modified for our application. The energy rate due to reactions, Q , at any time and temperature is represented by:

$$[\text{III-1}] \quad Q = (\text{HR})(\text{AM})$$

where HR is the heat of reaction, and AM is the mass rate of ammonia evolution or absorption.

$$[\text{III-2}] \quad \text{AM} = M(1 - P/\text{PE})S \text{ EXP}(-A/\text{RT}_g)$$

where M is the mass of ammoniate present in node i,

P is the total pressure at node i,

PE is the equilibrium vapor pressure of the reaction at node i,

S is the frequency factor in the kinetic rate equation,
A is the activation energy,

R is the gas constant, and

T_g is the temperature of the gas at node i.

The derivation of the kinetic rate equation (equation III-2) is contained in the Phase I report (Ref III-2). The vapor pressure, PE, is determined by

$$[\text{III-3}] \quad \text{PE} = P_o \text{ EXP}(\text{HR}/R)(T - T_o)T_o$$

where P_o is the arbitrary reference pressure,

T is the temperature of node i, and

T_o is the arbitrary reference temperature.

The average value of the mass of reactive ammonia present at node i, \bar{M} , over the time period $\Delta \theta$, is given by

$$[\text{III-4}] \quad \bar{M} = M - \text{abs}(\text{AM}) \Delta \theta / 2$$

where abs is the absolute value. Therefore, equation [III-1] can be rewritten as

$$[\text{III-5}] \quad \bar{Q} = (\text{HR})\bar{M}(\text{AM}/M) = Q[1 - \text{abs}(\text{AM})\Delta \theta / 2M].$$

We will approximate Q as a linear function of T over the time period $\Delta\theta$ by

$$[\text{III-6}] \quad Q = \gamma + \beta T$$

where $\gamma = + (HR)(AM) - \beta T$,

$$\beta = dQ/dT_o = -(HR)M_S \{ \text{EXP}(-A/RT_o) / RT_o^2 \} \{ A + (HR - A)(P/PE) \}, \text{ and}$$

A is the activation energy in the kinetic rate equation.

Therefore, the average value of Q becomes

$$[\text{III-7}] \quad \bar{Q} = (\gamma + \beta T)(1 + \delta)$$

where $\delta = -\text{abs}(AM) \Delta\theta / 2M$.

when $M=0$, $AM=0$, and $\delta = 0$.

An elementary energy balance over a time increment $d\theta$ gives the following nodal energy balance,

$$[\text{III-8}] \quad c(dT/d\theta) = \sum_j G_j (T_j - T) + \bar{Q}$$

where c is the heat capacity of the fluid,

G_j is the thermal conductance at node j , and

T_j is the temperature at node j .

Substituting equation III-7 into equation III-8 results in;

$$[\text{III-9}] \quad c(dT/d\theta) = \sum_j G_j (T_j - T) + (\gamma + \beta T)(1 + \delta)$$

or

$$-c(dT/d\theta) = [\sum_j G_j - \beta(1 + \delta)] T - [\sum_j (G_j T_j) + \gamma(1 + \delta)].$$

Equation III-9 can be rewritten as

$$[\text{III-10}] \quad -(c/\alpha_1)(dT/d\theta) = T - \alpha_2/\alpha_1$$

where $\alpha_1 = \sum_j G_j - \beta(1 + \delta)$, and

$$\alpha_2 = \sum_j (G_j T_j) + \gamma(1 + \delta).$$

For steady state conditions $dT/d\theta$ is zero by definition and

$$[\text{III-11}] \quad T = \alpha_2/\alpha_1.$$

The model temperature at the end of a time increment during transient operation is obtained by integrating equation III-10 between θ and $\theta + \Delta\theta$. The resulting equation is:

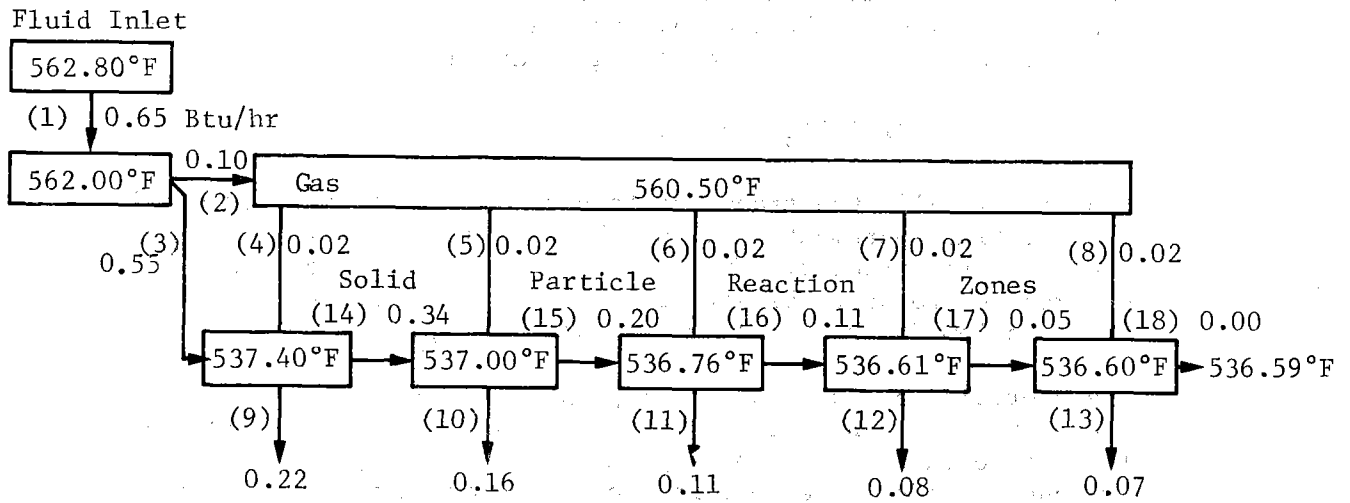
$$[\text{III-12}] T_{|\theta + \Delta\theta} = \alpha_2/\alpha_1 + (T_\theta - \alpha_2/\alpha_1) \text{EXP}(-\alpha_1 \Delta\theta/c).$$

Equation III-12, the transient temperature, is inherently stable for all time increments $\Delta\theta$, but the accuracy must be checked for each specific problem. The accuracy of this approach has been checked and found to be satisfactory for the reacting nodes in this problem for time increments approaching 10^{-2} hours.

The operation of the analytical program can be illustrated best by an energy balance of the five reaction zones surrounding the fluid tube (node 1) in the top layer. The energy balance approaches steady-state approximately one hour after the decomposition reaction is initiated. An energy balance is shown for the MgCl_2 decomposition reaction in Figure III-3. The temperature values shown in the boxes represent nodes and the rates of energy transfer are shown on the arrows connecting the nodes.

Figure III-3 shows the energy loss of the fluid between the inlet temperature of 562.8°F and the calculated temperature of layer 1 (562.0°F) is 0.649 Btu/hr . The number of parentheses (1) preceding the energy rate refers to the energy path. This energy is transferred by convection to the gas (2) at 560.5°F at a rate of 0.10 Btu/hr and to the solid (3) by conduction at a rate of 0.548 Btu/hr . The reaction zone adjacent to the tube wall receives energy by conduction from the tube at the rate of 0.548 Btu/hr (3) and by convection from the gas at the rate of 0.020 Btu/hr . The chemical reaction absorbs energy at the rate of 0.224 Btu/hr (9) and the bed conducts energy from node 9 to node 10 at the rate of 0.342 Btu/hr (14). The analytical program calculates the reaction nodal temperature of 537.48°F by making an energy balance on the node.

The second reaction node (node 10) receives energy by bed conduction from node 9 at a rate of 0.342 Btu/hr (14) and by convection from the gas at a rate of 0.020 Btu/hr (5). The chemical reaction absorbs energy at the rate of 0.163 Btu/hr and transmits heat to the third node (node 11) at a rate of 0.202 Btu/hr (15). The energy balances for each node are made in a similar manner.



Rate of Heat Absorption by Reaction

Figure III-3
Heat Transfer Rate for High-Temperature Reactor ($MgCl_2$) at One Hour, Btu/hr

B. COMPARISON WITH TEST DATA

This section presents a comparison of the pertinent reactor parameters calculated from the analytical model with those obtained from Cycle 26 of the subscale testing in Task 2 (Section V). Important reactor parameters compared include:

- 1) Reactor bed temperature;
- 2) Ammonia flowrate;
- 3) Rate of heat generated (absorbed);
- 4) Temperature of the fluid leaving the reactor.

The heat transfer parameters used in the analytical model are based on data obtained from tests performed at Colorado State University (Ref III-3). Two major heat transfer paths were identified from the heat exchanger surface to the reactor bed and incorporated in the analytical model. The first path is a direct course from the tube surface to the reacting solid, which is characterized by the heat transfer coefficient, h_{sw} .

The second path consists of a two-step convection route from the tube surface to the reacting solid consisting of (1) a convection path between the tube surface and the gas characterized by the heat convection coefficient, h_g , followed by (2) a convection path between the gas and the solid which is characterized by the convection parameter hA where A is the heat transfer area of the solid particles in the reaction zones. The heat transfer coefficient, U_2 , for the second path is given by

$$[III-13] U_2 = (h_g)(hA)/(h_g A_t + hA)$$

where A_t is the tube area. The overall coefficient of heat transfer, U_t , from the surface of the tube to the reacting solid is based on the two parallel, major heat-transfer paths and is

$$[III-14] U = h_{sw} + (h_g)(hA)/(h_g A_t + hA).$$

The numerical value of this coefficient, based on input parameters for the analytical model, is 1.07 Btu/hr-ft²-°F.

The input values of the preceding heat transfer coefficients were obtained from the study discussed in Section V. Generally, the heat transfer parameters are less than the overall heat transfer values obtained from the experimental data reported in Section V. For example, the value of overall coefficient of heat transfer

obtained experimentally was 2.2 Btu/hr-ft²-°F for the high-temperature reactor and 1.2 Btu/hr-ft²-°F for the low temperature reactor compared to the analytical value of 1.07 Btu/hr-ft²-°F presented previously.

The comparison of analytical and experimental reaction parameters (Table III-1 and III-2) used the same values of heat transfer parameters for both the high-temperature reactor with MgCl₂ and the low-temperature reactor with CaCl₂ operating in both the charging and discharging modes.

It should be recognized that because the solid particles serve as heat sinks during the decomposition and as heat sources during the recombination, the values of the empirical heat transfer coefficients shown in Tables III-1 and III-2 could be expected to be different even though they were assumed to be the same. These heat transfer coefficients could also be different in the two reactors because of the difference in the thermal properties, the surface structure, and reaction operating temperature between the MgCl₂ and CaCl₂ salts.

A detailed comparison of the analytically calculated flowrate of ammonia and the experimental flowrate for the discharge mode of the high-temperature MgCl₂ reactor shown in Table III-1 indicates that the input values of the heat transfer coefficients, h_g , h_A , and h_{sw} , are satisfactory.

The analytical predictions for the charge mode are lower than the experimental results because the analytical model was operated to maintain essentially the same reaction bed temperature for both the discharge and charge modes.

A detailed comparison of the analytically calculated flowrate of ammonia with the experimental flowrate for the low-temperature CaCl₂ reactor (Table III-2) indicates that the input values of the heat transfer parameters h_g , h_A , and h_{sw} are low for both the discharge mode (decomposition, heat absorption) and the charge mode (recombination, heat generation).

Two values are given for the analytical ammonia flowrate and the energy rate in Tables III-1 and III-2. The first value for each parameter represents the rate 0.2 hours after initiation and the second value represents the rate at the end of the operation; i.e., after five hours of decomposition and after three hours of recombination. These values shown little change during the operational periods.

Table III-1 Comparison of Experimental and Analytical Reaction Parameters

High Temperature Reactor: $\text{MgCl}_2 \cdot 2\text{NH}_3 \rightleftharpoons \text{MgCl}_2 \cdot \text{NH}_3 + \text{NH}_3$

Input Data to Analytical Model:

Heat Transfer Parameters (Ref III-3)

$$k_B = 0.113 \text{ Btu/hr-ft}^2 - ^\circ\text{F}$$

$$h_g = 3.07 \text{ Btu/hr-ft}^2 - ^\circ\text{F}$$

$$h_A = 8.5 \times 10^{-4} \text{ Btu/hr} - ^\circ\text{F}$$

$$h_{sw} = 0.688 \text{ Btu/hr-ft}^2 - ^\circ\text{F}$$

$$wc = 0.815 \text{ Btu/hr-}^\circ\text{F per tube}$$

Bed permeability - 100 grams NH_3 /hr mmHg

Chemical Reaction Parameters

(Ref III-2)

$$s = 4.213 \times 10^{10} \text{ hr}^{-1}$$

$$A = 43,133 \text{ Btu/lb mole}$$

$$H_r = 33,048 \text{ Btu/lb mole of ammonia}$$

$$T_o = 527^\circ\text{F at } P_o = 14.69 \text{ psia}$$

	Discharge Mode, Recombination		Charge Mode, Decomposition	
	Exp Cycle 26	Analytical	Exp Cycle 26	Analytical
Bed Temperature, °F	541.2	546	552	539
Bed Pressure, psia	20.99	20.99 (input)	17.91	17.9 (input)
NH_3 Flowrate, lb/hr	0.066	0.072	0.073	0.078
Energy Rate, B/hr	129	146	142.7	154.3
Temp, Fluid In, °F	514	514 (input)	573	573 (input)
Temp Fluid Out, °F	525	520	562	567
Temp Shroud, °F	553	541	521	539

Table III-2 Comparison of Experimental and Analytical Reaction Parameters

Low Temperature Reactor: $\text{CaCl}_2 \cdot 8\text{NH}_3 \rightleftharpoons \text{CaCl}_2 \cdot 4\text{NH}_3 + 4\text{NH}_3$

Input Data to Analytical Model:

<p><u>Heat Transfer Parameters</u> (Ref III-3))</p> <p>$k_B = 0.113 \text{ Btu/hr-ft}^2 - ^\circ\text{F}$</p> <p>$hg = 3.07 \text{ Btu/hr-ft}^2 - ^\circ\text{F}$</p> <p>$hA = 8.5 \times 10^{-4} \text{ Btu/hr-}^\circ\text{F}$</p> <p>$h_{sw} = 1.07 \text{ Btu/hr-ft}^2 - ^\circ\text{F}$</p> <p>$k \text{ (insulation)} = 1.02 \text{ Btu/hr-}^\circ\text{F per tube}$</p> <p>Bed permeability = 100 grams $\text{NH}_3/\text{hr mmHg}$</p>	<p><u>Chemical Reaction Parameters</u> (Ref III-2)</p> <p>$s = 1.076 \times 10^7, \text{ hr}^{-1}$</p> <p>$A = 15,714 \text{ Btu/lb mole}$</p> <p>$\text{HR} = 17,703 \text{ Btu/lb mole of ammonia}$</p> <p>$T_o = 89^\circ\text{F at } 14.69 \text{ psia}$</p>
---	--

	Discharge Decomposition		Charge Recombination	
	Exp Cycle 26	Analytical	Exp Cycle 26	Analytical
Bed Temp, $^\circ\text{F}$	100	101	89	93
Bed Pressure, psia	20.99	19.99 (input)	17.98	16.99 (input)
NH_3 Flowrate, lb/hr	0.066	0.054-0.053	0.073	0.052
Energy Rate, Btu/hr	68.9	56.3-55.3	76.4	54.3-54.3
Temp, Fluid In $^\circ\text{F}$	122	113 (input)	82	80 (input)
Temp, Fluid Out, $^\circ\text{F}$	115	111	86	82

Each reactor was initialized in a fully charged condition and operated for five hours in decomposition followed by three hours in recombination in the analytical program. The percentage of completion of the chemical reaction is shown as a function of time for each reaction in Figure III-4 and III-5. For example, the MgCl_2 decomposition reaction shown in Figure III-4 was started at time zero and operated for five hours. The node next to the tube surface (node 11) decomposed from zero percent $\text{MgCl}_2 \cdot \text{NH}_3$ to 86 percent during this time period. However, the node farthest from the tube surface (node 15) reached only 31 percent after five hours. The average percentage of completion for the total reaction bed reached approximately 50 percent after five hours.

The fluid temperature was reduced at five hours and the recombination reaction started with the bed in the condition existing at the end of the 5-hours decomposition period. The node adjacent to the fluid tube (node 11) started the recombination period at 86 percent $\text{MgCl}_2 \cdot \text{NH}_3$ and reached about 17 percent after eight hours. During the same period, the node farthest from the fluid tube (node 15) started recombination at 31 percent and reached 17 percent after eight hours. The total reaction bed started the recombination reaction at 50 percent completion and reached about 30 percent completion of the recombination reaction after eight hours.

The rate of reaction continuously decreased during these transient reaction periods, but the rate of ammonia generation (or evolution) and the corresponding rate of heat absorption (or generation) remained essentially constant because, for the conditions chosen, the overall process rate was limited by the heat transfer rate in and out of the reactor and not by the reaction rate. If the rate of heat transfer in and out of the reactor were significantly increased, the analytically predicted and the experimentally observed values of ammonia rate and heat generation (or absorption rate) would show a greater decline during the operational time period.

C. CONCLUSIONS

The following conclusions can be made based on the discussions in the preceding paragraphs.

- 1) An analytical model was constructed for a laboratory-scale experimental reactor. The results obtained from the analytical model compared favorably with the experimental data.

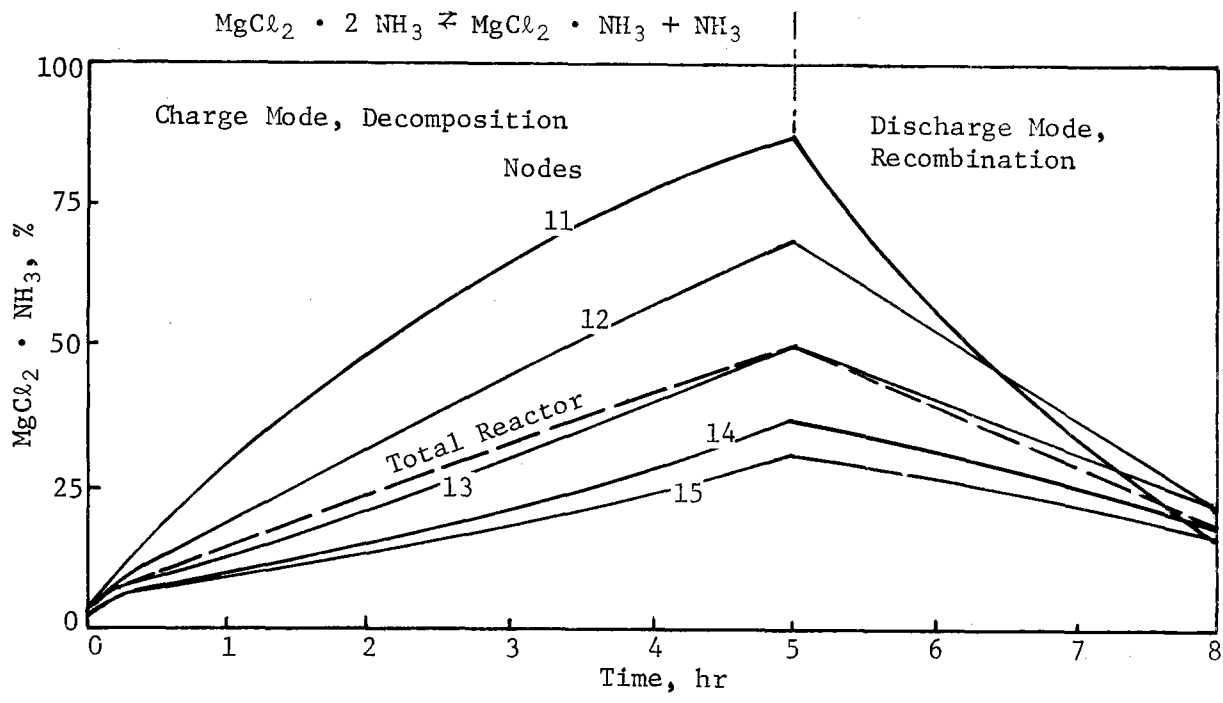


Figure III-4
Percent of $MgCl_2 \cdot NH_3$ as a Function of Time

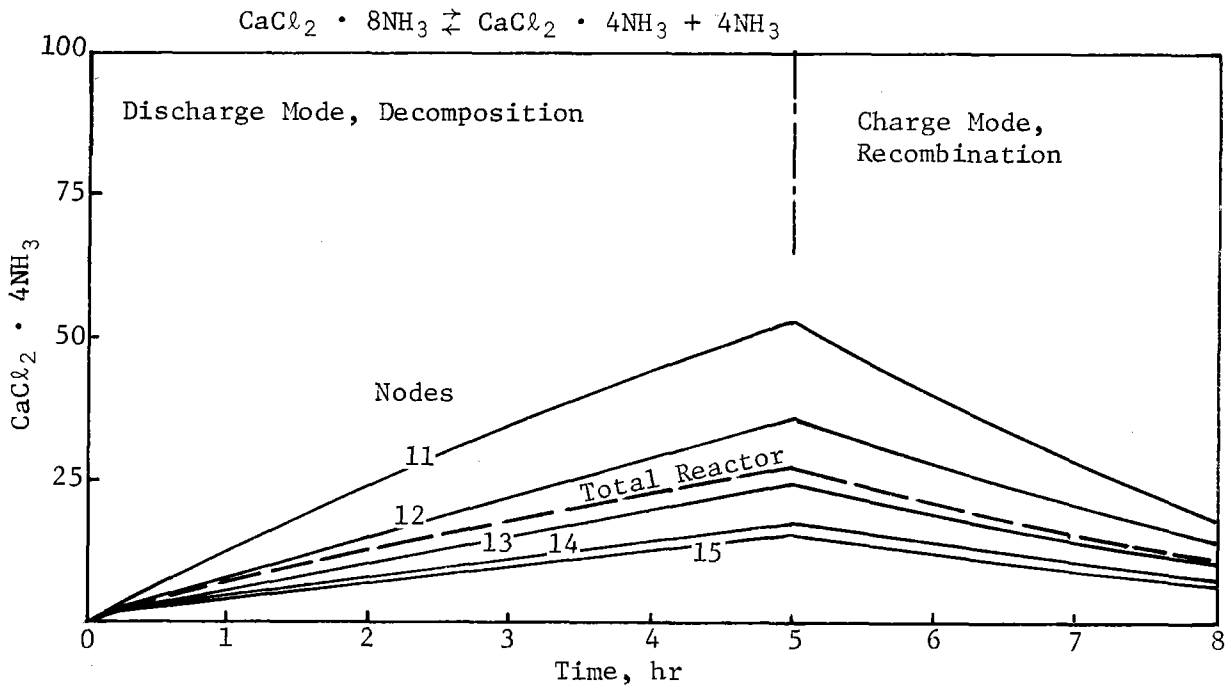


Figure III-5
Percent of $CaCl_2 \cdot 4NH_3$ as a Function of Time

- 2) The values of the heat transfer parameters are satisfactory for the MgCl_2 reactor but are low for the CaCl_2 reactor.
- 3) The overall rate of the process for the conditions studied is limited by the heat transfer rate to and from the reactor. The rate of chemical reaction does not control the process.

IV.

CHEMICAL AND PHYSICAL PROPERTIES TESTING

Chemical and physical properties testing conducted in this program covered four major areas of study. The testing was performed to determine the following:

- 1) The effect of ammoniation/deammoniation cycling on density, particle size, surface area, and the reversibility of the chemical reaction;
- 2) The effect of moisture on the reaction rates of two ammoniated salts;
- 3) The effect of nonaqueous impurities on the reaction rates of an ammoniated salt;
- 4) The heats of reaction for all CaCl_2 and MgCl_2 ammoniates.

In the cycling test all of the ammoniates of CaCl_2 and MgCl_2 were subjected to a total of 100 cycles of ammoniation/deammoniation. Measurements were made of the initial properties and the properties after 1, 5, 10, 20, 50, and 100 cycles. No change was noted in any of the properties measured as a result of cycling.

The effect of the addition of 1%, 2%, 4%, and 6% moisture on the dissociation/recombination kinetics of one calcium chloride ammoniate and one magnesium chloride ammoniate was measured in the second test series. No permanent degradation in the reaction rates of the salts resulted from the water impurity.

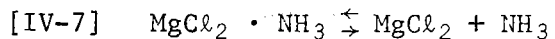
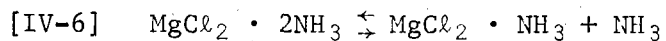
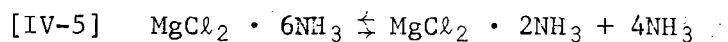
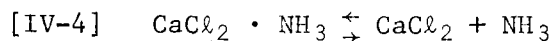
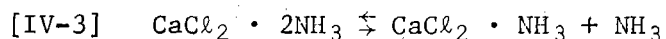
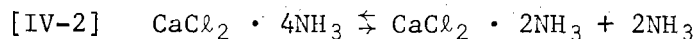
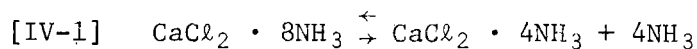
The third area of investigation tested the effect of other impurities (air and calcium sulfate) on the reaction rates of calcium chloride octammoniates. Again, no change in the reaction rates were noted with 1% to 2% of the impurity present.

Finally, the heats of reaction of all of the ammoniates of the calcium chloride and magnesium chloride were measured. These measurements had been made in Phase I of this program and were repeated here because of the disagreement between the measured

data and literature values. In this program a larger quantity of material was used in an attempt to improve the measurement accuracy.

A. DISSOCIATION/RECOMBINATION CYCLING (TASK 3)

The objective of this testing was to provide samples for a series of tests on changes in salt ammoniate morphology and trends of chemical irreversibilities after a number of dissociation/recombination cycles of the following salt ammoniate reactions:



1. Method

a. Original Apparatus - The original apparatus was designed to thermally cycle four separate salt specimens at preselected temperatures. It was deemed desirable to use transparent containers in order to observe any results of the reactions (ammoniation and cycling) and to readily obtain expansion measurements. Quartz was selected as the container material to accommodate the high temperatures associated with some of the cycling requirements.

Four containers (Fig. IV-1) were fabricated from 13.8-in. lengths of quartz tube having an outside diameter of 1.2 in. and a wall thickness of 0.070 in. Flanges (type 304 stainless steel, 2-3/4-in. OD) with graded seals were attached to the ends of each tube. The overall length of the finished tube was 22.0 in.

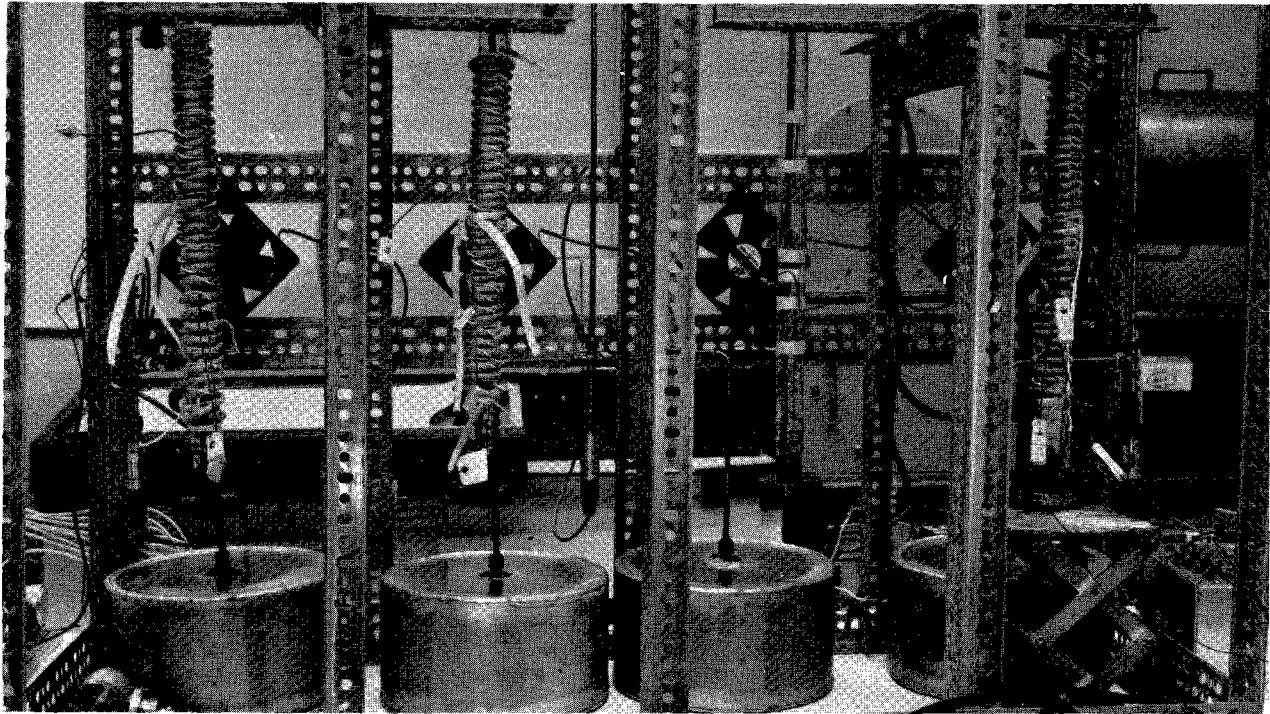


Figure IV-1 Cycling Test Apparatus

A "screen tube," 21.5-in. long with an outside diameter of 0.3 in., was fabricated from 250 x 1370 mesh, 304L stainless steel fabric. The screen tube was welded to the circumference of a stainless steel tube. This tube assembly was welded to a bore in a flange that mated with the flange on the quartz tube described previously. The purpose of the assembled screen tube and quartz tube was two-fold: to facilitate ammoniation throughout the salt, and to prevent salt from being pumped out of the quartz tube during evacuation.

Each quartz tube was fitted with three thermocouples; one in the center and one 3.4 in. from each end. The output signals from all thermocouples were monitored on a 12-channel recorder.

Heating coils were wrapped around the length of the quartz tubes and secured with asbestos cord. Current through the heating coils was controlled by two separate variable transformers for each tube; one each for the high- and low-temperature half-cycles. Selection of the appropriate variable transformer (high- or low-temperature half-cycle) was accomplished by an eight-switch recycling cam timer. The timer also controlled the cooling fans.

A fixture was assembled to accommodate the quartz tubes, cooling fans, valves, and attendant plumbing. A ballast tank (volume 345.3 cubic inches) minimized pressure fluctuations due to temperature changes. Statham PA707TC pressure transducers monitored pressures.

A quartz tube was filled with 6.1 in.³ of CaCl₂ (a height of 7-21/32 in.) and mounted vertically in the fixture. Ammoniation was started (after vacuum bake-out) and an initial temperature rise from room temperature to 135°F was observed. The salt returned to room temperature after approximately 20 minutes. As noted by the continuous drop in NH₃ pressure, ammoniation continued for approximately four hours. At this point the quartz tube fractured. Ammoniation was attempted twice more with the same method and with the same results.

A new tube was fabricated from a 12-in. length of 321 stainless steel having an outside diameter of one inch and a wall thickness of 0.065-in. Flanges similar to those used on the quartz tubes were welded to each end of the stainless steel tube. A screen tube 11-1/2-in. long was fabricated and thermocouples were attached at the center and 1/2 in. from each end. Strain gages were mounted 4-7/8 in. from the bottom and 5/8 in. from the top (top defined as entry point of screen tube). The tube was wrapped with a heating coil.

The tube was filled to a level of 5-1/4 in. (3.12 in.³) with 200 to 250-mesh CaCl₂ and attached to the cycling fixture. Ammoniation was started following vacuum bake-out. Thermal behavior similar to that observed with the quartz tube ammoniation was noted. After ammoniation, a radiograph revealed that the level of the salt had grown to 5-3/4 in. (3.412 in.³), a volume increase of only 9.6%. Also, the radiograph showed that the portion of the screen tube that was immersed in the salt was severely crushed. The strain gage located 4-7/8 in. from the bottom of the tube indicated 226 microinches per inch of lateral strain after salt ammoniation.

b. Modified Apparatus - The 12-in. tube described in the previous paragraph was cut to a length of 4.9 in. and a 0.1-in. x 2.5-in. x 2.5-in. stainless steel plate was welded to the unflanged end. A 2.5-in. long screen tube was fabricated for the flanged end. A thermocouple was attached 1/2-in. from the bottom of the tube. The tube was then wrapped with a heating coil.

The tube was charged with a relatively small amount (0.025 lb) of CaCl_2 and attached to the cycling fixture in a horizontal position to minimize constraint on the growth of the salt. The tube was agitated to achieve distribution of the salt and further minimize constraint of salt growth. Ammoniation was started after vacuum bake-out and was completed (as noted by cessation of NH_3 pressure drop) in four hours. The tube was then disassembled and examined. Weight measurements confirmed the proper stoichiometric addition of NH_3 . No ill effects were observed.

Three more identical tubes were fabricated and the cycling program was started. Ammoniation was done with the tubes in a horizontal position (to minimize constraint of salt growth) and cycling was performed with the tubes in a vertical position. The rest of the apparatus used was the same as that described for the original quartz tube arrangement.

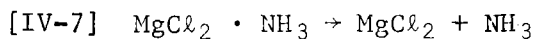
The salts were cycled between high and low ammoniate in each reaction for up to 100 cycles of dissociation/recombination.

Prior kinetic studies performed in the laboratory indicated the recombination reaction at a given temperature difference below the equilibrium temperature was slower than the corresponding deammoniation at the same temperature difference above the equilibrium temperature. Cycling temperatures were therefore selected on the basis of the recombination reaction, with equal temperature differences above and below the equilibrium temperature selected such that the recombination reaction had sufficient time to go to completion. This was confirmed experimentally by the cessation of NH_3 pressure drop and by a weight increase of the sample tube indicating a stoichiometric addition of NH_3 . The dissociation reaction was assumed to be complete when the ammonia pressure in the sample tube stabilized.

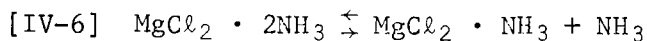
c. Results - A volume change during ammoniation of anhydrous CaCl_2 to form $\text{CaCl}_2 \cdot 8\text{NH}_3$ on the order of 240% was experienced by the salt. Any constraint that prevents a full and free expansion during the initial reaction ($\text{CaCl}_2 + 8\text{NH}_3 \rightleftharpoons \text{CaCl}_2 \cdot 8\text{NH}_3$) is likely to cause a rock-like, impermeable material to form instead of the preferred low density, highly permeable powder. Sufficient constraint existed during vertical ammoniation to cause fracturing of the quartz tubes. Apparently, the initial ammoniation occurs in the upper layer of salt and essentially "locks" the unreacted salt in the lower layers. As the recombination with ammonia proceeds, the accompanying volume expansion fills all available interstices and then begins exerting force on the chamber walls.

An attempt was made to measure the forces acting on a stainless steel chamber during initial ammoniation of calcium chloride. The test was unsuccessful because the salt formed during ammoniation crushed the ammonia feed-tube screen, absorbed the expansion force, and transferred little force to the chamber wall. After the initial ammoniation of the anhydrous calcium chloride to form the octammoniate, there is far less shrinkage or expansion (approximately 20% to 25% determined visually) on subsequent decompositions and recombinations.

The reaction:



was found to be highly corrosive to parts of the container in which the cyclic tests were conducted. The ammonia feed-tube screen, made from 304L stainless steel, was partially or completely corroded in all cyclic tests of magnesium chloride monoammoniate. Tubes used for cyclic testing were also 304 stainless steel and corrosion was found on the inside walls. "Kevex" X-ray analysis of the tested salts confirmed corrosion, indicating the presence of high amounts of iron, chromium, and phosphorous. The corrosion problem was also evident for the reaction,



but to a lesser extent than the monoammoniate reaction.

d. Conclusions - The conclusions obtained from the study are as follows:

- 1) Special care must be taken in the initial ammoniation of CaCl_2 to prevent formation of high-density phases. Large volume changes accompanying the ammoniate formations can be encouraged in a variety of ways. High-frequency vibration of the container during ammoniation has proved successful as has horizontal position of a 1-in. diameter cylindrical tube. Eight pounds of CaCl_2 were successfully ammoniated in a 12-in. diameter cylinder by maintaining the cylinder in a horizontal position and occasionally rolling the cylinder about its longitudinal axis.

The likelihood of forming rock-like, impermeable material suggests that if the octammoniate were to be used on a large scale reactor, it would be advisable to charge the reactor with the ammoniated salt rather than loading with anhydrous salt and ammoniating the container.

- 2) The corrosion exhibited by the reaction,



in contact with the stainless steel screen indicates a materials compatibility selection problem exists.

- 3) No trends of chemical reaction irreversibilities were noted as a result of cycling.

B. BULK DENSITY (TASK 3)

The objective of this portion of the study was to determine the bulk density of the various salt ammoniates and the effects of dissociation/recombination cycling on this parameter (if any).

1. Method

Bulk density measurements were made by independent measurement of sample mass and volume for each of the salt ammoniates before and after cycling (i.e., the "after" measurement for cycle n should ideally equal the "before" measurement for cycle n + 1).

2. Results

The influence of cycling on ammoniates of $MgCl_2$ is summarized in Table IV-1 and data obtained for $CaCl_2$ ammoniates is given in Table IV-2.

The bulk density of $CaCl_2$ used in the tests was relatively constant at 55.9 lb/ft³. For the $MgCl_2$ tests, a newly prepared batch of anhydrous salt was used for each cyclic test, and because of the variability of the initial bulk density of this salt, the density before and after cycling is noted.

3. Conclusions

The conclusions obtained from this portion of the program as follows:

- 1) The bulk densities of both the calcium and magnesium chlorides are low when compared with the true material densities (refer to Section V).

Table IV-1

Magnesium Chloride Ammoniates Bulk Densities before and after Cycling

Salt	MgCl ₂ · NH ₃		MgCl ₂ · 2 NH ₃		MgCl ₂ · 6 NH ₃	
	Before, lb/ft ³	After, lb/ft ³	Before, lb/ft ³	After, lb/ft ³	Before, lb/ft ³	After, lb/ft ³
1	12.5	11.9	13.1	13.7	15.0	14.4
5	13.1	14.4	14.4	16.9	12.5	17.5
10	11.9	13.1	13.1	16.2	13.1	16.9
20	6.9	8.1	15.6	18.7	9.4	13.7
50	13.1	11.9	20.0	16.9	22.5	18.1
100	26.8	31.2	20.0	21.2	21.8	16.9

Table IV-2

Calcium Chloride Ammoniates Bulk Densities after Cycling*

Salt	CaCl ₂ · NH ₃	CaCl ₂ · 2 NH ₃	CaCl ₂ · 4 NH ₃	CaCl ₂ · 8 NH ₃
Cycle	lb/ft ³	lb/ft ³	lb/ft ³	lb/ft ³
1	35.0	29.3	30.0	29.3
5	33.1	36.2	35.0	47.4
10	30.0	29.3	32.5	29.3
20	40.6	27.5	34.3	35.0
50	38.1	40.0	29.3	35.0
100	22.5	18.1	31.2	28.1

*Density before Ammoniating - 55.9 lb/ft³

The estimated measurement error is 12%.

- 2) The bulk density of both salts is not influenced in large measure by the state of ammoniation.
- 3) Though several questionable, perhaps anomalous points appear on Tables IV-1 and IV-2 (i.e., MgCl₂ · NH₃ 100 cycles and CaCl₂ · NH₃ 100 cycles) it should be made clear that in none of the salt ammoniates does a consistent trend appear to indicate a significant influence of dissociation/recombination on the bulk density.

C. THEORETICAL DENSITY (TASK 3)

The objective of this set of tests was to determine the true density of the various ammoniates (as opposed to the bulk density discussed previously).

1. Method

Determination of the theoretical density of the ammoniated salts was first attempted by X-ray diffraction (e.g., Debye-Scherrer)-- a method commonly used to measure lattice parameters from which theoretical density is routinely determined. However, for the ammoniated salts in question several complicating factors soon became apparent. First, nothing was known of the actual crystal structure of most of the ammoniates. Also, the difficulty of obtaining a suitably pure sample of a particular ammoniate made it essentially impossible to obtain an unambiguous diffraction pattern. The necessity for the latter is widely established (Ref IV-1), particularly in the case of those ammoniates whose crystal structure must be determined. We therefore used a modified weld-type pycnometer (modified in that temperature could be monitored directly) to determine the density of the various salts. Duo Seal pump oil was chosen as the inert liquid for the pycnometer.

The volume of the pycnometer was determined with distilled water at 77°F and the density of the oil calculated. Salt samples of known weight were then immersed in the oil-filled bottle and sonicated to release trapped air bubbles. The exterior of the bottom was cleaned with solvent and placed in a thermostat until the appropriate temperature was attained. The pycnometer was then weighed and density calculations made.

2. Results

Densities of the various ammoniates as determined experimentally are listed in Table IV-3. The method agreed well with the literature value for anhydrous CaCl_2 (Ref IV-2). Determinations on anhydrous MgCl_2 were difficult as the irreversible formation of the monohydrate takes place almost immediately when the sample is exposed to room conditions. Any value obtained for $\text{CaCl}_2 \cdot 8\text{NH}_3$ is suspect due to the instability of this ammoniate under ambient conditions, and particularly because ammonia evolution was detected during testing of the sample. The value obtained was 93.45 lb/ft^3 , but this value should only be considered to

indicate that the calcium chloride octammoniate is significantly less dense than the quadrammoniate.

Table IV-3 Densities of Ammoniates

Salt	Density, lb/ft ³
CaCl ₂	134.35*
CaCl ₂ · NH ₃	137.72
CaCl ₂ · 2 NH ₃	107.4
CaCl ₂ · 4 NH ₃	98.39
CaCl ₂ · 8 NH ₃	93.45
MgCl ₂	144.75 - 145.46†
MgCl ₂ · NH ₃	124.67
MgCl ₂ · 2 NH ₃	98.82
MgCl ₂ · 6 NH ₃	88.09

*Experimental value compared to literature value of 134.23.

†Literature value. *Handbook of Chemistry and Physics*, 48th Ed, p B-191, Chemical Rubber Company, Cleveland, Ohio, 1967.

3. Conclusions

Conclusions from this part of the program are as follows:

- 1) The density of calcium chloride octammoniate was the most difficult to obtain. However, the result obtained as mentioned previously, indicates the CaCl₂ · 8NH₃ follows the trend exhibited by all the other ammoniates, i.e., an increasing degree of ammoniation results in a decreased density.

D. SURFACE AREA (TASK 3)

The objective of this study was to determine the average surface area of the various ammoniates and the effect of cycling on the surface area.

1. Method

The BET (Ref IV-3) method for determining surface area was used for each of the ammoniated salts after a specified number of dissociation/association cycles. An Ainsworth RV-AU-2 Vacuum Automatic Recording Balance was used to determine gravimetrically the amount of argon required by each ammoniate for monolayer adsorption. The ammoniated salt was placed in the balance pan, weighed, and the system evacuated. The sample was cooled to -108°F via an externally applied acetone-dry ice bath and argon admitted to a final pressure of 100 torr. The amount of argon adsorbed was then corrected for the amount of argon adsorbed by the empty system. The surface area of the ammoniated salt particles was determined by assuming the molecular area of argon to be 14.4A (Ref IV-4).

2. Results

The results obtained for the calcium chloride octammoniate were questionable. The results for the other three ammoniates of CaCl_2 and for the MgCl_2 ammoniates are shown in Table IV-4. The calcium chloride ammoniates that could be tested yielded surface areas in the range of 1 to 2×10^3 ft² per pound of ammoniate. Examination of the data indicates that samples of a particular ammoniate vary in surface area depending on the number of dissociation/association cycles. An exception was $\text{MgCl}_2 \cdot \text{NH}_3$ for it appeared to be less finely divided than the higher ammoniates of MgCl_2 .

3. Conclusions

The following are the conclusions for this part of the study.

- 1) Errors inherent in the surface area determination were attributed to the calcium chloride ammoniates being grossly heterogeneous with respect to particle size, making a truly representative sampling difficult to accomplish.

Table IV-4

Surface Area of the Ammoniated Salts CaCl_2 and MgCl_2 *

Salt	No. of Dissociation/ Association Cycles	Surface Area, ft^2 / lb of Ammoniate
$\text{CaCl}_2 \cdot 4 \text{NH}_3$	50	1.09×10^3
	100	2.05×10^3
$\text{CaCl}_2 \cdot 2 \text{NH}_3$	0	1.72×10^3
	50	1.44×10^3
	100	2.19×10^3
$\text{CaCl}_2 \cdot \text{NH}_3$	0	1.30×10^3
	50	1.47×10^3
	100	1.71×10^3
$\text{MgCl}_2 \cdot 6 \text{NH}_3$	0	1.85×10^4
	100	1.19×10^4
$\text{MgCl}_2 \cdot 2 \text{NH}_3$	0	1.96×10^4
	100	1.67×10^4
$\text{MgCl}_2 \cdot \text{NH}_3$	0	8.88×10^{-3}
	100	8.54×10^{-3}

*The variation in values obtained for a particular ammoniate after altering the number of cycles to which it was subjected still falls within the range considered "good agreement" by Young and Crowell (Ref IV-4) in comparison of the BET method with other surface area determination methods.

- 2) Despite the sampling difficulty, certain trends or lack of trends, could be ascertained with a reasonable degree of certainty: one, cycling the salts through varying numbers of dissociation/association reactions had little if any effect on the surface area to weight of ammoniate ratio; and two, though results varied widely (at least an order of magnitude) for the octammoniate of calcium chloride, the largest surface area obtained ($9.86 \times 10^3 \text{ ft}^2/\text{lb}$) indicates that perhaps this ammoniate is significantly more finely divided than the other ammoniates of this salt. As the magnesium chloride monoammoniate appears less finely divided than its corresponding higher ammoniates, there may be a trend toward smaller particle size as the various salts achieve higher degrees of ammoniation.

E. PARTICLE SIZE DISTRIBUTION (TASK 3)

The objective of this test was to measure particle size distribution and the effect of cycling on particle size.

1. Method

A conventional, visible-light 35X microscope was used for determining particle size distribution of the cycled salt ammoniates. Using a vernier scale eyepiece, 400 representative particles of each cycled salt were sized in categories of 0 to 100 microns, 100 to 300 microns, and 300 to 3000 microns. These categories are those commonly used for particulate analysis.

2. Results

The results obtained in particle size analysis of the cycled salt ammoniates are given in Table IV-5.

3. Conclusions

The following are the conclusions for this part of the study.

- 1) In general, no trend that related to the number of association/dissociation cycles and particle size distribution was indicated.
- 2) Aside from the usual difficulties in sampling elucidated elsewhere (i.e., representative sampling and the actual altering of the particle size in getting the salt out of the ammoniation chamber), the tendency of all the salt ammoniates to clump or aggregate after a short time in the presence of air (water vapor) probably gave rise to some of the anomalous results (particularly among the magnesium chloride ammoniates) in Table IV-5.

F. EFFECTS OF MOISTURE ON SALT REACTION RATES (TASK 4)

The objective of this task was to determine the effect of 1%, 2%, 4%, and 6% moisture addition by weight of anhydrous salt on the dissociation/recombination reaction rates of one calcium chloride and one magnesium chloride ammoniate pair.

Table IV-5 Particle Size Distribution (in %) for Ammoniated Salts vs Cycles

Cycle Ammoniate	0			1			5			10			20			50			100		
	1*	2	3	1	2	3	1	2	3	1	2	3	1	2	3	1	2	3	1	2	3
CaCl ₂ • 8NH ₃	85	10	5	0	5	95	2	5	93	2	0	98	2	5	93	30	10	60	5	5	90
CaCl ₂ • 4NH ₃	85	10	5	0	0	100	5	10	85	0	0	100	0	5	95	10	10	80	5	0	95
CaCl ₂ • 2NH ₃	5	5	90	5	5	90	10	10	80	0	5	95	0	5	95	40	40	20	5	5	90
CaCl ₂ • NH ₃	2	5	93	0	0	100	5	0	95	2	0	98	0	0	100	2	0	98	3	0	97
MgCl ₂ • 6NH ₃	95	0	5	90	5	5	85	10	5	90	5	5	70	10	20	85	10	5	90	5	5
MgCl ₂ • 2NH ₃	70	20	10	85	10	5	70	10	20	80	10	10	70	20	10	50	20	30	90	5	5
MgCl ₂ • NH ₃	60	20	20	60	20	20	60	20	20	80	10	10	70	20	10	60	10	30	95	0	5

*1 = 0-100 microns
 2 = 100-300 microns
 3 = 300-3000 microns

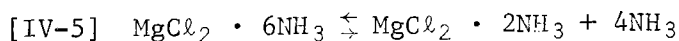
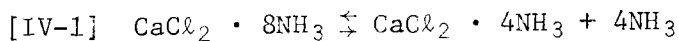
Note: The particle size distribution is based on number of particles.

1. Method

A Mettler TA-1 thermoanalyzer that continually monitors weight loss (or gain) and instantaneous rate of weight loss (or gain) versus temperature was used for these studies. Samples to be tested were weighed and placed in the instrument and baked in vacuum at 300°F to 390°F until a stable weight was obtained. The thermoanalyzer was bled back to atmospheric pressure with laboratory air and a small air flow was maintained through the balance with the air bubbled through a water trap before entering the balance. When the sample weight gain reached the desired 1%, 2%, 4%, or 6%, the thermoanalyzer was evacuated (with no detectable weight loss as a result of evacuation) and then backfilled with one atmosphere of anhydrous ammonia. The sample weight gain was recorded until no further ammonia was taken up. With the thermoanalyzer pressure held at one atmosphere of ammonia, the salt temperature was adjusted to a level that caused dissociation to occur. When the dissociation reaction was complete, and the next lower ammoniate was formed, the temperature was lowered until recombination to the higher ammoniate began. The temperature was raised and lowered cyclically in this fashion until the rate data in Figures IV-2 and IV-3 were obtained.

2. Results

Rate data were obtained for the reactions



as 1%, 2%, 4%, and 6% by weight moisture was added to the anhydrous salt.

Figure IV-2 gives the dissociation/recombination rates for $\text{CaCl}_2 \cdot 8\text{NH}_3$ that contained 1%, 2%, 4%, and 6% by weight moisture compared with rate data for the anhydrous salt.

Figure IV-3 shows the effects of 1%, 2%, 4%, and 6% moisture addition on the dissociation/recombination rates of $\text{MgCl}_2 \cdot 6\text{NH}_3$.

3. Conclusions

Conclusions for this task are as follows:

- 1) The values plotted were obtained after several conditioning cycles of dissociation/recombination in which the total amount of ammonia reacted with the salt gradually increased to the stoichiometric amount. In Figure IV-3 all values tend to be somewhat higher than the original values reported for the

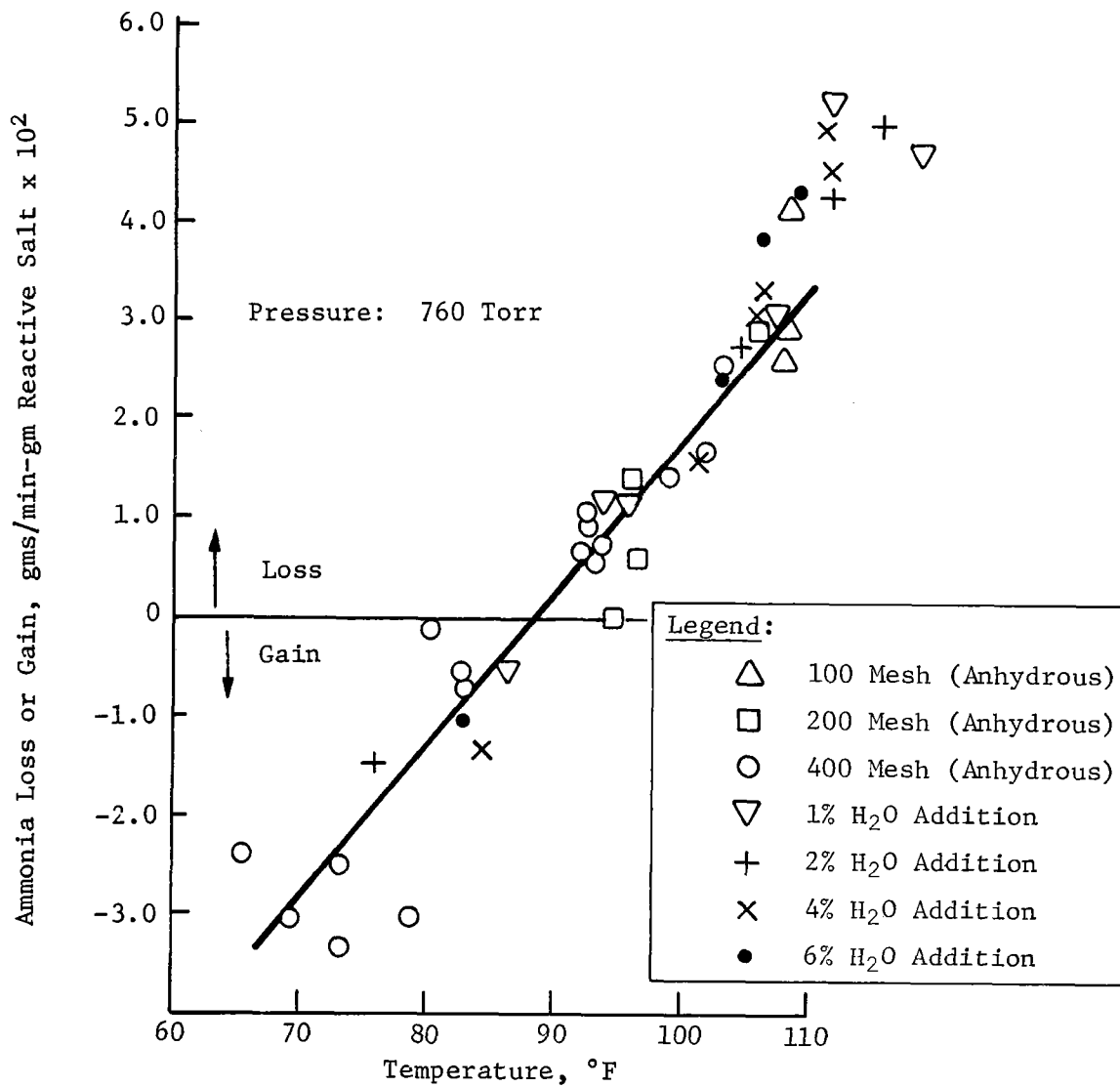


Figure IV-2
 Rate Data, $\text{CaCl}_2 \cdot 8\text{NH}_3 \rightleftharpoons \text{CaCl}_2 \cdot 4\text{NH}_3 + 4\text{NH}_3$ Effects of Moisture

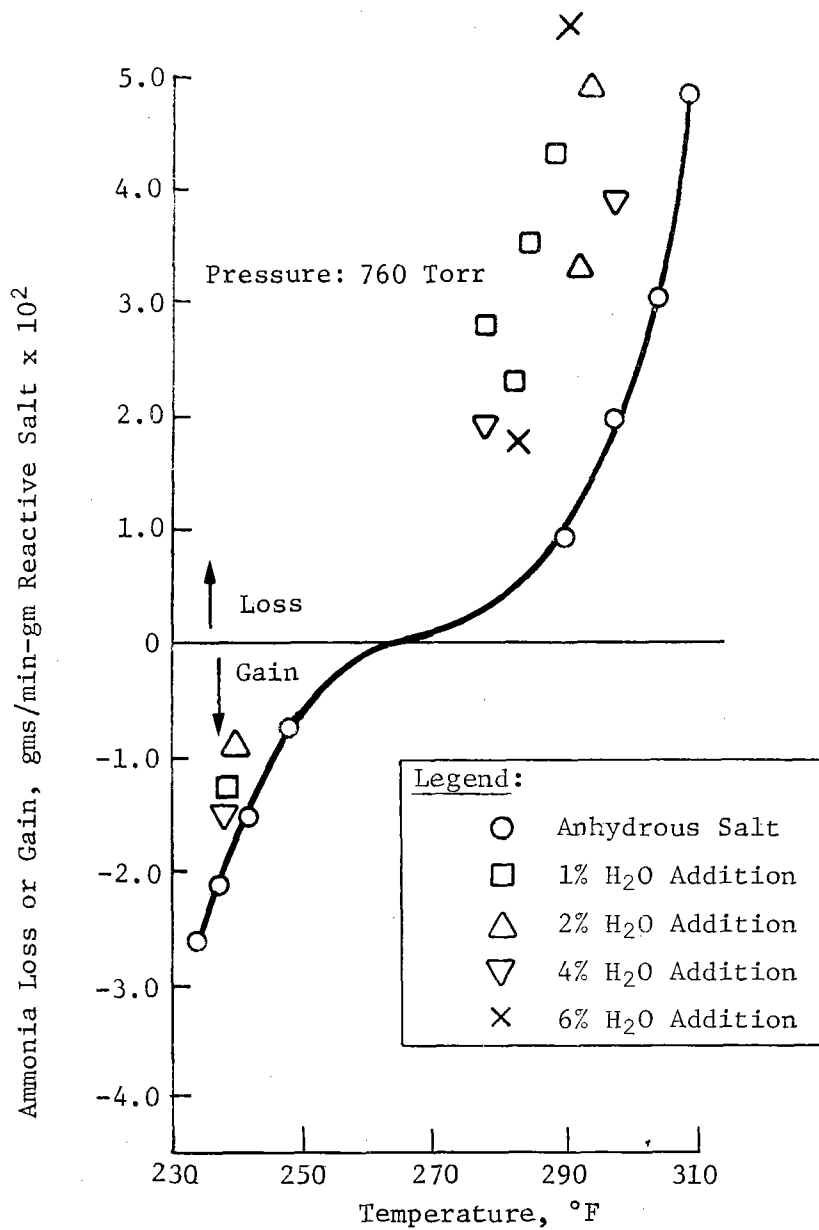


Figure IV-3
 Rate Data, $MgCl_2 \cdot 6 NH_3 \rightleftharpoons MgCl_2 \cdot 2NH_3 + 4NH_3$ Effects of
 Moisture

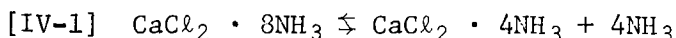
anhydrous salt after the conditioning of the moisture-containing salt. This anomaly is explained by the fact that there was no need for a conditioning period for dissociation/recombination with the anhydrous salt testing reported previously.

- 2) The results obtained in this effort indicate small amounts of moisture (1% to 6%) have no permanent affect on the dissociation/recombination rates of these salts as compared to those obtained for the anhydrous starting material; however, 6% moisture could cause material compatibility problems.

G. NONAQUEOUS IMPURITIES (TASK 10)

The initial objective of this task was to measure the influence of a maximum quantity of natural impurities expected with technical grade CaCl_2 and MgCl_2 on the dissociation/recombination reaction rates of one ammoniate of each salt.

During one of the cyclic tests on calcium chloride (Task 3), it appeared that a small air leak had a measurable effect on the rate of ammonia uptake by the calcium chloride. To determine the influence of air in the ammonia gas, rate data for the reaction

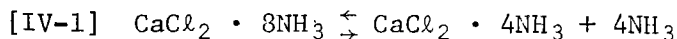


were obtained in the presence of 1% and 2% laboratory air by volume in one atmosphere of ammonia.

1. Method

Contact with Dow Chemical Company, who manufactures both magnesium chloride and calcium chloride, indicated that the principal impurity associated with technical grade magnesium chloride (97%) is calcium chloride. Because the calcium chloride reactions with ammonia have been well characterized, it was believed unnecessary to obtain additional data on the magnesium chloride-calcium chloride mixture.

The principal impurity in technical grade calcium chloride (99%) is calcium sulfate. One percent by weight reagent grade calcium sulfate was thoroughly mixed with reagent grade calcium chloride and dissociation/recombination rate data for the reaction



were determined.

The kinetic data in this task were obtained in the same manner as described in task 4 of the report.

2. Results

Figure IV-4 compares the rate data for dissociation/recombination of the octammoniate of CaCl_2 in the presence and absence of air and Figure IV-5 details the effect of the CaSO_4 impurity on the same reaction.

3. Conclusion

The conclusion from this task is that both types of impurity have an insignificant effect on the dissociation/recombination rates.

H. HEATS OF REACTION VERIFICATION (TASK 9)

During the previous phase of this program the heats of reaction for seven ammoniates of CaCl_2 and MgCl_2 were experimentally determined. There was some discrepancy between some of the values measured and the corresponding values reported in the literature. The objective of this task was to remeasure the heats of reaction determined previously.

1. Method

The heats of reaction were measured using the Differential Thermal Analysis (DTA) operating mode on the Mettler TA-1 Thermoanalyzer. Aluminum oxide was used as the reference material and NBS primary standard KNO_2 was used for calibration of the system. Samples larger by a factor of four than those used in the previous phase were tested to obtain larger recorded DTA peaks for improved precision in determining recorded areas. The estimated accuracy of this method is plus or minus 4%.

2. Results

Table IV-6 cites the heats of reaction measured, the heats of reaction measured previously, and the values obtained from the literature (Ref IV-5). The values under the heading ΔH_{EXPII} are values obtained in the program.

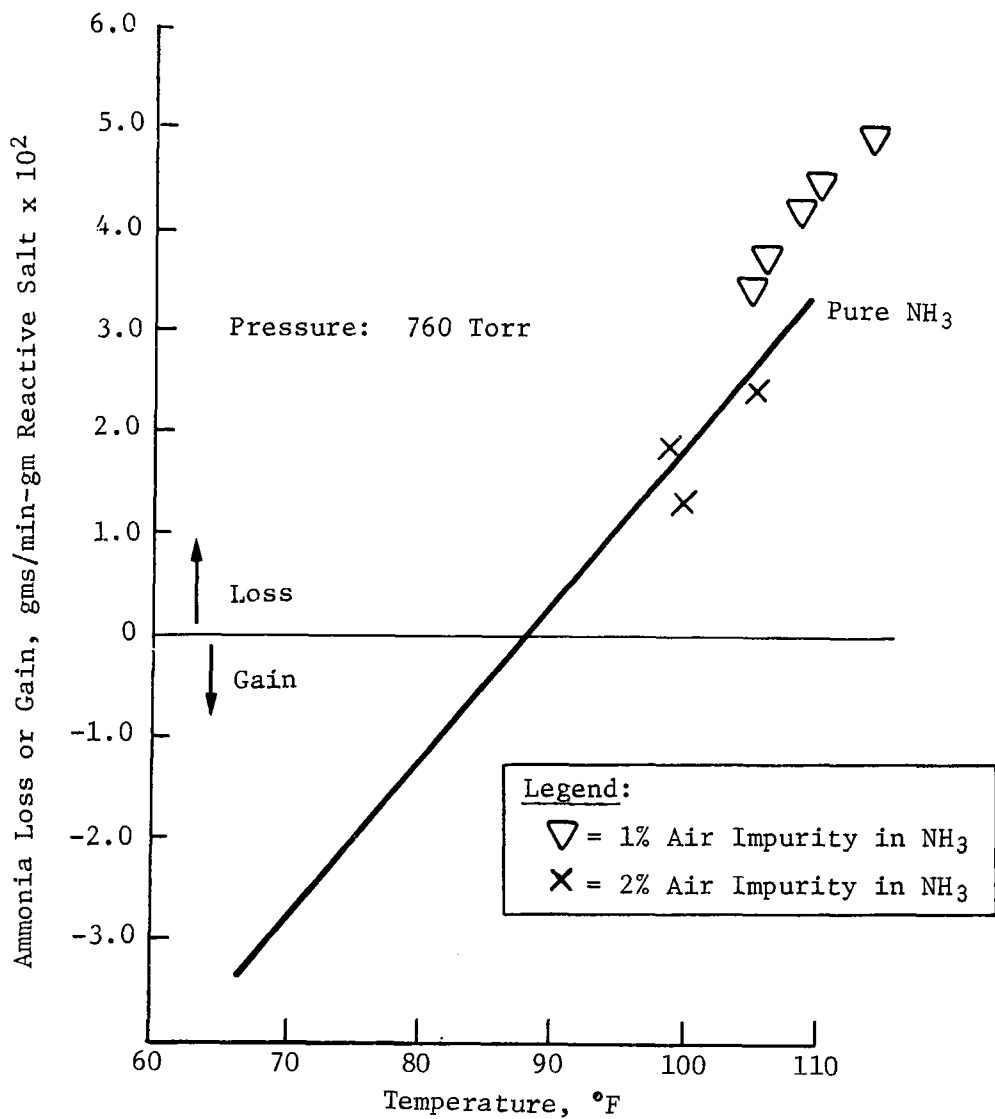


Figure IV-4
 Rate Data, $\text{CaCl}_2 \cdot 8\text{NH}_3 \rightleftharpoons \text{CaCl}_2 \cdot 4\text{NH}_3 + 4\text{NH}_3$, Influence of
 Air Impurity

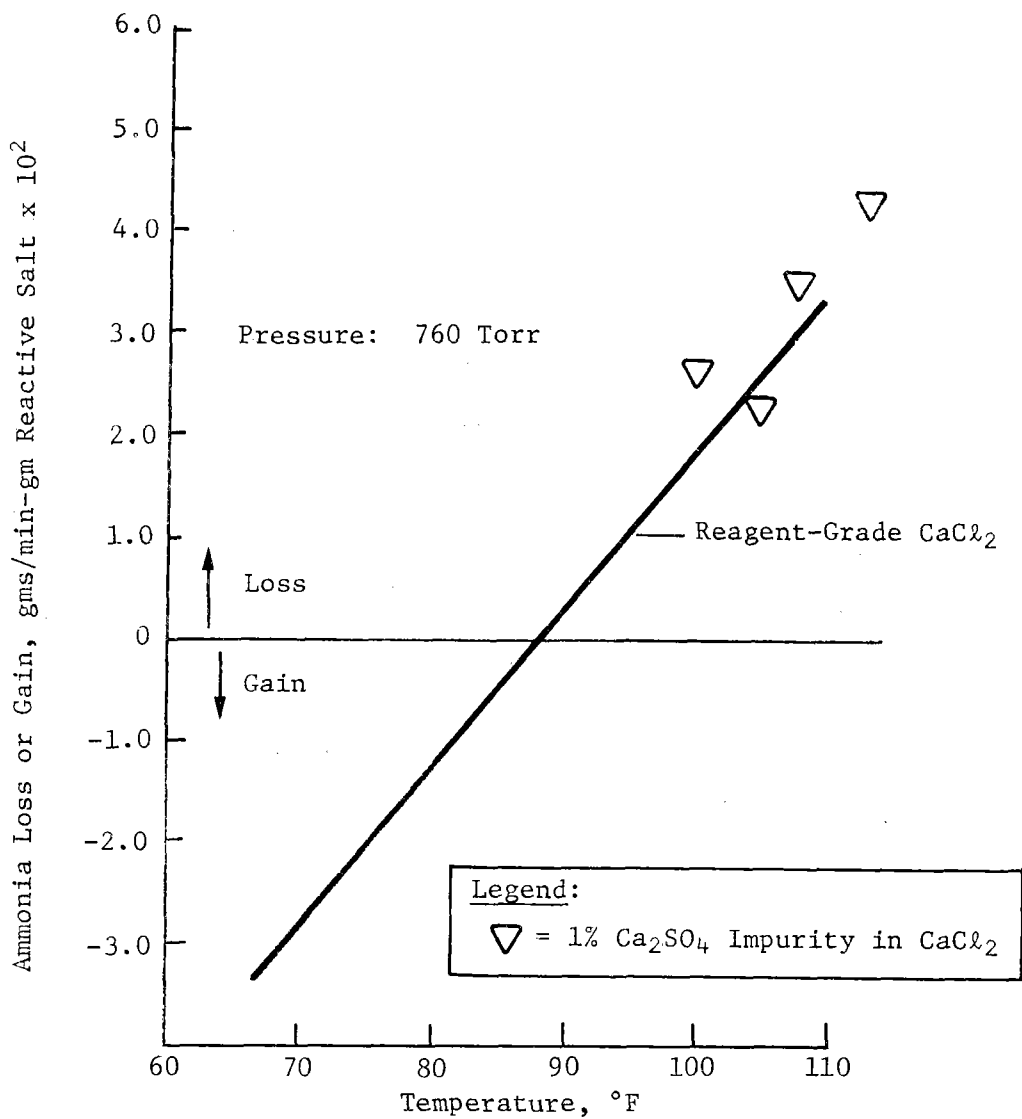


Figure IV-5
 Rate Data, $\text{CaCl}_2 \cdot 8\text{NH}_3 \rightleftharpoons \text{CaCl}_2 \cdot 4\text{NH}_3 + 4\text{NH}_3$ Influence of Calcium Sulfate Impurity

Table IV-6

Heats of Reaction for CaCl_2 and MgCl_2 Ammoniates (Btu/lb of higher ammoniate)

	T, °F	ΔH_{LIT}^*	ΔH_{EXPI}	ΔH_{EXPII}
CaCl₂				
$\text{CaCl}_2 \cdot 8\text{NH}_3 \rightarrow \text{CaCl}_2 \cdot 4\text{NH}_3 + 4\text{NH}_3$	88	71.6	73.8	68.7
$\text{CaCl}_2 \cdot 4\text{NH}_3 \rightarrow \text{CaCl}_2 \cdot 2\text{NH}_3 + 2\text{NH}_3$	108	101.8	111.8	100.8
$\text{CaCl}_2 \cdot 2\text{NH}_3 \rightarrow \text{CaCl}_2 \cdot \text{NH}_3 + \text{NH}_3$	329	180.5	159.4	158.1
$\text{CaCl}_2 \cdot \text{NH}_3 \rightarrow \text{CaCl}_2 + \text{NH}_3$	406	229.8	177.7	200.2
MgCl₂				
$\text{MgCl}_2 \cdot 6\text{NH}_3 \rightarrow \text{MgCl}_2 \cdot 2\text{NH}_3 + 4\text{NH}_3$	266		133.6	97.9
$\text{MgCl}_2 \cdot 2\text{NH}_3 + 4\text{NH}_3 \rightarrow \text{MgCl}_2 \cdot 6\text{NH}_3$	266			106.1
$\text{MgCl}_2 \cdot 2\text{NH}_3 \rightarrow \text{MgCl}_2 \cdot \text{NH}_3 + \text{NH}_3$	522	250.1	220.7	216.5
$\text{MgCl}_2 \cdot \text{NH}_3 + \text{NH}_3 \rightarrow \text{MgCl}_2 \cdot 2\text{NH}_3$	522			173.2
$\text{MgCl}_2 \cdot \text{NH}_3 \rightarrow \text{MgCl}_2 + \text{NH}_3$	702	334.5	270.1	260.5
$\text{MgCl}_2 + \text{NH}_3 \rightarrow \text{MgCl}_2 \cdot \text{NH}_3$	702			205.8
<p>Note: Heats of reaction determined for dissociation and recombination of the hexa-ammoniate of MgCl_2 agree reasonably with each other, but are considerably lower than the value measured previously. No literature value could be found for this reaction.</p>				
*64°F International Critical Tables, Vol V				

3. Conclusions

Conclusions from this task are as follows:

- 1) Heats of reaction determined for dissociation of the octammoniate and quadrammoniate of CaCl_2 generally agree with the literature values.
- 2) The ΔH value measured for dissociation of the diammoniate of CaCl_2 agrees closely with the value measured earlier, both values being 21.4 to 22.4 Btu/lb lower than the literature value.
- 3) The heat of reaction obtained for dissociation of the monoammine of CaCl_2 lies approximately midway between the value measured previously and the literature value.
- 4) Heats of reaction for the MgCl_2 ammoniates were determined for both the dissociation and recombination modes. Close agreement for heat of reaction of a given salt pair dissociating and recombining was not obtained. The principal reason for this apparent discrepancy is attributed to the longer times required for the recombination reaction to go to completion. As a given salt approaches completion of the recombination with NH_3 to the higher ammoniate, the rate of heat given up approaches zero, and the DTA curve indicating this exotherm is highly skewed, with a curve that approaches an indicated zero exotherm baseline over a time period of two or more hours. The ability to measure precisely the area under this type of DTA curve is less than when the DTA approaches a normal bell-shaped curve. For this reason, greater confidence is placed on the heats of reaction obtained for dissociation.

V. SUBSCALE TESTING (TASK 2)

The actual use-configuration of the ammoniated salt energy storage system is directly related to coupled reactions. The effect of various parameters on the coupled reaction system was studied in this phase of the program.

A. OBJECTIVES

The objectives of these studies were as follows:

- 1) Determine the effect of cyclic operation of coupled ammoniated salt systems;
- 2) Demonstrate that the test results are reproducible with time;
- 3) Demonstrate that the ammoniated salt reactions are reversible;
- 4) Demonstrate the operation at six different temperature-pressure conditions with one ammoniated salt reaction.

B. BASIS FOR COUPLED REACTION PROCESS

1. Reaction Equilibrium

The ammoniated salt reactions are assumed to be an equilibrium system. The characteristics of the reactions can be described by a thermodynamic relationship

$$[V-1] \quad \ln K = -\Delta H/RT + C$$

where K is $\frac{\pi_i (a_{pi})^n}{\pi_j (a_{rj})^n}$ the equilibrium constant,

a_{pi} is the activity of i th product,

a_{rj} is the activity of j th reactant,

ΔH is the heat of reaction,

n is the stoichiometric coefficient,

R is the international gas constant,

T is the absolute temperature,

C is a constant depending on an initial condition, and

π_k is the symbol for product of k factors.

Because the activity of all solid products and reactants is one, and the activity of gases at low pressure is equal to this pressure, the equilibrium constant can be written

$$[V-2] \quad K = P_{\text{NH}_3}$$

for the ammonia, salt reactions.

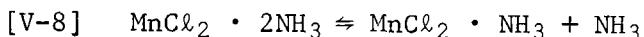
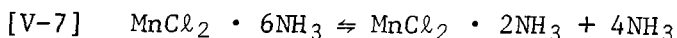
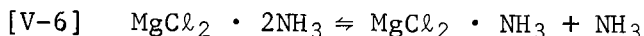
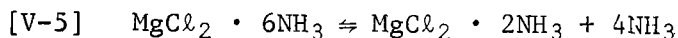
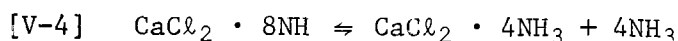
The thermodynamic equilibrium expression gives a function that describes the interaction between the ammonia pressure, the temperature, and the heat of reaction,

$$[V-3] \quad P_{\text{NH}_3} = C' \exp [-\Delta H/RT],$$

for these reaction systems. When all inert gases have been removed from the reactor system, the ammonia pressure is equal to the total pressure on the system. This relationship will be used in later discussions.

2. Chemical Reactions Studied

The following reactions were investigated during this phase of the program in cycling ammoniated salt systems.



The ammonia pressure over the ammoniated salts as a result of the equilibrium reactions given above is illustrated in Figure V-1 for various system temperatures and pressures. For these reactions, the curves are a representation of equation [V-3].

When the temperature and pressure in the reactor describe a point that is below and to the right of the vapor pressure curve that represents the solid in the reactor, NH_3 gas will be released-- a condition similar to the discharge condition in a reactor. When the temperature and pressure conditions in the reactor describe a point that is above and to the left of the representative

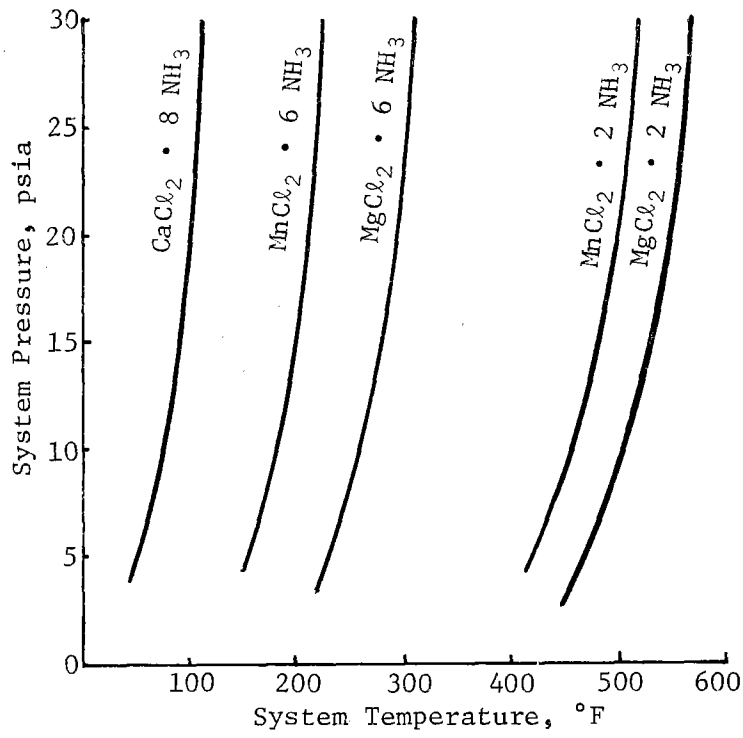


Figure V-1 Vapor Pressure of Ammoniated Salts

equilibrium curve, NH₃ gas will be absorbed by the salt until the reaction goes to completion. This condition is similar to the charge cycle for a reactor.

3. Coupled System

The reversible energy storage system operates by using the heat of reaction of ammoniated salts as a means of converting heat to a form of chemical energy that can be reclaimed. By coupling two reactions that take place at the same pressure but different temperatures, energy can be absorbed by the system at a temperature with one reaction and stored or released at a different temperature with another reaction. Using ammoniated salts, ammonia gas is endothermically released at a temperature from one salt and exothermically absorbed and stored at a different temperature by another salt. The system can be reversed by adding heat to the reactor where the ammonia is stored causing the gas to flow to the other reactor where the energy is again released.

The low temperature reaction, $\text{CaCl}_2 \cdot 8\text{NH}_3 \rightleftharpoons \text{CaCl}_2 \cdot 4\text{NH}_3 + 4\text{NH}_3$, was shown in previous work to operate reversibly at 15 psia and about 90°F. At these conditions, $\Delta H_r = 17,703$ Btu/lb mole of NH₃

absorbed must be removed from the reactor during the charging cycle. By replacing this energy at the same temperature and pressure conditions, one mole of ammonia gas will be released. The reaction was used as the low temperature ammonia sink for all experiments carried out during this program.

The other four reactions presented in Paragraph B, Section V, were individually coupled with the low temperature calcium chloride ammoniate reaction to serve as the high temperature NH₃ source or sink. Table V-1 shows the temperature and heat release that can be expected when these four reactions are operating at 15 psia.

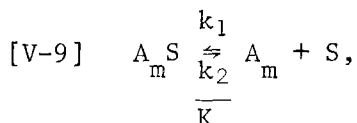
Table V-1

Reaction Temperature and Energies at 15 psia for Ammoniated Salts

Equation	Ammoniated Species	Temperature, °F	ΔH_r Heat of Reaction, Btu/lb mole NH ₃
V-5	MgCl ₂ · 6NH ₃	276	22,230
V-5	MgCl ₂ · 2NH ₃	507	33,048
V-7	MnCl ₂ · 6NH ₃	197	21,492
V-8	MnCl ₂ · 2NH ₃	480	30,006

When the system is operated at 15 psia, one of the reactions represented by equations [V-5] through [V-8] will consume or give up the heat of reaction at the temperature shown in Table V-1. The direction of heat flow is determined by the flow of NH₃ gas. When the coupled low temperature reactor is maintained at a temperature above the equilibrium point of the contained salt, NH₃ gas will be released and flow to the high temperature reactor where it will react and release energy. When the coupled high temperature reactor is in a similar condition due to addition of high temperature energy, NH₃ gas will be released, absorbing heat and causing the NH₃ gas to flow to the low temperature reactor.

The rate of NH₃ flow between reactors is determined by the rate of release and rate of absorption of the NH₃ gas in the reactors under prevailing conditions. The chemical rate of reaction for the equilibrium ammoniated salt systems can be written in general terms for the elementary reaction



where AS is the high ammoniated salt species in the reaction,

S is the low ammoniated salt species in the reaction,

A is ammonia,

k₁ is the decomposition rate constant,

k₂ is the combination rate constant,

K is the equilibrium constant, and

m is the stoichiometric coefficient.

and

$$[V-10] \quad \frac{dn_A}{dt} = V k_1 a_{AS} n_{AS} - V k_2 a_S n_S C_A$$

where $\frac{dn_A}{dt}$ is the rate of decomposition, moles free ammonia/unit time,

V is the void volume of the reactor (assumed constant),

a_S is the activity of low ammoniated salt (assume = 1),

a_{AS} is the activity of high ammoniated salt (assume = 1),

n_S is the moles low ammoniated salt,

n_{AS} is the moles high ammoniated salt, and

C_A is the concentration of ammonia in gas space.

A material balance for the ammonia exchanged during the Task 2 test showed that between 5% and 25% of the available NH_3 in the high ammoniated salt was exchanged during the one-hour run cycle. Because instantaneous data were recorded every 10 minutes, three flowrate values were available to calculate the average NH_3 flow over a 20 minute time span. This average flow represented the ammonia release when the molar amount of the ammoniated salt was changed by 2% to 8%. To simplify the data analysis, n_S and n_{AS} were considered constant and the average data values for the points between 30 and 50 minutes of run time were used to evaluate each charge and discharge cycle.

Using this simplification, the ammonia flow was based on a kinetic analysis of the coupled reaction because

$$[V-11] \quad \frac{dn_A}{dt} = Vk_1 - Vk_2 C_A.$$

This reaction rate was zero at equilibrium and therefore

$$[V-12] \quad k_1/k_2 = C_{Ae},$$

and the rate equation was rewritten as

$$[V-13] \quad \frac{dn_A}{dt} = Vk_1 \left(1 - C_A/C_{Ae}\right).$$

Ammonia was considered an ideal gas under the conditions of this task; therefore, the concentration was written as

$$[V-14] \quad C_A = n_A/V = P/RT$$

and the flowrate between the coupled reactors was

$$[V-15] \quad \frac{dn_A}{dt} = Vk_1 \left[1 - P/P_e\right] = \left[Vk_1/P_e\right] \left[P_e - P\right].$$

The energy available at the absorbing bed was determined by an energy balance on that bed. The sum of the following terms determined the energy released based on a zero (0) reference condition where

$$\frac{dn_A}{dt} = F_{NH_3}.$$

The sensible heat of the NH_3 at the gas inlet was

$$[\text{V-16}] \quad Q_1 = F_{\text{NH}_3} C_p (t_i - t_o).$$

The sensible heat to bring the NH_3 gas to the bed temperature was

$$[\text{V-17}] \quad Q_2 = F_{\text{NH}_3} C_p (t_o - t_B).$$

The heat of reaction in the absorbing bed was

$$[\text{V-18}] \quad Q_3 = F_{\text{NH}_3} (\Delta H).$$

The heat released in the absorbing bed was the sum of the above heats

$$[\text{V-19}] \quad Q_a = Q_3 + Q_2 + Q_1.$$

The energy needed to cause the reaction at the discharging bed was

$$[\text{V-20}] \quad Q_d = F_{\text{NH}_3} \Delta H.$$

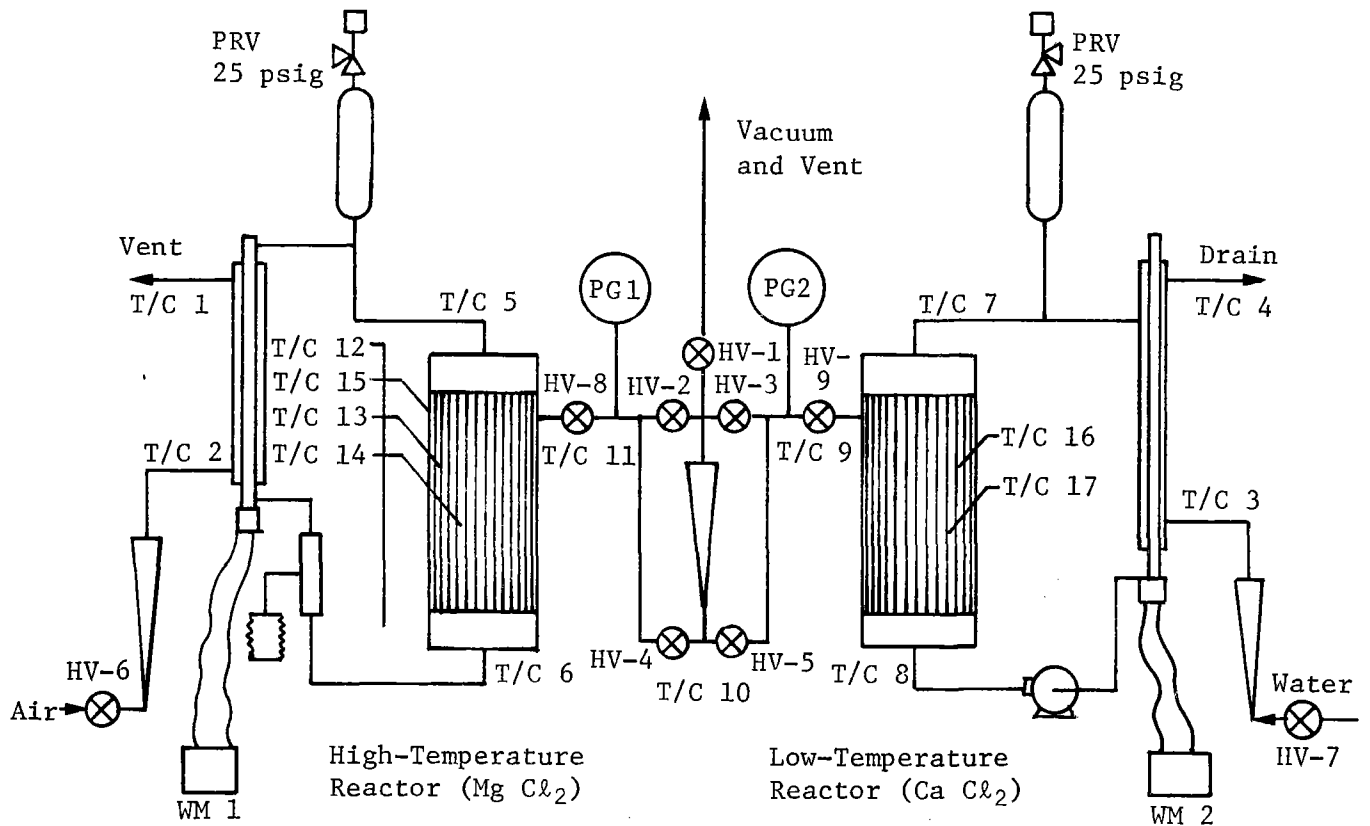
A heat balance on each of the reactors should show that the heat supplied or released in the reactor was equivalent to the above calculated values plus the heat losses to the environment.

C. EXPERIMENTAL TEST EQUIPMENT AND OPERATION

A schematic of the test setup used to obtain data on the coupled ammoniated salt system is shown in Figure V-2. The equipment used and its operation during tests will be discussed in this section of the report.

1. Ammoniated Salt Reactors

Ammoniated salt reactors were constructed as shell and tube heat exchangers with the salt contained on the shell side and the appropriate heat transfer fluid circulated through the tube side. A section view of the reactor is shown in Figure V-3. The shell was six inches in diameter and one foot long. It contained twenty-one $\frac{1}{2}$ -inch tubes on 1-inch triangular centers with a heat transfer area of 4.06 sq ft. The headers were constructed with the entire tube bundle exposed to one pass of the heat transfer fluid. Both the high- and low-temperature reactors were covered with an external layer of Fiberglas insulation to maintain adiabatic conditions.



Notation

PRV - Pressure Relief Valve

HV - Hand Valve

Figure V-2 Schematic of Test Equipment for Ammoniated Salt Systems

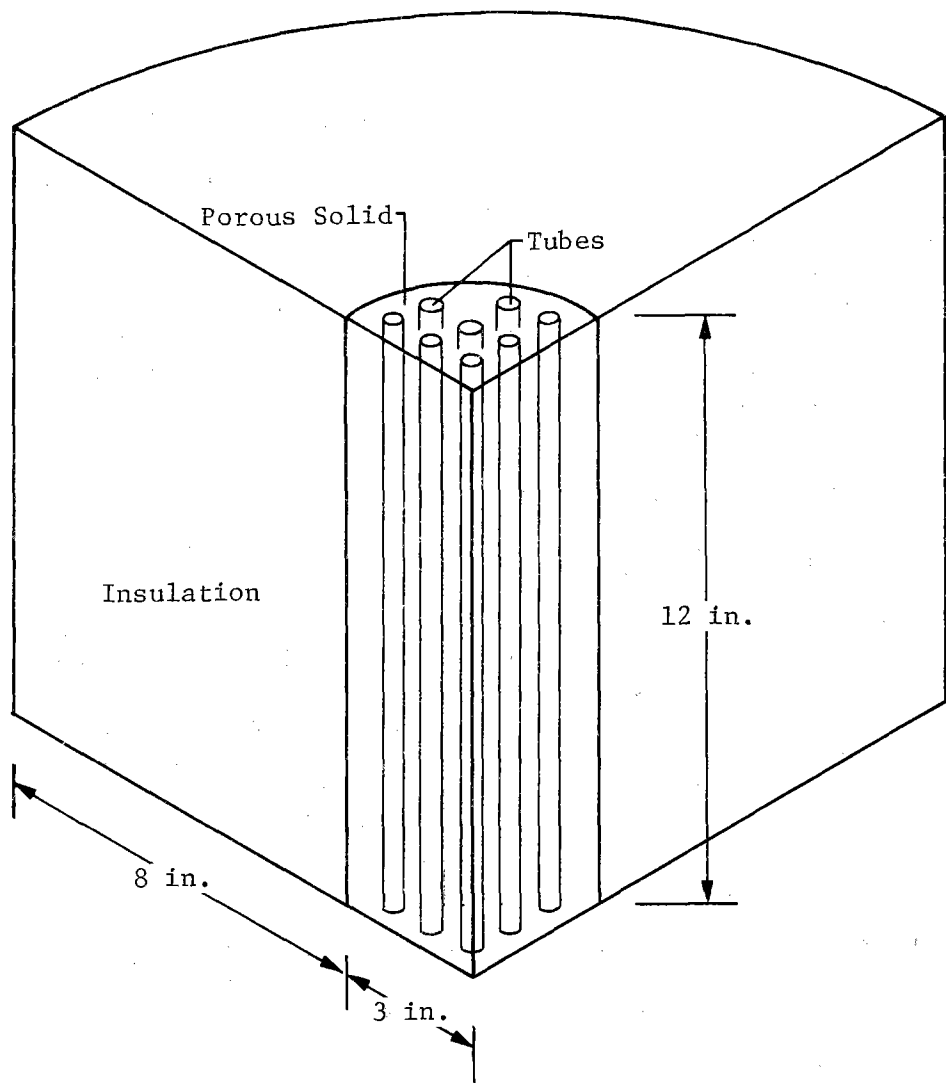


Figure V-3 Ammoniated Salt Reaction

2. Energy Transfer Equipment

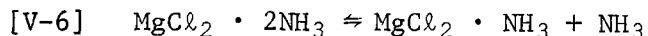
During operation, energy was transferred in the reactor with an external circulating loop that contained heat transfer oil for the high-temperature reactor and water for the low-temperature reactor. The loop connected the tube side of the reactors with an external heat exchanger, which was used to exchange energy with an outside source or sink. The fluid was moved around the loops at a known rate by a positive displacement pump. In both cases, electrical heaters were the source of energy for the external heat exchangers. Tap water was used for the heat sink on the low temperature reactor system and air was used on the high temperature system. Both loops contained thermocouples at the inlet and exit of the reactor to determine the energy transferred to the circulating fluid.

3. Ammonia Transfer System

The shell side of the low- and high-temperature reactors were connected with 3/8-inch stainless steel tubing that channeled the ammonia released in one reactor to the other where it was absorbed. The line contained a valving arrangement that directed the ammonia through a common flowmeter to determine the rate from either reactor. Gauges were connected in the line near each reactor to indicate the pressure at that point.

4. Material of Construction and Compatibility

The test equipment was made of 304 stainless steel. This material did not show corrosion or compatibility problems except in the case of the high temperature ammoniated $MgCl_2$ reactions



where visual evaluation showed surface corrosion. Kevex X-ray analysis of the salts after the tests confirmed that iron, chromium, and phosphorous were present in the salt residue. Material compatibility tests are needed to better understand the problem and to make recommendations for the construction of larger units.

5. Test Procedure

The test procedure discusses the steps that were followed to prepare the high-temperature salt beds for specific reaction conditions and the operation of the cyclic tests for each ammoniated salt. All tests were started with the low-temperature reactor containing $CaCl_2 \cdot 8NH_3$ and the high-temperature reactor containing the specified chloride salt ammoniated to a higher level than required. The test setup shown schematically in Figure V-2 was used in all tests.

a. *High Temperature Reactor Preparation* - The high temperature reactor filled with the appropriate ammoniated chloride salt and free of residual air was installed in the system with the hand valve (HV-8) closed. The low temperature reactor that contained fully ammoniated $\text{CaCl}_2 \cdot 8\text{NH}_3$ was isolated by HV-9. Valves HV-10, HV-1, HV-2, and HV-3 were opened and the vacuum pump was operated to remove the air from the connecting piping. Then HV-1, HV-2, HV-3, and HV-10 were closed and energy was added to the high-temperature reactor using the circulating oil loop and the guard heater until the temperature of the salt bed was at the level where the equilibrium pressure of the desired low ammoniated operating salt was approximately 25 psia. Ammonia gas was then released through the flowmeter by opening HV-8, HV-4, HV-1, and HV-11. The pressure in the reactor was maintained above 15 psia by throttling HV-1. Energy was continually added to the reactor with the circulating oil loop to maintain the reactor temperature and the NH_3 evolution rate between 1.5 and 2 standard liters/Min. The operation was continued until the ammonia evolution rate approached zero. The salt composition approached the desired low-ammoniated compound at that condition and was ready to receive NH_3 from the low-temperature reactor. Valves HV-1 and HV-4 were closed to maintain the equilibrium NH_3 condition and the low-temperature reactor was prepared to discharge NH_3 .

b. *Low Temperature Reactor Discharge Cycle* - The high-temperature reactor conditions remained as shown in Section V, paragraph C5a., except the temperature was brought to the equilibrium values for NH_3 gas at 15 psia. Heated water was circulated through the low temperature reactor to raise the contained $\text{CaCl}_2 \cdot 8\text{NH}_3$ salt to 97°F . When the pressure of the low temperature reactor exceeded that in the high temperature reactor by 5 psi, HV-5 and HV-2 (Fig. V-2) were opened to allow the NH_3 gas generated in the $\text{CaCl}_2 \cdot 8\text{NH}_3$ reactor to flow to the high-temperature reactor through the flowmeter. Cooling air was simultaneously allowed to flow through the external exchanger on the high-temperature reactor to serve as a sink for the energy released by the high-temperature NH_3 reaction. The temperature of the circulating heat transfer fluids was continually adjusted to maintain the NH_3 flowrate constant and at a constant pressure.

The low-temperature discharge cycle was run for 60 minutes. The system was then stopped by closing HV-2 and HV-5 to isolate the reactors and was prepared to run a 60-minute low-temperature reactor charge cycle.

c. *Low Temperature Reactor Charge Cycle* - The isolated low-temperature reactor was cooled by deenergizing the electrical heat source in the circulating heat transfer loop and starting cooling water through the external heat exchanger to serve as

a sink for energy released in the reactor. Simultaneously, the coolant air to the exchanger in the high-temperature circulating loop was turned off and the electrical heat source was started. When the pressure of the NH_3 gas from the high-temperature reactor exceeded that of the low-temperature reactor by 5 psi, HV-4 and HV-3 were opened to allow gas to flow from the high-temperature reactor to the low-temperature reactor. The rate of heat added to the high-temperature circulating loop and removed from the low-temperature loop was adjusted to maintain constant flow at approximately the same rate as in the charge cycle. The charge cycle was continued for 60 minutes and then HV-4 and HV-3 were closed again and the apparatus was prepared for the next discharge cycle.

d. Data - Temperature, pressure, power, and flow data were recorded at 10-minute intervals during the 60-minute low-temperature discharge and charge cycles. The following data points were recorded.

Flows:

- NH_3 rate
- High-temperature heat transfer fluid
- Low-temperature heat transfer fluid

Temperatures:

- Heat transfer fluid to high-temperature reactor
- Heat transfer fluid from high-temperature reactor
- Heat transfer fluid to low-temperature reactor
- Heat transfer fluid from low-temperature reactor
- NH_3 at flowmeter
- Hot reactor wall
- Hot reactor salt
- Cold reactor wall
- Cold reactor salt
- Guard heater on high-temperature reactor, sides
- Guard heater on high-temperature reactor, top

- Air to high-temperature loop heat exchanger
- Air from high-temperature loop heat exchanger
- Water to low-temperature loop heat exchanger
- Water from low-temperature loop heat exchanger

Pressure:

- High-temperature reactor
- Low-temperature reactor

Power:

- High-temperature loop heat exchanger
- Low-temperature loop heat exchanger
- Guard heater, side
- Guard heater, top

The preceding data were used to determine heat balances and reaction rates for the experimental test run during the program.

D. RESULTS

The experimental results obtained with the coupled reaction systems during this phase of the project were evaluated to show the effect of the cyclic operation on the reversibility of the chemical reactions and the reproducibility of the system at different operating conditions. The reactor energy balance described in Section V, paragraph B was investigated and the conclusions are presented here. The rate equation developed in Section V, paragraph B was also used to examine the data and the results are presented.

1. Reactor Heat Balance

A heat balance was carried out using the experimental data from the low- and high-temperature reactors for both the charge and discharge segment of the cycles. Each condition will be discussed here.

The analysis was done for thirteen cycles using the energy data developed from a single point after 50 minutes of operation for each cycle.

During the discharge cycle for the low-temperature reactor, the absolute value of the difference between the heat of reaction (determined as the product of the measured ammonia flowrate and the molar heat of reaction in that reactor) and the rate of energy loss of the water cycling through that reactor was calculated to be an average of 14% of the heat of reaction. This difference can be attributed to unknown variation of results for the ammonia flow, water flow, sensible heat change of the salt, measurement of circulating water temperature differential, and heat exchange between the reactor and the environment. A similar analysis was conducted for the high-temperature reactor during the same segment of the cycles. The absolute value of the difference between the expected heat of reaction and the sum of the energy picked up by the circulating fluid plus that needed to bring the temperature of the ammonia gas up to reaction temperature was 30% of the heat of reaction. The difference could be caused by the same reasons as enumerated for the low-temperature reactor plus the heat exchanged between the reactor and a guard heater placed in the reactor insulation.

The analysis was conducted for the low-temperature reactor charge cycle. The analysis showed that the ratio of the absolute value of the differences between the expected heat of reaction and the heat transferred to the exchanger fluid in the circulating loops for the same thirteen cycles was 28% for the high-temperature reactor and 16% for the low-temperature reactor. All of the uncertainties listed for the low-temperature reactor discharge part of the cycles are applicable to describe these differences.

The magnitude of these average differences is due to the impact of the sensitivity of the small scale experimental setup and the inherent inaccuracies in instrumentation and control.

The NH_3 gas flowrate and thus, the rate at which heat is stored in this system was shown in Section V, paragraph B to be linearly proportional to the difference between the equilibrium vapor pressure of the ammoniated salts in the system and the system pressure. Because this equilibrium pressure is an exponential function of temperature, the bed temperature is important in the reproducibility analysis for these experiments.

2. Process Reproducibility and Reaction Reversibility

This section discusses the use of the reaction analysis shown in Section V, paragraph B and its application to show the process reproducibility and reaction reversibility. The analysis scheme is based on reversible equilibrium kinetics, which shows that the reaction rate for combination or decomposition of the ammoniated salts used in these tests is

$$[V-15] \quad dn_A/dt = V(k/K)(P_e - P) = V(k/K)\Delta P$$

The rate constant, k , and the equilibrium constant, K , are both exponential functions of $1/T$ and can be written in the form

$$a \exp [A/RT].$$

Their quotient, k/K_e , is much less sensitive to temperature than is either of the individual parameters. The rate of NH_3 evolution will be nearly linearly proportional to the difference between the ammonia equilibrium pressure over the salt at its temperature and the system pressure. This is also dependent on the fact that the amount of ammoniated salt that is decomposing or combining with NH_3 remains constant because the rate constant is specified per unit of salt.

The equilibrium pressure of NH_3 over the salt was calculated with the thermodynamic relationship given in Section V, paragraph B using the temperature indicated by a thermocouple in the salt bed,

$$[V-3] \quad \ln P_v = -\Delta H/RT + C$$

A linear relationship between the pressure-driving force and the ammonia flow rate for a series of cycles is a necessary condition for reaction reversibility and proven reproducibility.

The data gathered during the experimental portion of the program was used with a linear curve fitting program for each set of conditions evaluated in the reactor. Table V-2, Data Analysis Results, follows and gives the best fit equations and their statistical significant for each set of run conditions. The curves and data points are shown for cycle 13 through 18 and a discussion of the curve-fit results is presented for all sets of conditions.

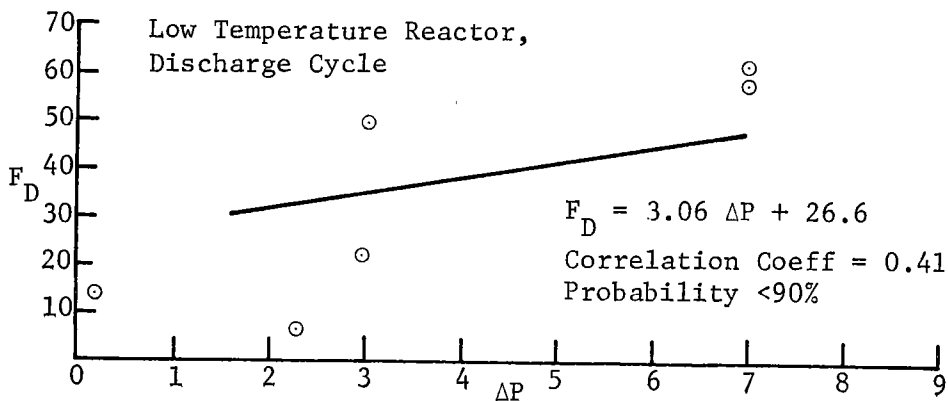
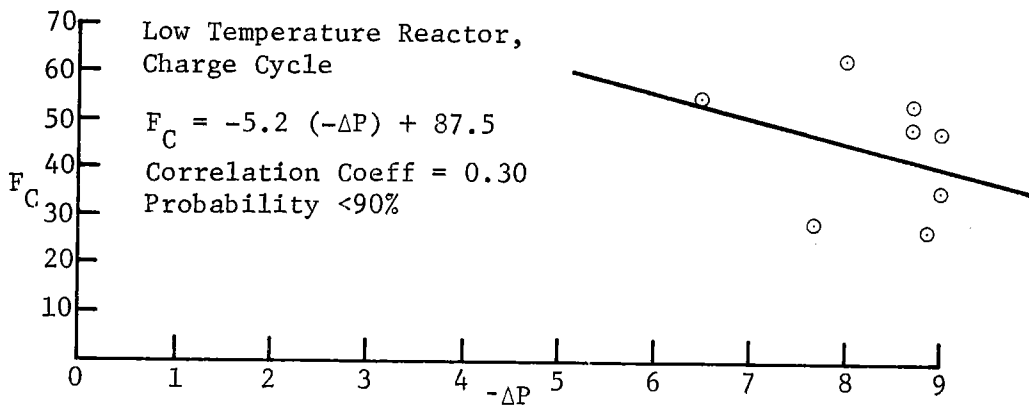
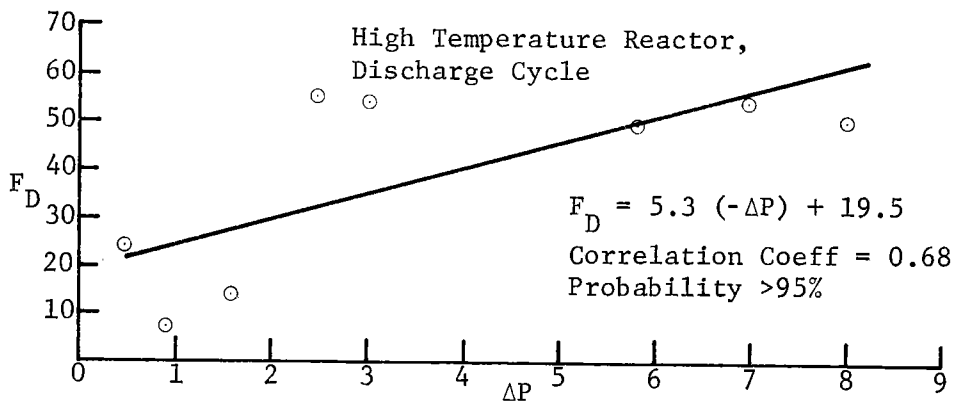
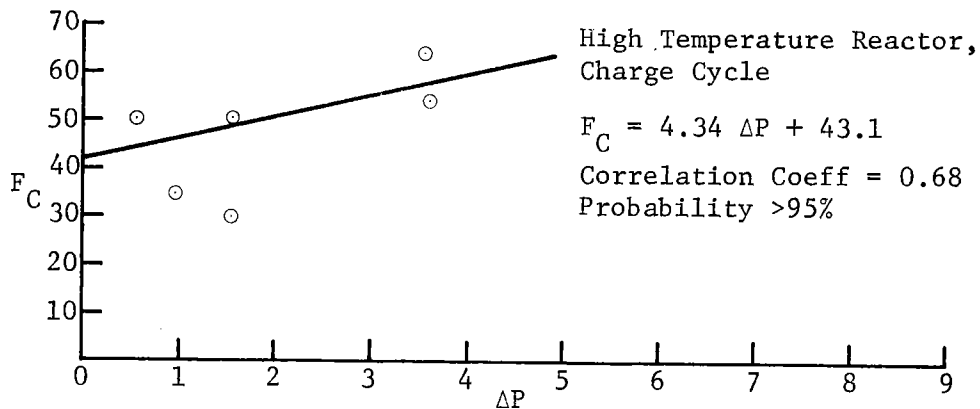


Figure V-4 Reactor Performance Cycles 11 through 18, $Mg Cl_2 \cdot 6 NH_3$

Table V-2
Data Analysis Results

Operating Cycle Numbers	Condition of Low Temperature Reactor	NH ₃ Flow vs Driving Force Function and Statistical Parameters					
		High Temperature Reactor	Correlation	Probability	Low Temperature Reactors	Correlation	Probability
11-18	Charge	$F_c=4.34(\Delta P)+43.1$	0.68	>95%	$F_c=5.2(-\Delta P)+87.5$	0.3	<90%
	Discharge	$F_D=5.3(-\Delta P)+19.5$	0.68	>95%	$F_D=3.06(\Delta P)+26.6$	0.41	<90%
21-39	Charge	$F_c=-2.5(\Delta P)+47.9$	0.0314	<90%	$F_c=0.581(-\Delta P)+31.87$	0.116	<90%
	Discharge	$F_D=2.59(-\Delta P)+18.26$	0.48	>95%	$F_D=3.5(\Delta P)+5.8$	0.686	>99%
64-72&78	Charge	$F_c=0.56(\Delta P)+53.4$	0.255	<90%	$F_c=-0.21(-\Delta P)+53.98$	0.26	<90%
	Discharge	$F_D=0.379(-\Delta P)+55.26$	0.18	<90%	$F_D=0.309(\Delta P)+57.18$	0.15	>90%
79-85*	Charge	$F_c=2.8(\Delta P)+0.54$	0.853	>99%	$F_c=7.48(-\Delta P)+8.5$	0.75	>90%
	Discharge	$F_D=-0.5(-\Delta P)+23.98$	-0.316	<90%	$F_D=-1.16(\Delta P)+19.8$	0.59	<90%
89-98	Charge	$F_c=0.569(\Delta P)+52.26$	0.331	<90%	$F_c=0.42(-\Delta P)+56.87$	0.063	<90%
	Discharge	$F_D=0.866(-\Delta P)+24.8$	0.114	<90%	$F_D=5.537(\Delta P)-30.64$	0.888	>90%
	Charge	$F_c=0.71(\Delta P)+15.6$	0.47	>99%	$F_c=-1.5(-\Delta P)+32.6$	0.383	96%
	Discharge	$F_D=0.0084(-\Delta P)+14.4$	0.00019	0	$F_D=0.0042(\Delta P)+14.92$	0.0046	<90%

*System apparently contained too much NH₃

The first 20 cycles were run with $\text{MgCl}_2 \cdot 6\text{NH}_3$ in the high-temperature reactor and $\text{CaCl}_2 \cdot 8\text{NH}_3$ in the low-temperature reactor. Cycles nine through 18 were arbitrarily selected for use in this analysis. The series includes two low-temperature reactor discharge cycles at reduced temperature to simulate an air conditioning mode, cycles 13 and 18. The conditions were controlled so the pressure differential was low in both reactors during these cycles, and therefore the reaction rates were slow and the heat loads were small. Different operating conditions should produce different heat transfer rates.

The results of the high- and low-temperature reactors during the charge and discharge portion of operating cycles 11 through 18 are also shown in Figure V-4. The plots show the ammonia evolution rate versus the pressure difference between the equilibrium pressure and the system pressure. The equation and the plot of the best fit linear function, the correlation coefficient, and the results of a probability analysis are also shown and are based on Reference V-1. The linear plot fits the high temperature reactor output in the 95% level of significance for the eight points analyzed. The reactor contained $\text{MgCl}_2 \cdot 6\text{NH}_3$ during the cycles. The results show that the mechanism chosen, a reversible equilibrium reaction, results in a rate function that describes the data. The curve fit over eight cycles also shows that the results are reproducible. This is significant because the operation was changed to a cooling cycle twice and then back to the normal operation during the series of data points examined.

The data points for the low temperature reactor were analyzed using the same technique because the $\text{CaCl}_2 \cdot 8\text{NH}_3$ reaction should follow the same mechanism with only a change in the magnitude of the generated constants. The test data obtained during the low-temperature reactor charge cycle were grouped so closely that the apparent NH_3 flow to pressure differential function showed only random variation. This explains the low correlation coefficient and the resulting low probability of significance.

The discharge cycles for the low-temperature reactor gave similar low probability of significance. The data recorded for two cycles show a net mass movement against the pressure gradient. This tends to show that the experimental data have a built-in bias. The discrepancy, which is tentatively suggested to be caused by poor contact between the temperature indicating

thermocouple and the salt bed, disappeared during the first low temperature cycle. The results for the last six cycles of this set (cycles 13 through 18) show a linear relationship between the NH_3 flow and the pressure differential with a level of significance of greater than 95%. This again shows the reversability of the reaction and process reproducibility when the monitoring equipment is performing properly.

Cycles 21 through 58 were operated with the lower ammoniate, $\text{MgCl}_2 \cdot 2\text{NH}_3$, in the high-temperature reactor. The analysis was carried out on cycles 21 through 39 because the remainder of the cycles was impaired by a plug of salt particles forming in a filter at the outlet of the high-temperature reactor, which reduced flow between the reactors.

The results of the analysis of the first 19 cycles is shown in Table V-2. The linear regression and the statistical analysis of both the low-and high-temperature reactors during the discharge cycle show that the reversible chemical model fits the data and the process is reproducible. The level of significance of the linear curve fit is greater than 95% in both reactors during discharge. The data obtained during the low-temperature reactor charge portion of the cycles were grouped closely, and a curve fit was not possible.

Cycle 59 through 99 were operated with ammoniated MnCl_2 in the high-temperature reactor. This series of cycles was separated in three discrete segments. The first series, cycles 59 through 78, was operated with $\text{MnCl}_2 \cdot 6\text{NH}_3$ as the high-temperature reactor salt. During the next series of cycles, cycles 79 through 85, the ammonia flow was reduced and the high-temperature reactor salt was $\text{MnCl}_2 \cdot 2\text{NH}_3$. During the remainder of the MnCl_2 runs, cycles 86 through 98, the NH_3 was reduced further but the $\text{MnCl}_2 \cdot 2\text{NH}_3$ reaction continued in the High-temperature reactor.

During cycles 59 through 78, the analysis of NH_3 flowrate versus delta P did not show a significant relationship in either reactor. The flowrate was nearly independent of the proposed pressure driving force. The overall pressure in the reactor had to be raised and the delta P in the MnC system was about twice that of the MnCl_2 system when 50 gph of NH_3 gas was being transferred. This indicates that the absorption reaction rate constant is lower for the $\text{MnCl}_2 \cdot 2\text{NH}_3 + 4 \text{NH}_3 \rightleftharpoons \text{MnCl}_2 \cdot 6\text{NH}_3$ than the similar MgCl_2 reaction.

The low-temperature reactor charge reaction appeared to proceed under conditions similar to the $MgCl_2$ system, which indicates that the preceding reverse reaction is similar to the $MgCl_2$ reaction.

After cycle 78, NH_3 gas was released from the system. The next set of runs, cycles 79 through 85, was operated with $MnCl_2 \cdot 2NH_3$ as the reacting salt in the high temperature reactor. When NH_3 gas was flowing from the ammoniated $MnCl_2$ -filled reactor the low-temperature reactor charge cycle showed a greater than 95% level of significance that the reaction was following the reversible kinetics posed for the model and that the process was reproducible.

The opposite reaction again was not significantly affected by the range of pressure differentials that were determined from the experimental data at reactor pressures up to three times those used with $MgCl_2$ reactions. Following cycle 85, more NH_3 was vented from the system, the flow was about one-half that found with the $MgCl_2$ reactions. This increased the reactivity of the coupled salt system and allowed the reactions to proceed at a lower pressure. This suggests that both salt beds were near saturation during the previous set of runs and that the data obtained are not a true representation of the $MnCl_2 \cdot 2NH_3$ reaction system.

The reaction pressure necessary to produce a delta P that would cause the $MnCl_2 \cdot NH_3$ to absorb NH_3 gas at an equal rate to that of $MgCl_2$ are significantly higher and little significance can be drawn from this high-temperature data because of the small range in which the important variables were investigated for the $MnCl_2 \cdot 2NH_3$ reaction. The reaction rate appears to be constant over the operating range that has been tested but the mode suggested will necessarily need longer test runs before a true understanding of the system is available.

The final 29 test cycles were run with $MgCl_2 \cdot 2NH_3$ as the main reacting salt. The data analysis showed that the test did not cover a large enough range of operating conditions to draw any conclusions from this information on whether the rate is controlled by the defined pressure differential. The flow-rates were nearly constant over the pressure-driving force calculated from the available test data.

The empirical constant generated for the slope of the flow versus driving force delta P in the high-temperature reaction during the charge cycle is different for this series of runs than it was

for cycles 11 through 18. This can be accounted for by the fact that the constant is a function of the rate constant and therefore the amount of available $\text{MgCl}_2 \cdot 2\text{NH}_3$ in the high-temperature reactor. The $\text{MgCl}_2 \cdot 2\text{NH}_3$ fraction was not determined during either set of test cycles; therefore, it is not possible to compare one series of test data to another.

E. CONCLUSIONS

The conclusions arrived at from this task are as follows:

- 1) The experimental work showed that a coupled, ammoniated salt system is technically feasible and can be used as an energy storage system.
- 2) The reaction analysis evaluation showed that the systems tested met the necessary condition for reaction reversibility and process reproducibility when the experimental conditions covered an adequate range of pressure and temperature.
- 3) The data obtained showed that the effects of system temperature and pressure variations were consistent with results of a reversible chemistry-based mathematical model.
- 4) The experimental data indicate that the operation of the ammoniated salt systems remains unaffected by cyclic operation within the experimental conditions examined.

VI. SYSTEM DESIGN AND ECONOMIC ANALYSIS

This section presents an economic analysis that compares a chemical heat storage system using ammoniated salts with a state of the art oil storage system. Also, fluidized bed reactors and alternative reactor designs are evaluated.

A. ECONOMIC ANALYSIS OF POWER PLANT STORAGE

The objective of this task was to generate a conceptual design of a chemical storage system and an oil storage system that supply the same bus bar energy. The two systems were to be compared by evaluating the storage-related cost and the power-related cost for each system.

The oil storage system was selected as the basis of comparison because preliminary studies (Ref VI-1) have indicated that oil storage systems are one of today's most economical types of storage systems. Therefore, if the chemical storage system can be shown to be economically more attractive than an equivalent oil system, there is justification for further development of the chemical storage system, at least for the applications considered.

1. Discussion

The study was limited to the following types and sizes of power plants:

- 1) Solar power plant, 50 MWe, 10-hour storage;
- 2) Conventional power plant, 100 MWe, 24-hour storage.

The storage systems considered:

- 1) Chemical storage, fluidized bed and flow-through bed;
- 2) Sensible heat storage, oil.

The following factors were considered in the economic analysis of the power plant storage:

- 1) Addition of the storage capability permits a power plant to be flexible in meeting varying demands of the customer. This flexibility in terms of storage capability can result in a lower power cost for a network of plants with a given power load profile.
- 2) The net value of storage can only be determined for a given utility network with its load profile. Thus, the value of stored energy is not within our ability to evaluate in general terms. However, there are some utilities using water pumping storage systems to store energy.

If a chemical storage system can be shown to be economically more attractive than an equivalent oil system the preceding considerations imply that there is justification for further development of the chemical storage systems. It must be recognized that the results of the economic analysis presented herein are limited because each utility network has its own unique requirements.

The approach that has been employed in this analysis is as follows:

- 1) The requirements have been defined;
- 2) A storage system is defined for a given power plant, the system is sized, and the power-related and storage-related costs determined;
- 3) The definition, sizing and costing process is repeated for each storage system of interest;
- 4) The costs are compared to determine what factors influence the economic benefits of the various forms of energy storage considered.

Details of the analysis are presented in Appendix A.

The approach followed has certain drawbacks. The cost numbers obtained are not absolute numbers; therefore, only relative numbers are obtained that permit ranking of one storage system against another. Although extremely important, operating and maintenance costs are difficult or impossible to obtain at this time because of the conceptual nature of the designs considered. However, it is reasonable to assume that these costs are about the same regardless of the system. Therefore, the results of the analysis are valid for indicating whether one storage system is more attractive economically than another based on equipment costs.

a. *Requirements* - Two types of systems were considered, a solar power plant and a conventional power plant. Their requirements are presented, in Tables VI-1 and VI-2.

Solar Power Plant - The energy system considered is a steam generator, solar power plant providing electrical power in a manner similar to the Barstow central receiver plant. The requirements for this system are presented in Table VI-1.

Table IV-1. *Solar Power Plant Requirements*

Power:	50 MWe
Duration:	10 hr
Storage Capacity:	5.3×10^9 Btu

Conventional Power Plant - The charge and discharge conditions for the steam plant are the same as those proposed for the Barstow central receiver pilot plant and are presented in Table VI-2.

Table VI-2. *Charge and Discharge Steam Conditions*

	Pressure, psi	Temperature, °F	Saturation Temperature, °F
Charging Steam	1465	950	593
Discharging Steam	400	530	445

The requirements for the commercial power plant are presented in Table VI-3.

Table VI-3. *Conventional Power Plant Requirements*

Power:	100 MWe
Duration:	24 hr
Storage Capacity:	21.9×10^9 Btu

The charge and discharge states for the steam are similar to those used in modern steam plants and are presented in Table VI-4.

Table VI-4. *Charge and Discharge Steam States*

	Pressure, psi	Temperature, °F	Saturation Temperature, °F
Charging Steam	2200	1000	650
Discharging Steam	423	560	450

b. *Chemical Storage System* - The following description is for the chemical storage system used in the solar power plant. A similar description of the system for the conventional power plant is presented in Appendix A.

The pair of chemical reactions chosen for the chemical storage power application is as follows:

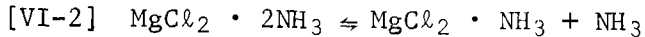
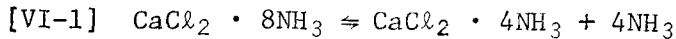


Figure VI-1 presents a schematic representation of a chemical storage module in the heat storage mode (charge mode). Heat is extracted from the power plant boiler during the charge mode in the form of superheated steam (1465 psi, 950°F). The steam is condensed in a heat exchanger that is submerged in a 519°F fluidized bed of ammoniated MgCl_2 . Each module has four beds of ammoniated MgCl_2 . The number of modules is dictated by the molar balance shown in equations [VI-1] and [VI-2]. The heat from the condensing steam drives the ammonia off the ammoniated MgCl_2 . The ammonia flows to a CaCl_2 fluidized reactor at 100°F where it is absorbed to make ammoniated CaCl_2 . This absorption releases energy that is removed by ambient temperature cooling water.

Figure VI-2 presents a schematic representation of a chemical storage module in the discharge mode. The storage system during this mode is supplying heat to the power plant. The heat is supplied to the plant in the form of saturated steam at 445°F, 400 psi. Low-temperature energy from the power plant's heat rejection system is used to raise the ammoniated CaCl_2 bed temperature energy added to the ammoniated CaCl_2 bed drives ammonia off this bed. This ammonia is transferred to the 519°F MgCl_2 bed where it combines with MgCl_2 and releases energy. The energy is removed from the bed by a water loop that brings in 160°F water and expels 445°F saturated steam that can be used for feed-water heating.

The process just described is shown on a pressure-temperature diagram for the ammoniated MgCl_2 and ammoniated CaCl_2 in Figure VI-3. Figure VI-3 shows the charge and discharge status of each reactor and the direction of ammonia flow. The process is also shown for the conventional plant in this figure.

Figure VI-4 illustrates a fixed-bed concept for using the chemical energy in the ammoniated salt thermal storage system. Ammonia is pumped through the fixed bed in this system, but at velocities low enough that the bed is not fluidized.

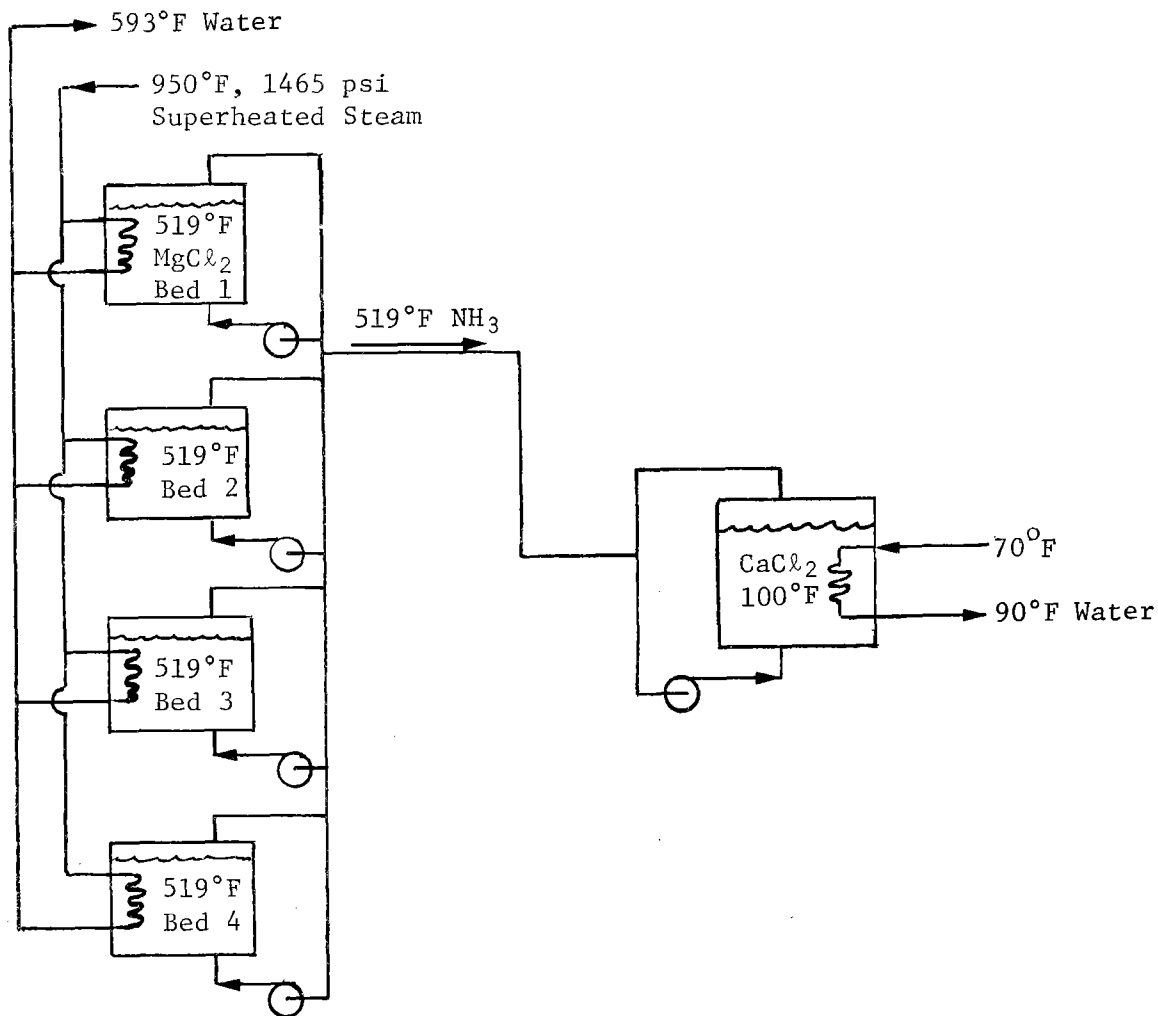


Figure VI-1 Schematic - Chemical Storage, Fluidized Bed Concept (Charging)

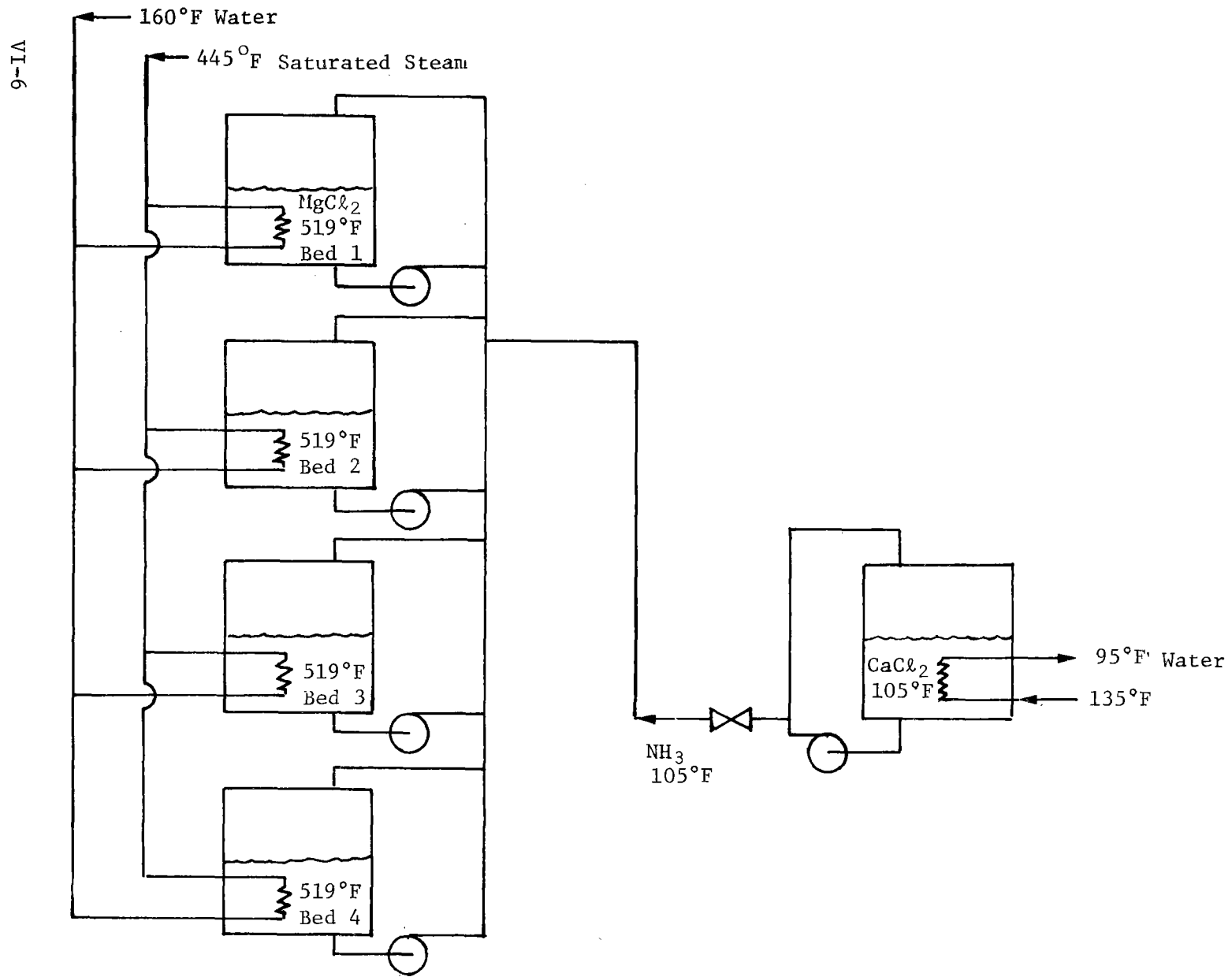


Figure VI-2 Schematic - Chemical Storage, Fluidized Bed Concept (Discharging)

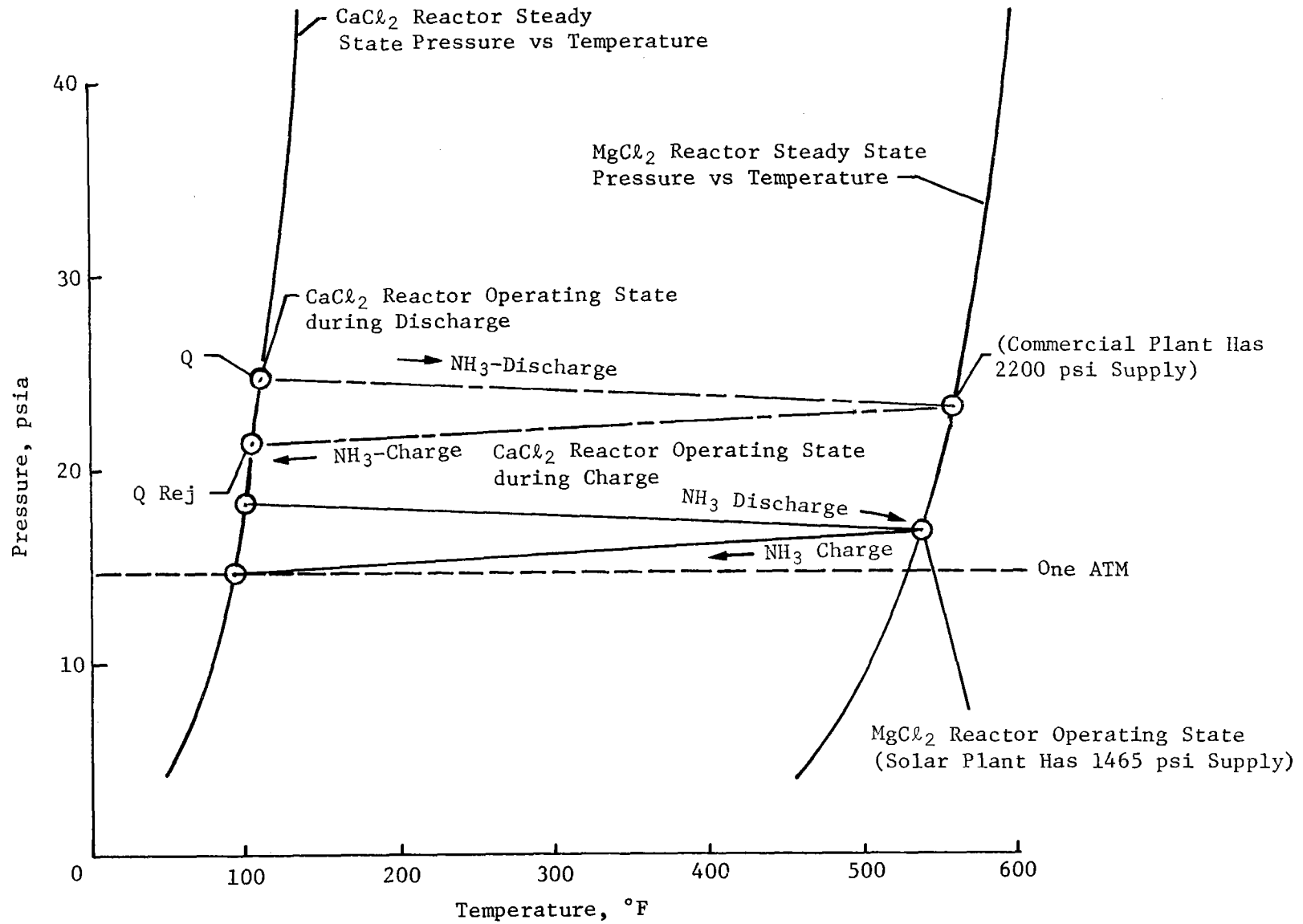


Figure VI-3 Operating Characteristics of Salt Pair

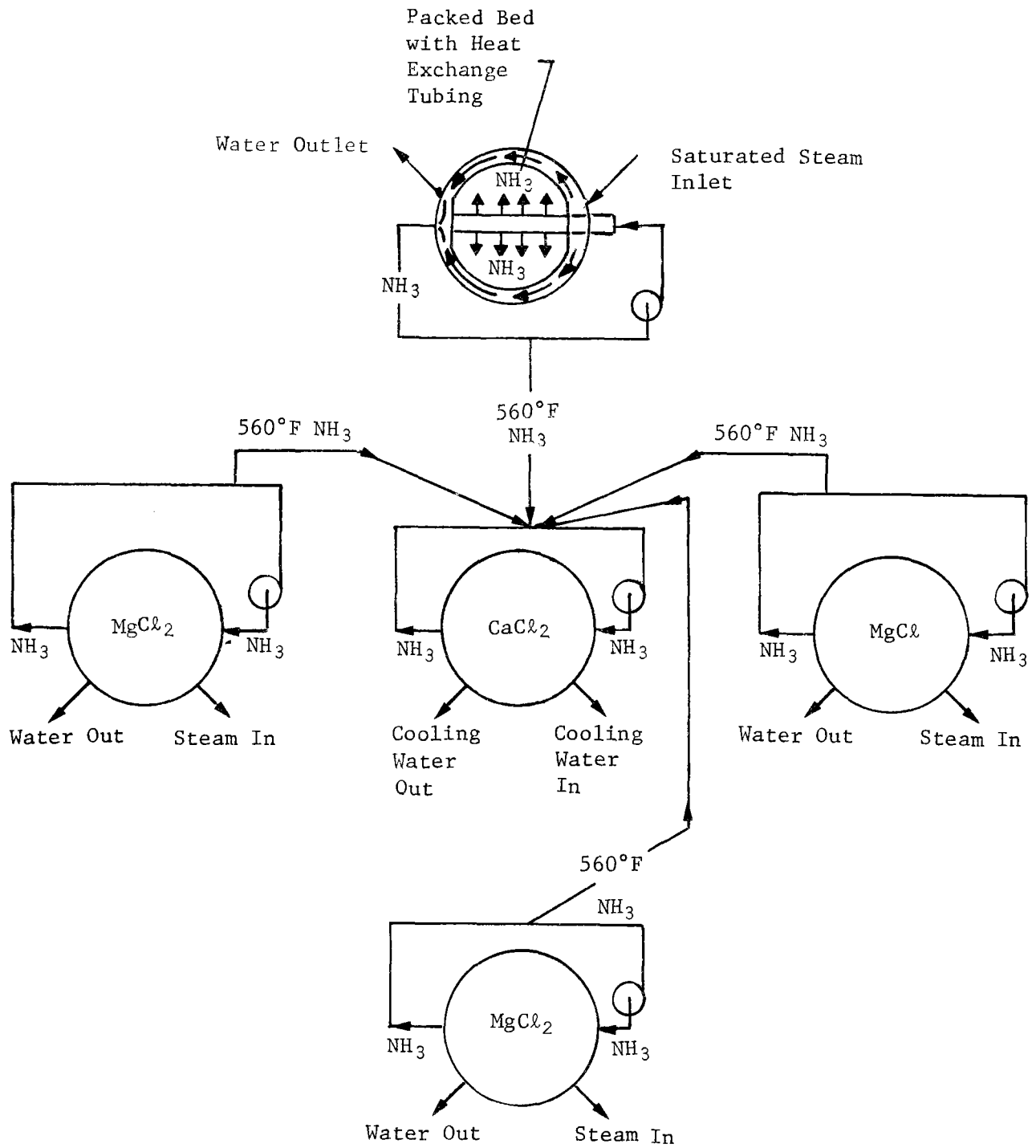


Figure VI-4 Chemical Storage - Flow Through Bed-Charging Concept

c. *Oil Storage System* - The oil storage system, shown schematically in Figure VI-5, operates in the following manner. Heat is extracted from the power plant boiler during the charge mode in the form of saturated steam (650°F, 2200 psi). The steam is condensed in the heat exchanger that transfers the latent heat of the steam to the hydrocarbon oil storage fluid. The oil is heated from 450°F, its cold reservoir temperature, to 560°F, its hot reservoir temperature.

During the discharge mode the oil flow is reversed to bring hot oil, 560°F, into the heat exchanger and cool it to 450°F. The heat the oil releases is transferred to feedwater, which enters the heat exchanger at 160°F and exits the exchanger as saturated steam at 450°F.

2. Results and Conclusions

Results of the economic analysis are presented in Table VI-5 and VI-6 for the 50 MWe and 100 MWe storage systems, respectively.

The following conclusions can be drawn from the results.

- 1) The batch fluidized reactor chemical storage system is competitive with the oil storage system for the 50 MWe system, considering the system investment cost (\$23.7 million versus \$22.8 million) or the total system cost (\$473.3 versus \$457.3/kWe) even though both parameters are higher. The flow-through bed chemical storage system is the least attractive due to its high $MgCl_2$ reactor and compressor costs.
- 2) The flow-through bed chemical storage system is the most attractive system for the 100 MWe system based on system investment cost (\$64.8 million) or total system cost (\$27.kWe). This can be explained by the lower storage-related cost compared to the competing systems.
- 3) This analysis indicates that it is impossible to draw general conclusions on the value of chemical storage without limiting the conclusions to a particular utility application. Recognizing this, the following comments are offered:
 - 1) Increasing the storage requirement is not advantageous to an oil storage systems due to the increased cost of oil and storage tanks.
 - 2) Chemical storage systems are subject to the high cost of reactor and heat exchanger components. If fluidized beds are used, the power required is a large part of the power stored (20 to 40%).
 - 3) The power-related costs for the oil storage system were al-

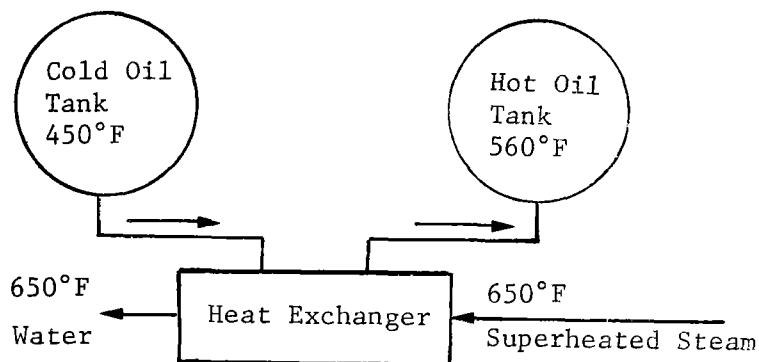


Figure VI-5 Schematic of Oil Storage System-Charging

Table VI-5
Comparison of 50 MWe, 10-Hour Storage Systems for Solar Power Plant

	Batch Fluidized Reactor, \$/kWe-hr	Flow Through Bed \$/kWe-hr	Oil \$/kWe-hr
Storage Related Costs			
MgCl ₂	7.11	7.11	Oil 20.44 Tanks 16.90
CaCl ₂	0.52	0.52	
NH ₃	1.91	1.91	
MgCl ₂	18.20	34.72	
CaCl ₂ Reactor	2.80	8.68	
Power Related Costs	\$/kWe	\$/kWe	\$/kWe
Compressor/Motor	32.2	21.0	Heat Ex 31.5 Piping, 52.5 Pumps, Valves
Heat Exchanger/MgCl ₂	20.5	40.4	
Heat Exchanger/CaCl ₂	40.5	22.4	
Piping, Valves	35.7	6.23	
System Investment Cost, \$	23,712,000	43,227,000	22,863,200
Total System Cost, \$/kWe	474.3	864.5	457.3
Storage Related Cost, \$/kWe-hr	30.54	52.94	37.34
Power Related Cost, \$/kWe	168.9	317.1	84.0

Table VI-6

Comparison of 100 MWe 24-Hour Storage Systems for Conventional Power Plant

	Batch Fluidized Reactor,	Flow Through Bed	Oil,
Storage Related Costs	\$/kWe-hr	\$/kWe-hr	\$/kWe-hr
MgCl ₂	6.56	6.63	Oil 18.79
CaCl ₂	0.48	0.36	Tanks 14.08
NH ₃	1.76	0.86	
MgCl ₂ Reactor	16.79	4.23	
CaCl ₂ Reactor	2.58	1.06	
Power Related Costs	\$/kWe	\$/kWe	\$/kWe
Compressor/Motor	71.3	75.0	Heat Ex 28.9
Heat Exchanger/MgCl ₂	50.5	48.0	Piping, Pumps, 129.0
Heat Exchanger/CaCl ₂	178.3	165.0	Valves
Piping, Valves	51.0	44.9	
System Investment Cost, \$	102,738,650	64,779,000	94,689,000
Total System Cost \$/kWe	1027.4	648.8	946.9
Storage Related Cost, \$/kWe-hr	28.17	13.14	32.87
Power Related Cost, \$/kWe	351.2	332.9	157.9

ways lower than for other systems regardless of application. This is attributed to the small heat exchangers required for the oil system versus the large heat exchangers for the chemical storage systems.

B. ALTERNATIVE BED CONFIGURATION—FLUIDIZATION

The objective of this task was to analyze the effects of bed fluidization on the performance of reversible thermal storage systems and to determine the fluidization characteristics of $MgCl_2$ and $CaCl_2$ salt beds. A small scale reactor was built to determine the gas velocity required to fluidize the salt beds. Power requirements for bed fluidization were determined for the economic feasibility studies.

1. Discussion

The fluidized-solid technique has several advantages over the fixed-bed concept. When a particulate bed or material, such as an ammoniated salt, is being fluidized, turbulent agitation of the solids and gas provides a bed with nearly isothermal conditions. Such temperature control allows close regulation of the reaction rates and the completion of the desired chemical reactions. The time to complete the ammoniation and deammoniation of the chemical salts can be expected to proceed much more quickly than in the fixed bed because of the isothermal conditions and the efficient gas-solid phase contact. The heat transfer rates are higher to embedded surfaces, such as heat exchangers, because of efficient gas-solid mixing and higher gas velocities through the bed. The fluidized-bed technique also prevents compaction of material--a problem that can reduce the material surface area and thus bed reactivity.

The disadvantages of fluidized beds are chiefly associated with operation of "nonideal" solid beds. Problems may be encountered in attempting to fluidize solids that do not flow freely or tend to agglomerate. Cohesive solid beds tend to channel, spout*, or slug, drastically reducing fluidization efficiency. Fine solid particles may be formed during the fluidization process, which will become entrained in the gas leaving the fluidized bed. This phenomenon requires recovery operations that must be included in the design. The pressure drop, ΔP , in fluidized

*Beds are said to "spout" when there is a jet of fluid passing up through their central parts. The solid particles in the jet move upward as a pneumatic transport regime, falling back and settling in an annular zone near the walls after the jet leaves the bed.

beds is larger than in other types of reactors, i.e., kiln, tray, etc. This pressure loss results in additional pumping and energy costs.

Whether the advantages of the fluidized bed outweigh the disadvantages depends on the material being fluidized and the application. Three basic factors control the design of a fluid-solid reactor:

- 1) The reaction kinetics for single particles;
- 2) The size distribution of the solids being reacted;
- 3) The flow patterns of the solids and fluid in the reactor.

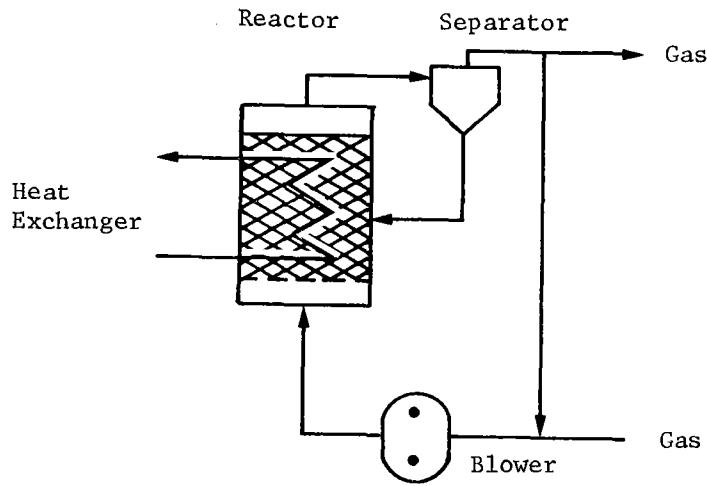
To date, a reliable method has not been established for the optimization of fluidized bed reactors. This is due to the lack of a general model to characterize the complex phenomena occurring in fluidized beds; therefore, most of the results of the fluidization process must be empirically derived for the particular application. Care must also be exercised in extrapolating results for scale-up determinations.

2. Fluidized-Bed Configurations

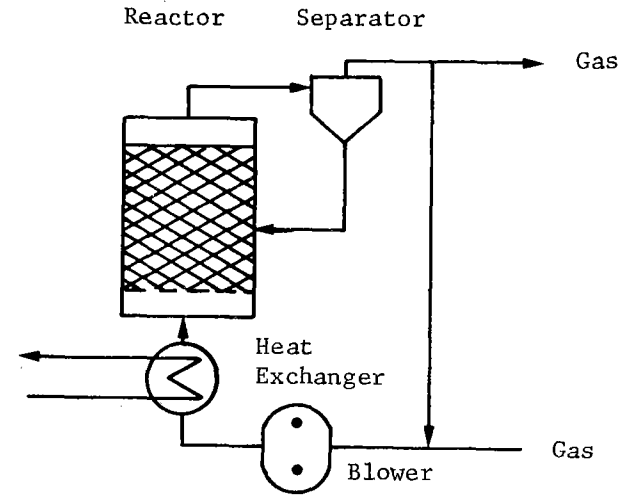
Several configurations are feasible for applications of thermal energy storage. These configurations consider batch versus continuous solid feed reactors using internal or external heat exchangers. The unit operation modules are shown in Figure VI-6. A cyclone separator is required in all configurations to separate the entrained solids from the gas leaving the reactor and to return the solids to the bed. A gas recycle loop is provided to minimize the use of the fluidizing gas and to improve the process efficiency.

The heat exchanger configuration has certain advantages. The internal heat exchanger promotes more efficient contact of the exchanger surface area with the solid bed and thus increases heat transfer. However, the heat exchanger affects the bed fluidization characteristics because it is located in the bed. Folk, et al. (Ref VI-2), have shown the beneficial effects of reactor internals (regularly spaced vertical rods spanning the height of the bed) on the quality of fluidization. Therefore, fluidization may be improved with internal heat exchangers employing proper heat exchanger and reactor design. The disadvantage of internal heat exchangers is their susceptibility to the corrosive environment of the bed material and fluidizing gas. Also, repair or maintenance of the heat exchanger would involve the costs of emptying the bed of solids and possible contamination of the solids from the heat exchanger leakage. The external heat exchanger removes the risk of direct contact

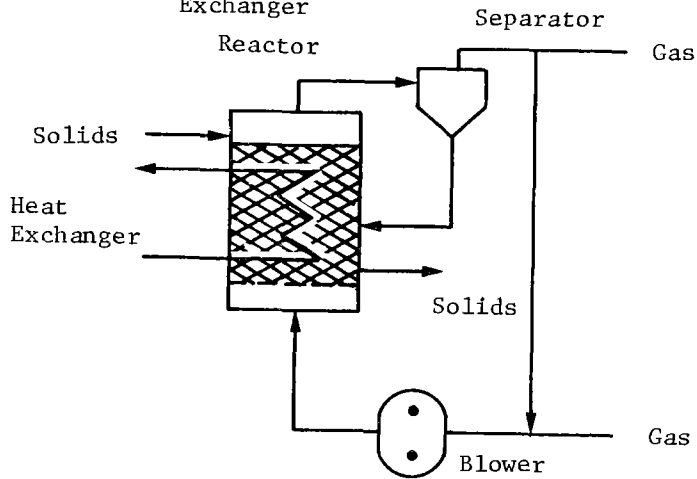
(1) Batch Mode
Internal Heat
Exchanger



(2) Batch Mode
External Heat
Exchanger



(3) Continuous Feed
Mode Internal Heat
Exchanger



(4) Continuous Feed
Mode External Heat
Exchanger

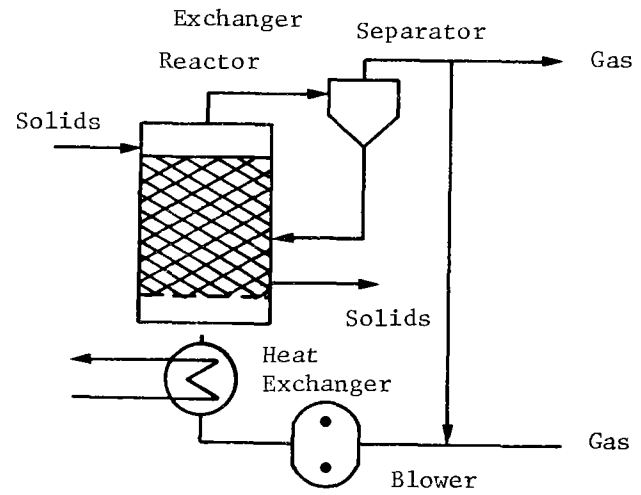


Figure VI-6 Fluidized Bed Concepts

of the transfer medium tubes with the solids resulting in a sacrifice in heat transfer. In this case, the heat transfer agent to the bed is the fluidizing gas. Such a configuration eliminates the possibility of heat exchanger surface and solids compatibility. Ease of maintenance is also a characteristic of this system.

Heat transfer calculations for fixed and fluidized beds (internal and external heat exchangers) for application to thermal energy storage are shown in Table VI-7 for comparison purposes. The heat transfer coefficients were estimated from recent correlations of fixed-bed and fluidized-bed studies. The required heat exchanger areas were determined using a constant heat rate for a given ammonia evolution rate from the bed. The heat transfer coefficient for the fixed bed was estimated and verified empirically during this program. The internal heat exchanger coefficient range was calculated from correlations developed by Wender and Cooper (Ref VI-3), and Mickley and Trilling (Ref VI-4). Heat transfer coefficients for the external heat exchanger configuration were estimated from data of Sharlovskaya (Ref IV-5) for the gas to particle heat transfer and Perry (Ref VI-6) for the heat exchanger tube surface to gas heat transfer.

Table VI-7 indicates that the optimum configuration for minimizing the heat exchanger surface area is the internal heat exchanger. The external heat exchanger configuration requires a large horizontal surface area for the gas flow to provide the required rate of heat transfer. The large heat transfer area of the gas to the solid particle can be obtained with the range of particle sizes used in fluidization.

3. Pumping Power Requirements

The power required to fluidize a particulate solid bed is a function of: the gas flow capacity (ft^3/sec) for fluidization; the pressure drop across the bed, ΔP ; and the efficiency of the blower unit. Fluidized beds operate between two superficial gas velocities: (1) the minimum fluidization velocity, and (2) the terminal velocity for a single bed particle. The minimum fluidization velocity can be determined experimentally or estimated from empirically derived correlations. Recently developed correlations by Broadhurst (Ref VI-8) were used to estimate the minimum fluidization velocity required for fluidization of $\text{MgCl}_2 \cdot \text{XNH}_3$ and $\text{CaCl}_2 \cdot \text{XNH}_3$ beds. Particle sizes were estimated for the ammoniated salt beds by using data developed earlier in this program (Table IV-5). These data show that most of the $\text{MgCl}_2 \cdot \text{XNH}_3$ salt can be expected to be in the 0 to 300 micron range and $\text{CaCl}_2 \cdot \text{XNH}_3$ will be in the 300 to 3000 micron range. The power costs were also estimated for each bed configuration in the range of expected gas velocities.

Table VI-7 Heat Exchanger Characteristics

	Fixed Bed, Wall to Solid	Internal Heat Exchanger, Wall to surface	Fluidized Bed, Wall to Gas	External Heat Exchanger, Bas to Solid
Heat Transfer Coefficient, Btu/hr-ft ² -°F	5	50 to 100	5	0.242
ΔT, °F	15	7.5	7.5	7.5
Required Heat Exchange Area, ft ² for $Q = \frac{1500 \text{ Btu}}{\text{hr}}$	20	2.0 to 4.0	40	820

Incipient fluidization of a bed occurs when the pressure drop is equal to the weight of the bed divided by the reactor cross sectional area. For the beds sized for the economic analysis, the pressure drop during fluidization across the $\text{MgCl}_2 \cdot \text{XNH}_3$ (30 ft dia x 30 ft length) bed is 900 lbf/ft² and the $\text{CaCl}_2 \cdot \text{XNH}_3$ (28.5 ft x 28.5 ft) is 854 lbf/ft². The correlation developed by Broadhurst (Ref VI-8) was selected to determine the minimum fluidization velocity, V_{mf} , because of its broad range of applicability over the flow conditions in fluidized beds. The correlation is

$$[\text{VI-3}] \quad V_{mf} = 0.00203 \left(\frac{\gamma D_p}{\rho_p} \right)^{0.5} \left(\frac{\rho_p D_p}{\mu^2} \right)^{0.425} \left(\frac{\rho_p}{\rho_f} \right)^{0.01}$$

where D_p is the particle diameter.

ρ_f is the fluid density,

ρ_p is the particle apparent density,

γ is $g(\rho_p - \rho_f)$,

μ is the viscosity, and

g is the gravitational acceleration.

The minimum fluidization velocities are presented in Figures VI-7 and VI-8. One can expect minimum fluidization velocities in the range of 0 to 0.15 ft/sec for the 0 to 300 micron range of $\text{MgCl}_2 \cdot \text{XNH}_3$. The 300 to 3000 micron $\text{CaCl}_2 \cdot \text{XNH}_3$ bed should require from 0.2 to 1.5 ft/sec to fluidize.

The pumping power requirements can be determined knowing the range of fluidization velocities. The energy requirements for the pumping of ammonia gas through the bed can be determined by the equation:

$$[\text{VI-4}] \quad \text{Pumping Power} = \frac{Q \times \Delta P}{550 \cdot \text{eff}}$$

where Q is the flow capacity, ft³/sec,

ΔP is the pressure drop, lbf/ft², and

eff is the blower efficiency, approximately 0.60.

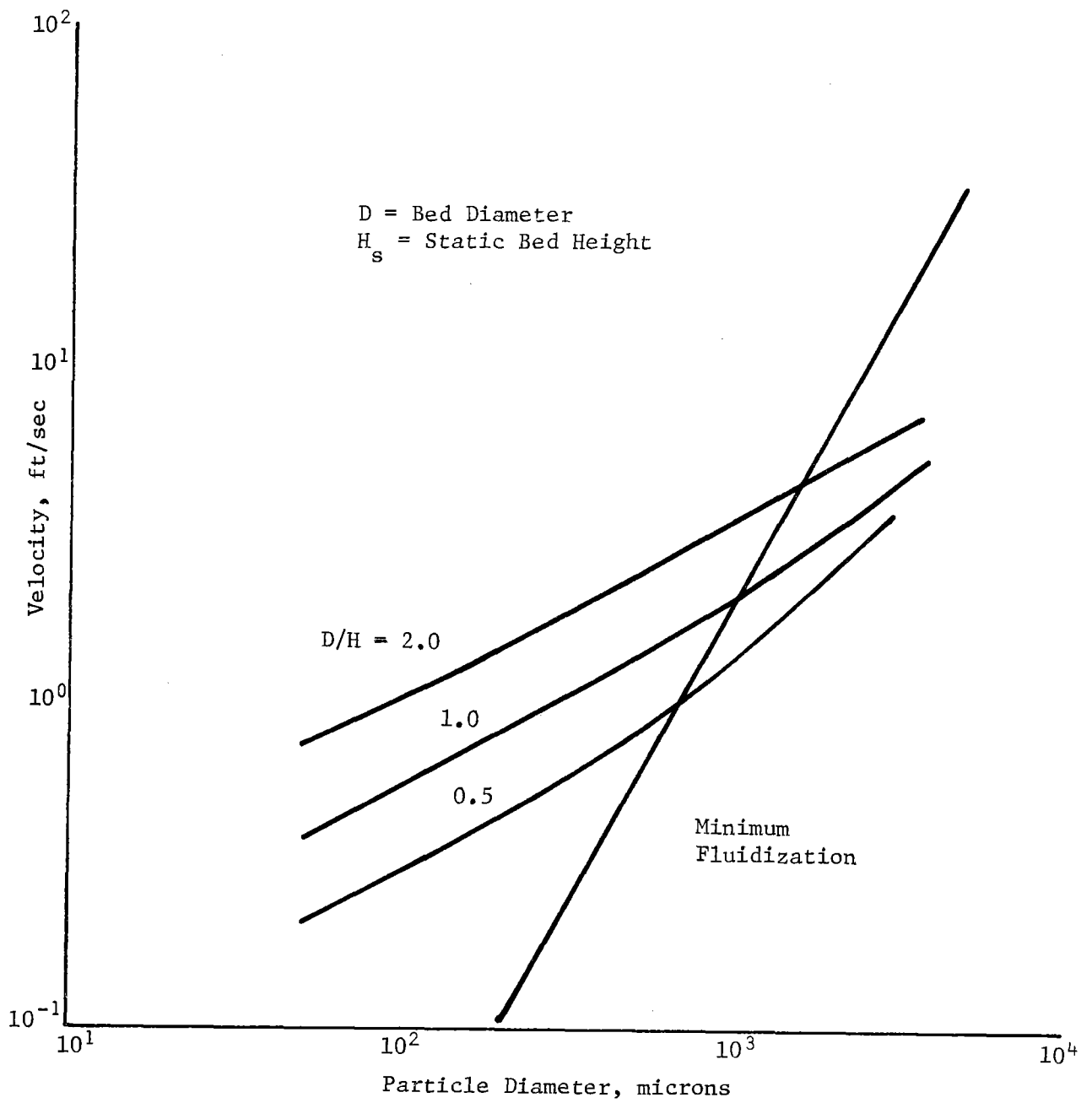


Figure VI-7 $\text{CaCl}_2 \cdot x \text{NH}_3$ Fluidization Using Broadhurst Correlations

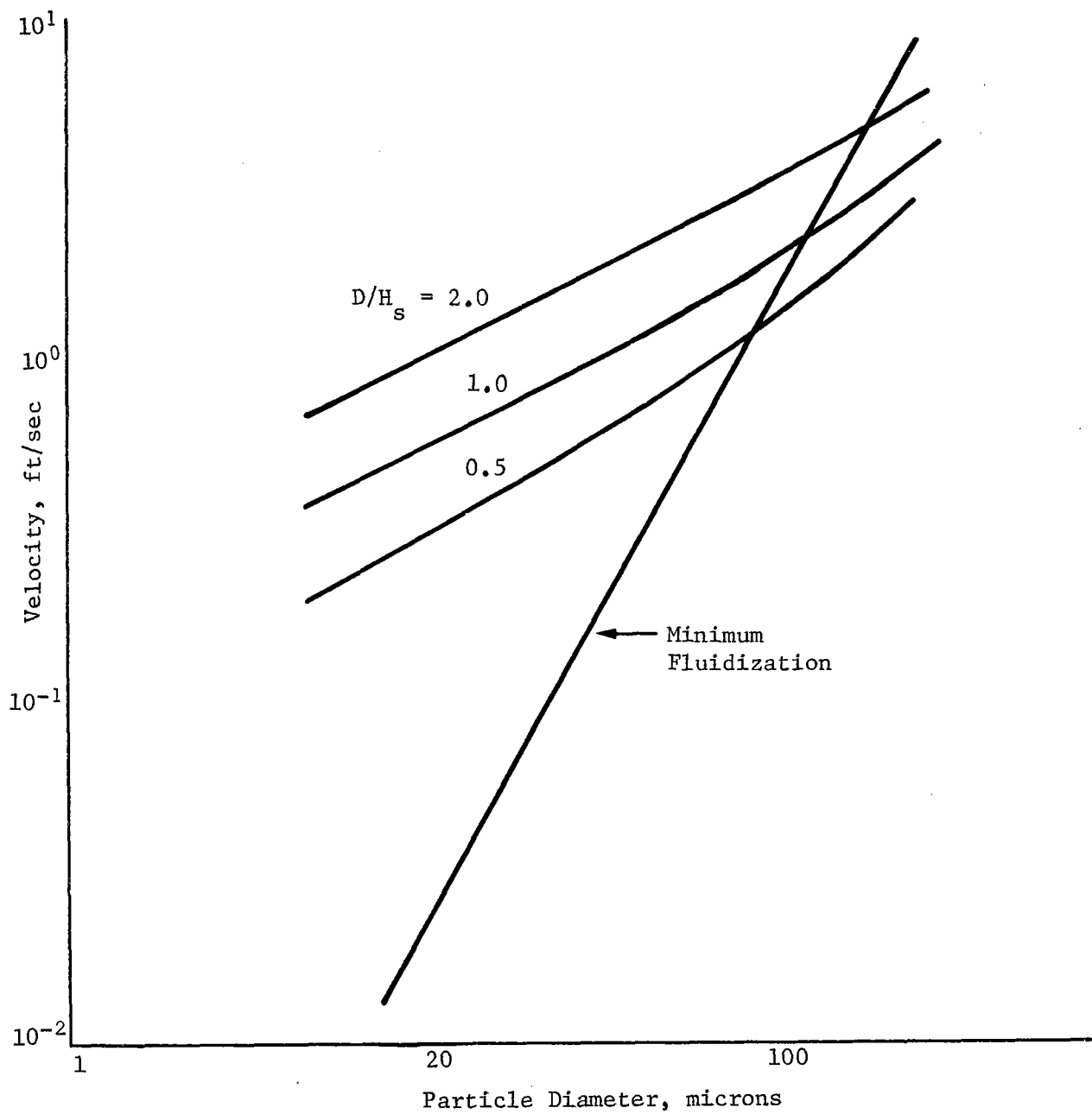


Figure VI-8 $MgCl_2 \cdot x NH_3$ Fluidization Using Broadhurst Correlations

For the 100 MWe plant the pumping requirements over the range of expected gas velocities were calculated for each bed and are presented in Figure VI-9. The cost breakdown can be determined based on the following assumptions:

- 1) 124 $\text{MgCl}_2 \cdot \text{XNH}_3$ beds;*
- 2) 31 $\text{CaCl}_2 \cdot \text{XNH}_3$ beds;
- 3) 0.2 ft/sec fluidization velocity for each bed;
- 4) 30 mills/kWh for cost of electricity;
- 5) continuous 365-day operation.

*(124 beds) (400 hp/bed) (0.7456 kW/hp) (\$0.030/kWh) (365 days/yr) (24 hr/day) = $\$1.94 \times 10^6$ /year.

These cost figures show that fluidization will cost over \$11 million a year in electricity alone. In another sense, fluidization will require between 35% to 40% of the energy that is stored for a 100 MWe storage plant.

4. Fluidization Tests

A laboratory scale 1.5-in. ID glass reactor was used to assess the fluidization characteristics of MgCl_2 and CaCl_2 solid beds. Tests were conducted for solid beds of varying particle size and bed heights. Gas flowrates were regulated to determine minimum fluidization velocity and fluidization quality. Bed densities at the minimum fluidization velocity were also determined.

Tests were conducted with apparatus shown schematically in Figure VI-10. The glass tube reactor was fed by a cold NH_3 supply to fluidize and ammoniate the salt bed. The salt bed was supported by a fine mesh wire screen (250 x 1370 mesh, 304L stainless steel). A fine mesh wire screen filter was also placed in the ammonia exit stream to prevent fine solids from escaping the reactor. Three thermocouple probes were placed on the grid, in the bed, and in the NH_3 exit. A water-filled manometer was used to measure the pressure drop, ΔP , across the reactor.

Several fluidization tests were performed with CaCl_2 , $\text{CaCl}_2 \cdot 8\text{NH}_3$, MgCl_2 and $\text{MgCl}_2 \cdot 6\text{NH}_3$. Each salt had its own fluidization characteristics. The anhydrous CaCl_2 fluidization tests showed significant volume change as it was fluidized and ammoniated. The anhydrous CaCl_2 used in these tests had nearly uniform particle sizes (approximately 60 to 80 microns). A minimum fluidization velocity was not obtainable for anhydrous CaCl_2 because part of the bed had been ammoniated before fluidization began.

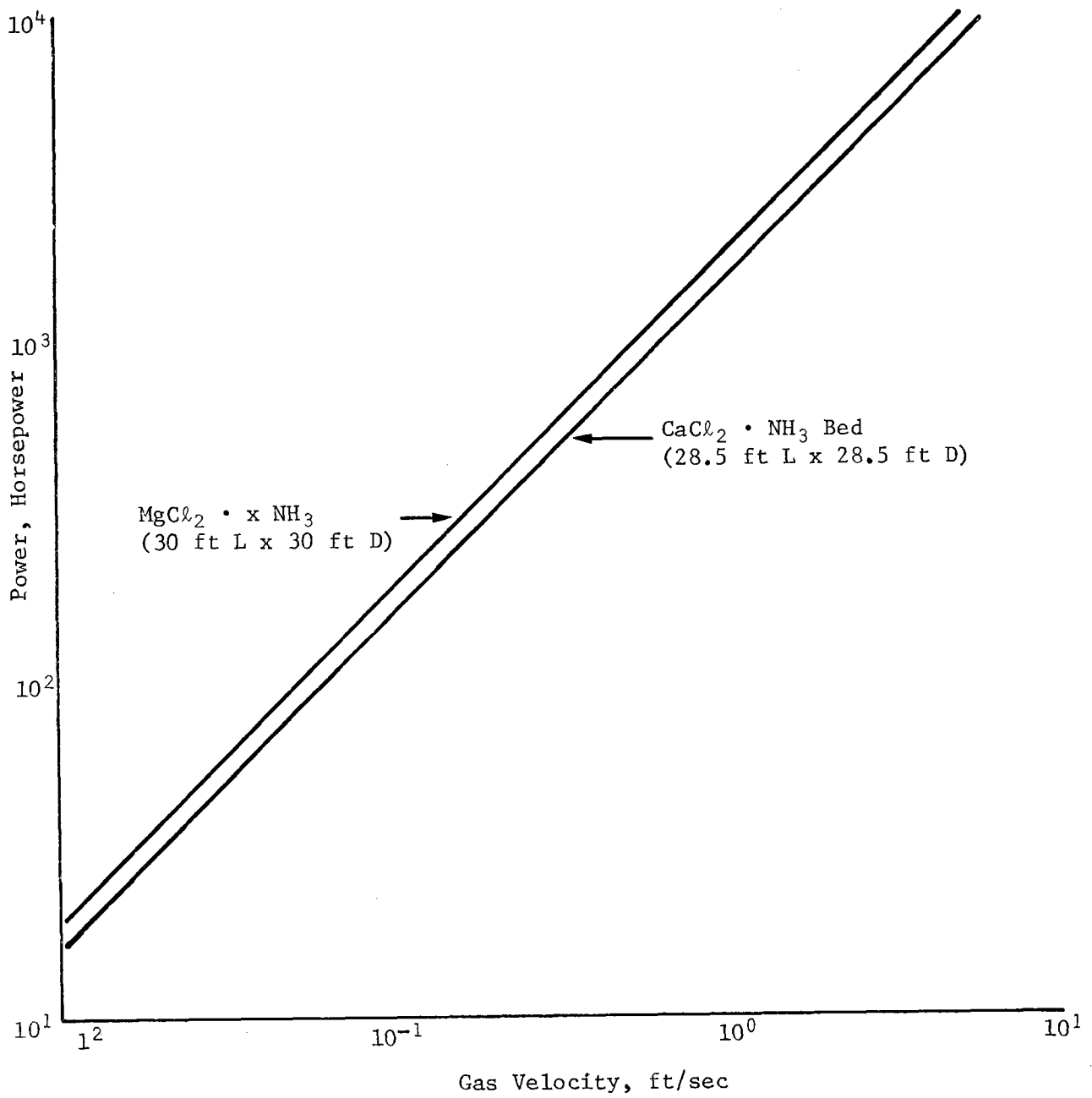


Figure VI-9 Power Requirements to Fluidize One Reactor Bed

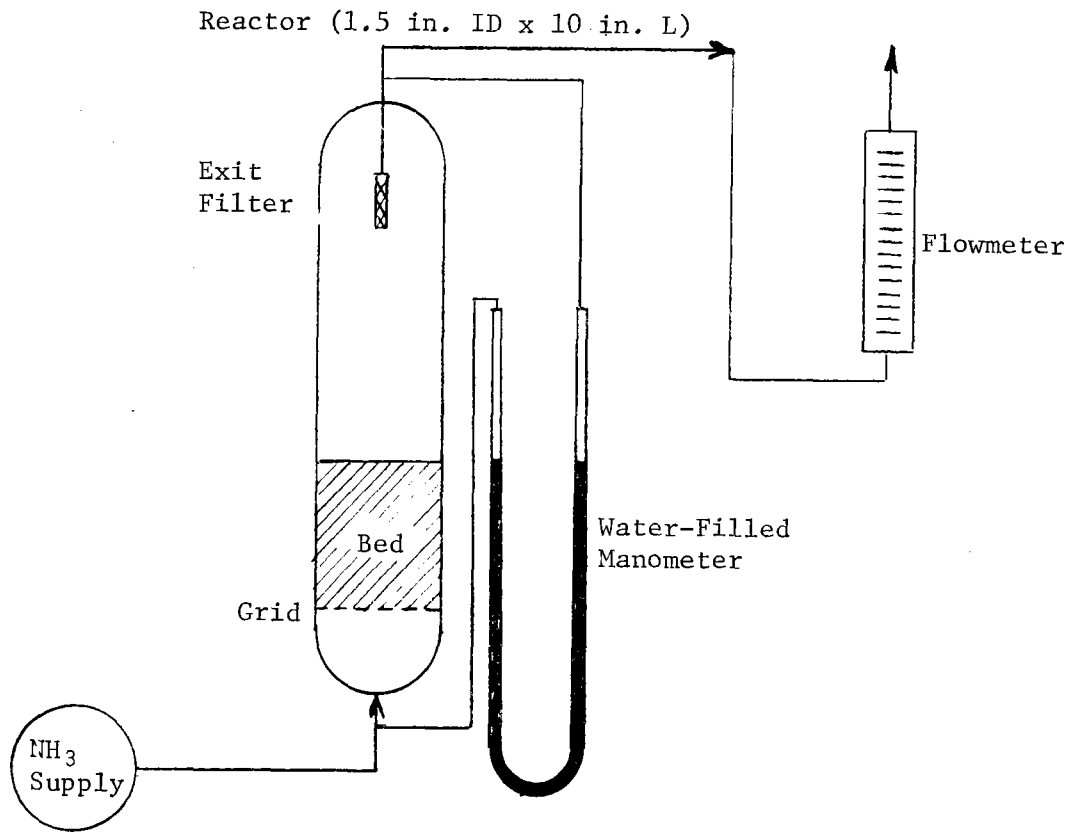


Figure VI-10 Test Reactor Schematic

As the CaCl_2 was ammoniated to $\text{CaCl}_2 \cdot 8\text{NH}_3$, small channels appeared and disappeared while the bed fluidized. Bubbles broke near the surface of the bed and over all the surface of the bed. Overall fluidization efficiency (i.e., recirculation, backmixing, etc) appeared to be good. Initially the anhydrous CaCl_2 was at ambient temperature (approximately 75°F). As the salt was fluidized, a temperature rise of approximately 30°F to 40°F was observed indicating the exothermic ammoniation reaction; however, this peak temperature was short lived as the cold ammonia gas quickly cooled the bed.

A second series of tests were conducted with $\text{CaCl}_2 \cdot 8\text{NH}_3$ prepared from the batch reactor. Seven pounds of ammoniated salt were prepared by starting with anhydrous CaCl_2 particle sizes in the range of 60 to 300 microns and ammoniating the salt in a closed vessel. Portions of this batch were placed in the fluidized bed laboratory reactor to achieve initial bed heights of 0.75 in., 1.5 in., and 2.5 in. Attempts to fluidize the ammoniated salt, $\text{CaCl}_2 \cdot 8\text{NH}_3$, were unsuccessful. None of the three different bed heights provided recirculation. Instead, all beds developed channels and spouts, providing conduits for the gas to pass through. Most of the channels formed near the glass surface of the reactor. The 0.75-in. high bed exhibited only channeling and spouting, while the 1.5-in. and 2.5-in. beds exhibited slugging tendencies. Slugging is a fluid bed phenomena of gas pockets that develop across the entire width of the reactor between packets of bed material. The occurrence of slugging in reactors tends to provide wide variations in ΔP across the reactor. In these series of tests, slugging occurred due to the cohesiveness of the bed material. The difference in the solid material used in this series of tests and the ammoniated salt material prepared in the fluidization series of tests cannot be readily explained. Differences in preparation and particle size range may provide the reason for differences in the cohesive properties of the salts.

External means of agitation of the cohesive $\text{CaCl}_2 \cdot 8\text{NH}_3$ improved the fluidization to the point of little or no slugging. Agitation of the reactor was done by tapping the glass reactor. If the cohesion or agglomerating tendencies of this ammoniated salt are the rule, then a mechanical stirrer in a large scale application may provide the necessary agitation to overcome this cohesion. Such devices have been successfully used in fluidizing flour and corn starch (Ref VI-7).

The problem of incipient slugging before fluidization in the preceding tests can be readily explained with the fluidization and slugging velocity correlations developed by Broadhurst (Ref VI-7). Calculated minimum slugging velocities for various bed diameter to fixed bed height ratios are shown in Figures VI-7 and VI-8.

The minimum slugging velocity equation used is

$$[VI-5] \quad V_{ms}^2 = \frac{\gamma D}{\rho_f} \left[51.4 \left(\frac{D}{H_s} \right)^{1.79} \left(\frac{\rho_f}{\rho_p} \right)^{1.09} + 0.00416 \left(\frac{\rho_f D^3}{\mu^2} \right)^{0.41} \left(\frac{\rho_f}{\rho_p} \right)^{0.59} \right]$$

where V_{ms} is the minimum slugging velocity,

γ is $g \rho_p - \rho_f$,

D_p is the particle diameter,

D is the bed diameter,

H_s is the static bed height,

ρ_p is the particle apparent density,

ρ_f is the fluid density, and

μ is the fluid viscosity.

Figures VI-7 and VI-8 show that slugging may occur before fluidization for large particle sizes. Slugging always occurred in the case of the $\text{CaCl}_2 \cdot 8\text{NH}_3$ fluidizing attempts. Because previous particle size measurements of this salt showed it to be in the 300 to 3000 micron range, slugging before fluidizing is consistent with the calculation presented in Figure VI-7. The trend of incipient slugging at lower gas velocities with increasing static height (decreasing D/H_s) was qualitatively observed. This trend is also consistent with correlation calculations presented in Figure IV-7. As will be discussed later, the $\text{MgCl}_2 \cdot \text{XNH}_3$ fluidization tests were much more successful (slugging seldom occurred). Because this bed has smaller particle sizes (0 to 300 micron), as determined in previous laboratory tests, fluidization should have occurred before slugging according to Figure VI-8.

A $\frac{1}{4}$ -in. metal rod was placed in the center of the bed to determine the effect of internal devices on fluidization quality. The rod provided a means for the solid bed to develop more channels around the metal surface. Superficial gas velocities as high as 3.0 ft/sec did not affect the static state of the bed. All gas passed around the periphery of the metal rod.

A final series of tests were conducted using anhydrous $MgCl_2$. The material varied in particle size from 50 to 500 microns. The reactor was filled with magnesium chloride to provide an initial bed height of 1.25 inches. The salt material was directly transferred from an oven to the reactor; therefore, the initial bed temperature was quite hot (approximately 630°F). Initially, the salt bed was difficult to fluidize. Channels formed and bed material was not mixing. However, as the magnesium chloride ammoniated, fluidization efficiency improved. Tapping the reactor at the beginning of the tests was required to close channels and maintain mixing. However, extensive bubbling and backmixing occurred without external vibration as the ammoniated salt, $MgCl_2 \cdot 6NH_3$, formed. The gas velocity at incipient bubbling of the bed occurred at approximately 0.4 ft/sec.

Salt particle striations were observed at lower fluidization velocities. For example, ammonia gas with velocities greater than 0.4 ft/sec and less than 3 ft/sec, the lower portion of the bed remained static and the upper portion fluidized. Channels formed in the lower portion of the bed and the upper portion bubbled and mixed. The relative amount of static bed and fluidized bed were determined depending on the degree of ammonia flowrate through the reactor. At high gas velocities, the volumetric proportion of static bed decreased indicating stratification due to settling of heavier and larger particles. No volume increase was noticed after ammoniation.

Gas entrainment of fine solids was noticed during fluidization of all salts. Excessive entrainment required reactor shutdown to clean the exit filter in both the anhydrous and ammoniated $CaCl_2$ tests. The $MgCl_2$ tests, however, produced little entrainment of solids. Fluidization of this salt did not require reactor shutdown to clean the exit gas filter.

Bed densities before and after fluidization of the salts were calculated (Table VI-8). The void fraction of the bed before fluidization was calculated from bed density. The values of the bed density and the void fractions determined from measurements of salts in the reactor are given in Table VI-8.

Table VI-8 Bed Densities

	Bed Density, lbm/ft ³	ϵ
$CaCl_2$ (before fluidization)	55	0.59
$CaCl_2 \cdot 8NH_3$ (after fluidization)	20	0.79
$MgCl_2$ (before fluidization)	12	0.86
$MgCl_2 \cdot 6NH_3$ (after fluidization)	23.9	0.73

The void fraction is simply calculated as

$$[\text{VI-9}] \quad \epsilon = 1 - \frac{\rho_{\text{bulk}}}{\rho_m}$$

where ρ_{bulk} is the weight of material in the bed divided by the measured volume of the bed, and

ρ_m is the apparent particle density.

The relatively large values of void fraction, ϵ , indicate highly porous and/or nonspherical salt particles. The void fractions calculated for the metallic salts used in this program were determined using the material densities determined from the pycnometer method. However, with this method the fluid enters the pores of a highly porous material and the pycnometer method underestimates the volume of the particles and overestimates the bed porosity. Therefore, the void fraction reported in the previous table includes the bed void fraction as well as the void fraction due to the porosity of the salt particle. Zabrodsky (Ref IV-9) outlines a method to determine the apparent particle density by measuring the hydraulic resistance, ΔP , of the bed.

5. Conclusions

Conclusions obtained from this portion of the study are as follows:

- 1) Results from the fluidization tests and the comparison with recent minimum fluidization and slugging correlations indicate that both $\text{MgCl}_2 \cdot \text{XNH}_3$ and $\text{CaCl}_2 \cdot \text{XNH}_3$ salts will fluidize if proper conditions of particle size and bed configuration are maintained.
- 2) The pumping power costs of fluidizing these beds for a 100 MWe, 24-hour storage unit represent about 35% to 40% of the stored energy, which will probably prohibit fluidization as a serious alternative bed configuration.

C. ALTERNATIVE REACTOR DESIGNS

The objective of this task was to evaluate reactor designs other than the fixed-bed reactor and to compare the various concepts on an economic basis. The economic comparison was to be on a relative and not an absolute basis. The costs are split in two factors; (1) a power-related cost, C_p , and (2) a storage-related cost, C_s , because this task was focused on application of the energy storage system to large-scale power plants. The two factors were combined to obtain a total cost, C , through a linear relationship in terms of storage discharge time, T , by

$$[\text{VI-7}] \quad C = C_p + C_s * T.$$

In the energy storage system under consideration, the power-related cost, C_p , is associated primarily with the cost of the heat exchanger, and the storage cost, C_s , consists of the salt and container costs.

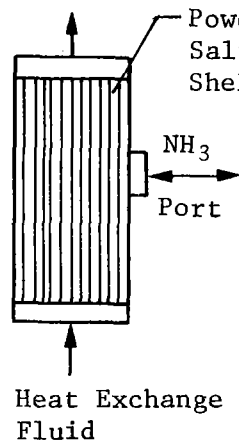
1. Reactor Design Description

a. Fixed Bed without Gas Recirculation - The fixed-bed, shell, and tube exchanger shown in Figure VI-11(a), requires a large heat transfer area per unit quantity of energy transferred. The large heat transfer area required is due to the low heat transfer coefficient between the heat transfer fluid and the reacting solid. As will be shown subsequently, the configuration is uneconomical relative to other designs.

b. Fixed Bed with Gas Recirculation - The overall coefficient of heat transfer can be increased by forcing the flow of ammonia gas perpendicular to the heat transfer surface. This fixed-bed concept with gas recirculation results in a smaller required heat transfer area and a lower cost than a reactor without gas recirculation. Also, assuming large quantities of stored material are involved, container costs can be reduced by considering large volume containers. One such concept is shown in Figure VI-11(b) where a large diameter (e.g., 80-ft) spherical container is equipped with an integral heat exchanger inside the reactor with a forced gas circulation. The power required for gas recirculation is estimated to be about 20 kW per reactor. As the volume of container is increased, the number of containers required is reduced. The resulting decrease in surface area per unit volume decreases the heat loss per unit volume as well as the cost per unit volume.

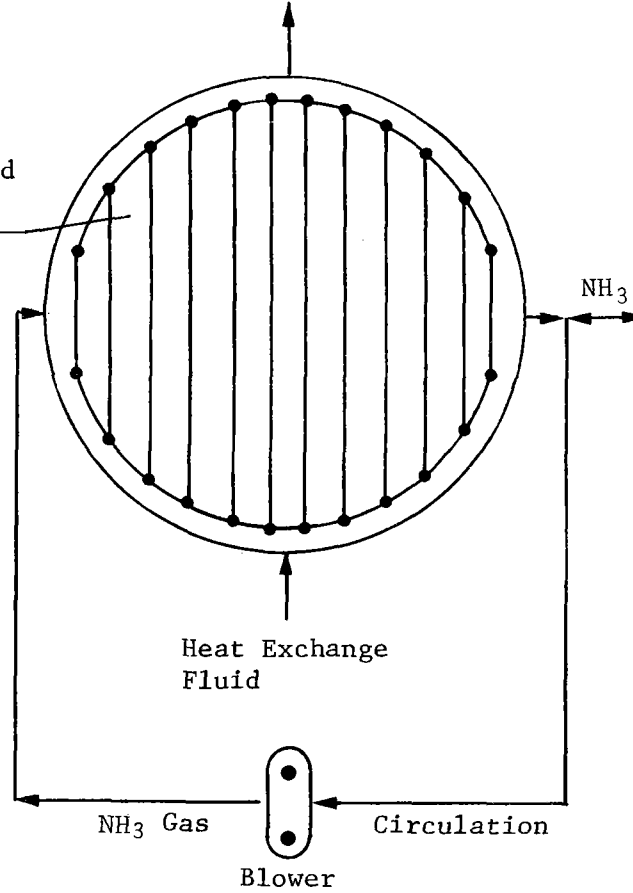
c. Fluidized Bed Reactor - The heat transfer surface area can be reduced further by considering the fluidized bed concept shown in Figure VI-11(c). The container in this system is usually cylindrical in order to promote fluidization of the solids by

Fixed Bed,
Shell and Tube
Exchanger



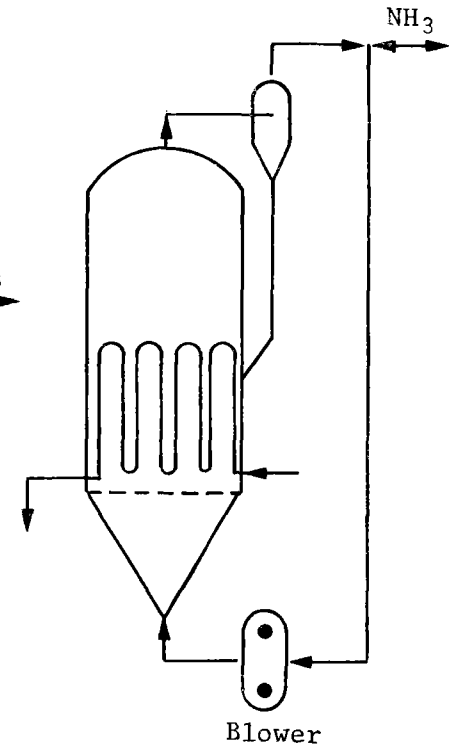
(a)

Fixed Bed with
Gas Circulation



(b)

Fluidized Bed



(c)

Figure VI-11 Reactor Concepts

recirculating ammonia gas. The relatively high heat transfer coefficient (nominally 50 to 80 Btu/hr-ft²-°F) obtainable with this approach permits the size of the heat exchanger surface to be reduced to a relatively low value. However, pressurized cylindrical containers for storing large volumes of solids are expensive compared to spherical containers and the power required to fluidize the total quantity of salt is excessive.

d. Fluidized Bed Reactors with Spherical Storage Containers and Pneumatic Transport of Solids - The advantages of the fixed bed and fluidized bed can be realized by combining them as shown in Figure VI-12. In this concept, the solids are stored in large spherical containers (with conical bottoms and without heat exchangers) to minimize storage costs and the reactions are conducted in a centralized fluidized bed reactor to minimize the power-related exchanger costs. The quantity of solids contained in the fluidized bed reactor is small relative to the quantity of stored solids. Solids are transferred pneumatically from one container, through the fluidized bed, and to an empty container during operation.

Operation of the fluidized bed reactor is as follows. Assume, for example, that all of the solids are in the higher ammoniated state and that all of the containers, except one, are full. The operation is started by raising the temperature of the fluidized bed with the heat source to a value above the equilibrium temperature. The higher ammoniate in the reactor decomposes endothermically under these conditions. When the concentration of solids in the reactor approaches that of the lower ammoniate, pneumatic conveying of higher ammoniate solids is started. Simultaneously, the solids are withdrawn from the reactor at the same volumetric rate. Because the fluidized bed operates essentially at a uniform temperature and concentration throughout, the reaction conditions approximate those of a completely back-mixed reactor where the concentration of the effluent solids is the same as the average concentration of solids in the reactor. In this case, the average bed concentration is that of the lower ammoniate, which is pneumatically conveyed to the empty container. The higher ammoniate container can be used to receive the lower ammoniate when it is empty. This operation can be continued until all of the higher ammoniate has been converted to the lower ammoniate.

The reverse operation takes place as follows. The fluidized bed is cooled slightly below the equilibrium temperature and ammonia gas is supplied to start the exothermic recombination reaction. When the lower ammoniate in the reactor has been converted to the higher ammoniate, pneumatic conveying of the lower ammoniate is started from the storage containers. Because the reactor now contains a high concentration of the higher ammoniate, the solids withdrawn are essentially the higher ammoniate and are conveyed to the empty storage container. The operation is continued until the original conditions are restored.

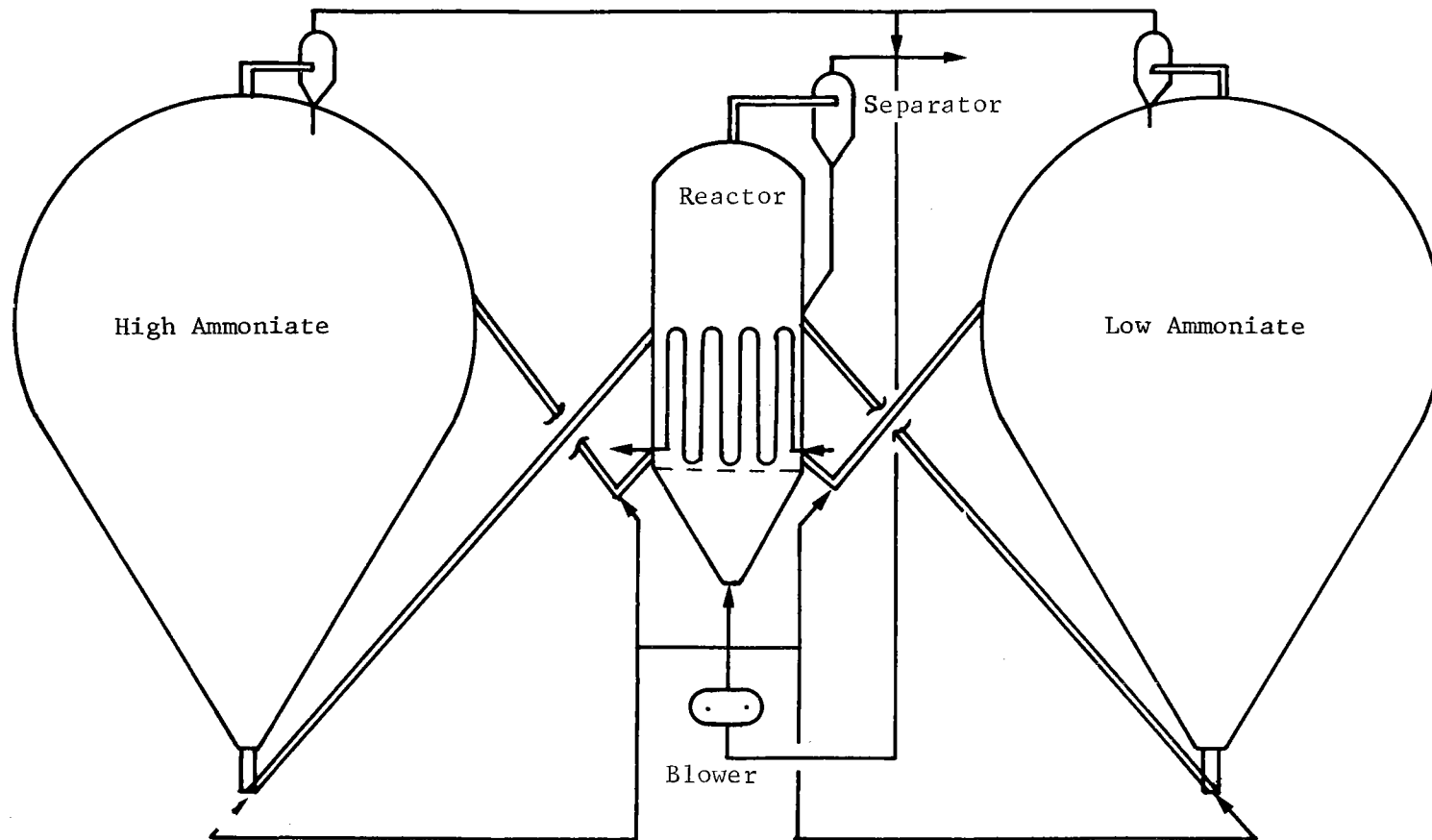


Figure VI-12 Fluid Bed Reactor with Solids Transport

2. Economic Analysis

A preliminary economic analysis was made to support the previous discussion. A relative comparison was made assuming that the energy storage system was used in a power plant application in which the base rate is 100 MWe and the storage discharge time is 10 hours at the base rate. Details of the analysis are presented in Appendix B.

Results of the economic analysis are presented in Table VI-9.

Table VI-9 Economic Comparison of Alternative Reactor Designs

	Number	Cs, \$/kWHe	Cp, \$/kWe	C, \$/kWe
Fixed-Bed Cylinders without Gas Recirculation	494	15.9	3000	3159
Fixed Bed with Gas Recirculation	12	9.0	750	840
Fluidized Bed D = L/2 = 20 ft	494	25.2	187.5	439.5
Storage Spheres with Fluidized Bed Reactor with Solids Transport	11 } 15 }	9.38	187.5	281.3

3. Conclusions

The conclusion from this phase is that the concept of spherical storage containers with fluidized bed reactors is the most economically attractive concept of the four considered.

VII. CONCLUSIONS

The overall conclusions from the Phase 1B Development of Ammoniated Salts Thermochemical Energy Storage Systems are as follows:

- 1) The concept is technically feasible,
- 2) The reactions tested are chemically reversible, and show no degradation over 100 cycles of ammoniation and deammoniation.
- 3) The concept is economically attractive for those specific applications considered, i.e., a 50 MWe steam-generator, solar power plant with a 10-hour storage capacity, and a 100 MWe conventional steam-generated power plant with a 24-hour storage capacity.
- 4) No technical problems were encountered that would preclude the use of this concept.

The overall conclusions are supported by the following specific conclusions:

A. COMPUTER MODELING

An analytical model was constructed for a laboratory-scale experimental reactor. Results obtained from the analytical model compared favorably with experimental data. The model has sufficient flexibility to evaluate a wide range of possible operating conditions.

The overall rate of the process for the conditions studied is limited by the heat transfer rate to and from the reactor. The rate of chemical reaction does not control the process.

B. CHEMICAL AND PHYSICAL PROPERTIES TESTING

- 1) Cycling does not affect the density, particle size, or surface area of the salts.
- 2) The reactions tested are chemically reversible, and show no degradation over 100 cycles of ammoniation and de-ammoniation.

- 3) Special care must be taken in the charging of a reactor to avoid formation of high density phases of the ammoniates.
- 4) Small amounts of moisture do not influence the reaction rates of the ammoniated salts.
- 5) The nonaqueous impurities tested do not influence the reaction rates of the ammoniated salts investigated.
- 6) The heats of reactions have been determined for the CaCl_2 and MgCl_2 ammoniates; however, their accuracy compared to the literature values was influenced by the experimental technique used.

C. SUBSCALE TESTING

- 1) The coupled ammoniated salt reactions are chemically reversible and the process is reproducible.
- 2) The heat balances conducted for the high temperature and low temperature reactors indicate the test hardware was operating as expected.

D. SYSTEM DESIGN AND ECONOMICS

The economic analysis indicated that:

- 1) The fixed bed chemical storage system without gas recirculation is not economically competitive with other systems considered in this study.
- 2) For a 50 MWe, 10 hr storage system the oil storage system had the lowest cost of the systems considered.
- 3) For a 100 MWe, 24 hr storage system the flow through chemical storage system had the lowest capital cost.
- 4) The comparisons are therefore somewhat inconclusive and are highly dependent on the specific power plant. This suggests that future work on this storage system should concentrate on other applications.

VIII.

RECOMMENDED FOLLOW-ON EFFORT

Several areas of future investigation were suggested by the results of the studies performed to date. The most significant area changes emphasis from a power plant application to applications that use a heat pump capability of the system to provide business and residential home heating and cooling. Reasons for the change in emphasis are: (1) the maximum temperature of any of the salts studied is limited to 650°F, which is below the 1000°F steam turbine inlet temperature most commonly used today, and would result in a loss in turbine efficiency; (2) the cost differential between the ammoniated salt storage system and the state-of-the-art oil system does not appear to be a compelling factor that would merit concentration on the power plant application; (3) the heat pump application can be developed and demonstrated on a much smaller scale and still provide data for other applications; and (4) it appears that the time required to develop and commercialize the heat pump application would be much less and therefore would result in a larger near-term energy savings.

Specific tasks suggested by the results of this program are as follows:

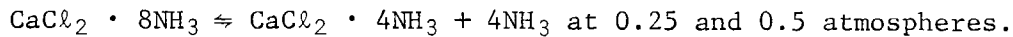
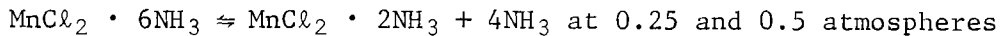
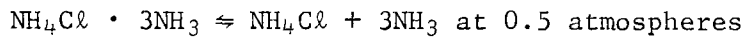
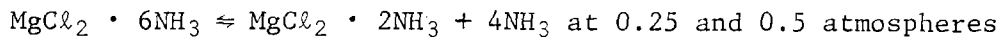
- 1) Chemical Testing - The subscale tests performed to demonstrate feasibility of using the paired reactions for cooling indicated that the reaction rate of the pairs tested ($\text{MgCl}_2 \cdot 6\text{NH}_3$ and $\text{MnCl}_2 \cdot 6\text{NH}_3$ with $\text{CaCl}_2 \cdot 8\text{NH}_3$) are relatively low at the operating temperature and pressures required; therefore, reaction rate testing of these salts at pressure below ambient is recommended. Further, a new low temperature ammoniate, $\text{NH}_4\text{Cl} \cdot 3\text{NH}_3$, might be a desirable alternative to the CaCl_2 , and should be characterized by measuring its chemical and physical properties.
- 2) Laboratory Scale System Testing - Heat transfer rates of the present reactors are low as indicated by data from the subscale testing and from the related heat transfer investigation (Ref III-3). To improve this low condition new solid salt reactors should be designed with multiple pass liquid heat exchangers and the capability of forced ammonia recirculation in each reactor. Also, a reactor to accommodate the liquid $\text{NH}_4\text{Cl} \cdot 3\text{NH}_3$ should be designed and fabricated. Ideally, the reactors should be sized so the amount of salt in each reactor contains an equal amount of transferrable ammonia. Thus, the paired reactions can be run to completion in either direction to provide data on the energy transfer rates near the reaction end points. The reactor test system should also be designed so each reactor can be run separately and effects of varying ammonia recirculation rate on heat transfer rate can be assessed.

- 3) Computer Models - A computer model of a typical home heat pump system should be coded so that system design calculations and tradeoffs can be made.

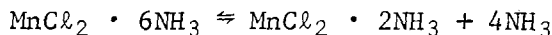
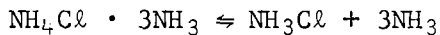
The proposed program for Phase II (Fig. VIII-1) is summarized in the following paragraphs.

A. TASK 1-CHEMICAL TESTS

Determine kinetics of dissociation/recombination for the following reactions.



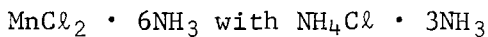
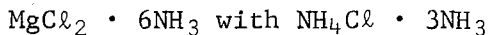
Determine heats of reaction for the following reactions.



Measure density and viscosity of $\text{NH}_4\text{Cl} \cdot 3\text{NH}_3$.

B. TASK 2-LABORATORY SCALE SYSTEM TESTS

Demonstrate the feasibility of the following pair of reactions.



Demonstrate the reversibility of the reactions of the salt pairs when the reactions are taken to completion.

Determine the effect of forced ammonia recirculation on reactor performance.

Obtain design and operating data to be used on the full-scale home heat pump system.

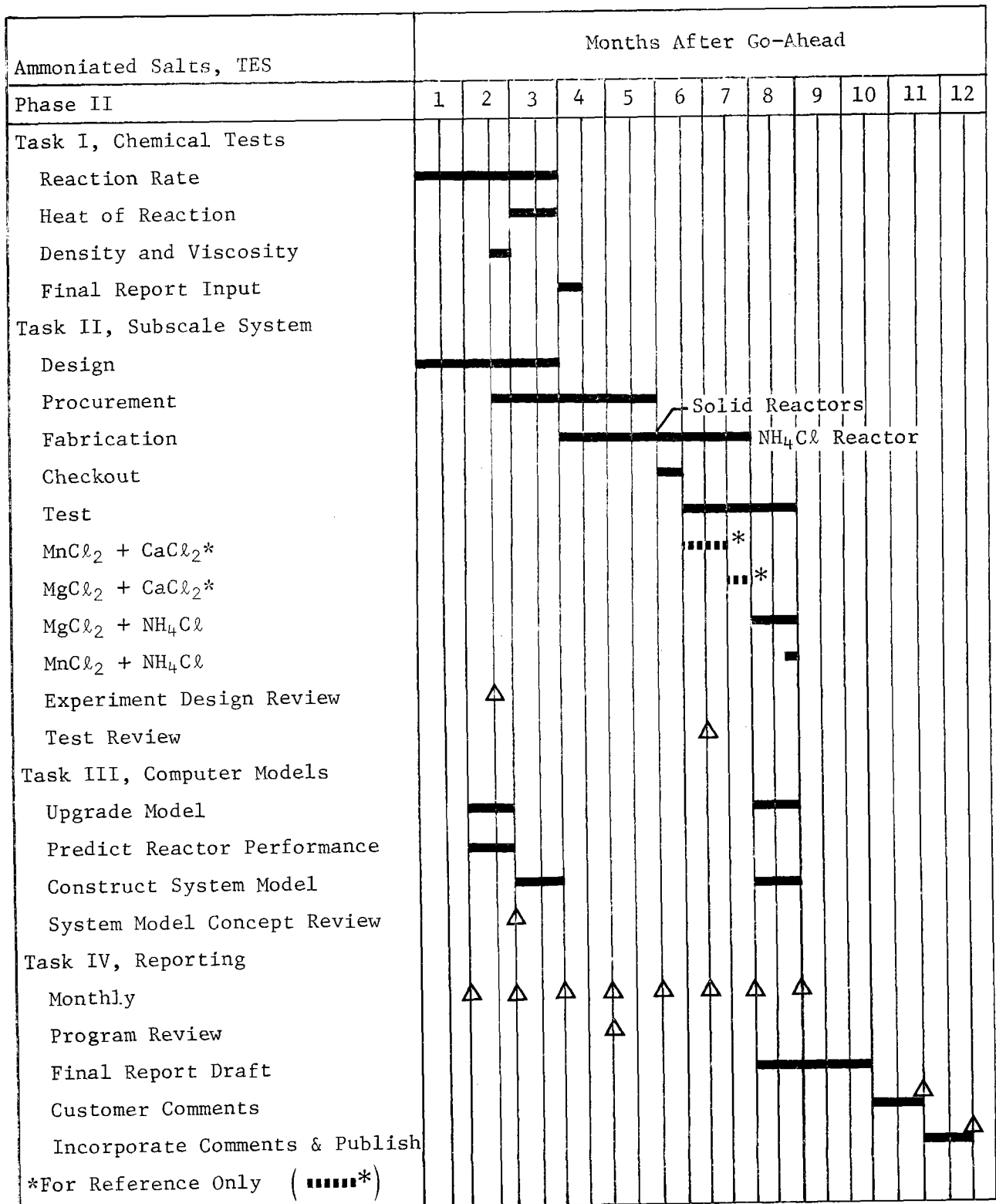


Figure VIII-1 Phase II Program Schedule

Design and fabricate the reactors to be used in this task and the reactors to be used in the solar cooling contract.

C. TASK 3—COMPUTER MODELS

Upgrade the reactor model developed in Phase Ib using data from Task I of Phase II.

Construct a computer model of a heat pump system and predict the performance of the prototype home cooling system.

D. SCHEDULE

The program span time is ten months. Reaction rate data will be obtained in the first three months and will be used as an aid in designing the reactors. The critical path for this contract is embodied in Task II. The sequence begins with the design phase, procurement, fabrication and assembly, checkout, and test and data reduction, and is estimated to take 8-½ months. A four-month final report preparation and approval phase is anticipated.

- III-1. Holmstead, G. M.: *Martin Marietta Interactive Thermal Analysis System, Version 2.0 (MITAS-II), User's Manual*. M-76-2, Martin Marietta Corporation, Denver, Colorado, May 1976.
- III-2. *Phase I, Initial Assessments, Final Report*. MCR-76-562, Martin Marietta Corporation, Denver, Colorado, 24 September 1976.
- III-3. Prenger, F. C.: *Heat Transfer in Packed Beds at Low Reynolds Number, Final Report*. Sandia Contract 87-8253, Martin Marietta Corporation, Denver, Colorado, Denver 1977.
- IV-1. Cullity, B. D. and Wesley, A.: *Elements of X-Ray Diffraction*. Chapter 10, 1967.
- IV-2. Chemical Rubber Company: *Handbook of Chemistry and Physics*. 48th Edition, Cleveland, Ohio, 1967, p B-163.
- IV-3. ASTM, "Symposium on Properties of Surfaces." ASTM Special Technical Publication No. 340, Philadelphia, PA, 1962, p 59-74.
- IV-4. Yound, D. M. and Crowell, A. D.: *Physical Absorption of Gases*. Butterworth Inc., Washington, D. C., 1962.
- IV-5. *International Critical Tables*
- V-1. Wnek, W. J. and Hass, W. R.: "The Equivalence and Numerical Solution of Regression, Optical Policy, and Boundary Value Problems Involving Differential Equations." *Journal of Computational Physics*, Vol 18, No. 3, July 1975, pp 326-341.
- VI-1. *An Assessment of Energy Storage Systems Suitable for Use by Electric Utilities*. Public Service Electric and Gas Co, Report ERDA E(11-1)-2501, 3 Volumes, July 1976.
- VI-2. Folk, W., Johnson, C. A., and Stotler, H. H.: "Effect of Reactor Internals on Quality of Fluidization," *Chem Engr Progr Symp, Serial No. 28*. 1962, p 58.
- VI-3. Wender and Cooper: *AIChE Journal*, Vol 4, March 1958, p 15.
- VI-4. Mickley, H. S. and Trilling, C.: "Heat Transfer Characteristics of Fluidized Beds." *Ind. Eng. Chem.*, Vol 41, 1949, pp 1135-1147.
- VI-5. Sharlovskaya, M. S.: *Convective Heat Transfer in a Fluidized Bed*. (in Russian), Kand Dissertat Tomsk Politchkn, Int, 1959 (Data Reported in Ref 9, Zabrodsky).

VI-6. Perry, J. N., *Chemical Engineers Handbook*, McGraw-Hill Publishing Co, New York, NY, 4th Ed. 1963, p 10-31.

VI-7. Brekhen, R. A., Lancaster, E. B. and Wheelock, T. D.: "Fluidization of Flour in a Stirred, Aerated Bed. Part I. General Fluidization Characteristics," *Chem. Eng. Progr. Symp. Serial No. 101*, 1970, p 66.

VI-8. Broadhurst, T. E., and Becker H. A.: "Onset of Fluidization and Slugging in Beds of Uniform Particles." *AIChE Journal*, Vol 21, No. 2, March 1975, pp 238-247.

VI-9. Zabrodsky, S. S., *Hydrodynamics and Heat Transfer in Fluidized Beds*, MIT Press, Cambridge, Mass, 1966, pp 1-12.

APPENDIX A - STORAGE SYSTEM SIZING AND COST CALCULATIONS

I. INTRODUCTION

Appendix A presents the approach and calculations used to size the storage system for two different sizes and types of power plants and defines the costs associated with the storage systems of interest. The study was limited to the following types and sizes of power plants:

- 1) Solar Power Plant, 50 MWe;
- 2) Conventional Power Plant, 100 MWe.

The storage systems considered were as follows:

- 1) Chemical Storage, fluidized bed and flow-through bed;
- 2) Sensible Heat Storage, oil.

The objective of the economic analysis was to provide insight to the economic attractiveness, if any, of a conceptual chemical storage system relative to a conceptual oil system supplying the same bus bar energy. If such an advantage exists, then the pursuit of the chemical storage system will be meaningful, at least for the power plant applications considered.

The following factors were considered in the economic analysis of the power plant storage:

- 1) Addition of storage capability must necessarily increase the bus bar cost of power over that from a power plant without the storage capability.
- 2) Addition of the storage capability permits a power plant to be flexible in meeting varying demands of the customer. This flexibility in terms of storage capability can result in the elimination of peaking equipment (turbines), which could result in a lower power cost for a network of plants with a given power load profile. This statement is particularly significant when we talk about the development of a new power plant.
- 3) The net value of storage can only be determined for a given utility network with its specific load profile. Thus the value of stored energy is not within our ability to evaluate in general terms. However, there are some utilities presently using water pumping storage systems to store energy. Also, preliminary studies indicate that thermal storage using the sensible heat of oil can be made competitive with the water pumping storage system (Ref A-1).

The preceding considerations imply that if a chemical storage system can be shown to be economically more attractive than an equivalent oil system, there is justification for further development of the chemical storage systems, at least for the applications considered. It must be recognized that the results of the economic analysis presented here are limited because each utility network has its own unique requirements.

The approach employed in this analysis is as follows:

- 1) The requirements are defined.
- 2) A storage system is defined for a given power plant, the system is sized, and the power-related and storage-related costs determined.
- 3) The definition, sizing, and costing process is repeated for each storage system of interest.
- 4) The costs are compared to determine the factors that influence the economic benefits of the various forms of energy storage considered.

The approach followed has certain drawbacks. The cost numbers obtained are not absolute numbers; therefore, only relative numbers are obtained that permit ranking of one storage system against another. Although extremely important, operating and maintenance costs are difficult or impossible to obtain at this time because of the conceptual nature of the designs considered. However, it is reasonable to assume that these costs are about the same regardless of the system. Therefore, the results of the analysis are valid for indicating whether one storage system is more attractive economically than another based on equipment costs.

II. SOLAR POWER PLANT

This section discusses the sizing and costing for a solar power plant. The section is divided in the following areas.

- A. Requirements
- B. Quantity of Storage Required
- C. Description of the Chemical Storage System
- D. Sizing of the Chemical Storage System with Fluidized Beds
- E. Cost of the Fluidized Bed Chemical Storage System
- F. Sizing the Chemical Storage System with a Flow-Through Bed
- G. Cost of the Chemical Storage System with a Flow-Through Bed
- H. Cost of the Oil Storage System

A. REQUIREMENTS

The energy storage system considered includes a steam generator, and a solar power plant providing electrical power similar to the Barstow Central Receiver Power Plant (Ref A-1). The requirements of this system are presented in Table A-1.

*Table A-1
Solar Power Plant Requirements*

Power:	50 MWe
Duration:	10 hr
Storage Capacity:	5.3×10^9 Btu

The charge and discharge states for steam are the same as those proposed for the Barstow Central Receiver Pilot Plant (Ref A-1) and are presented in Table A-2.

Table A-2 Charge and Discharge Steam States

	Pressure, psi	Temperature, °F	Saturation Temperature, °F
Charging Steam	1465	950	593
Discharging Steam	400	530	445

QUANTITY OF STORAGE REQUIRED

The $MgCl_2$ bed temperature is maintained at a temperature midway between the saturation temperature of the charging steam (593°F) and the saturation temperature of the discharging steam (445°F). The saturation temperature of the charging steam represents the source temperature for the charging power. The superheat energy is assumed at the saturation temperature for the heat exchanger sizing calculations (Ref A-2). The $MgCl_2$ bed temperature is the source temperature for the discharging steam. An equal driving potential, the temperature difference, is available for charging and discharging. This potential provides a nearly equal charging and discharging rate capability based on the temperature of the $MgCl_2$ bed being 519°F.

The storage system is sized to supply feedwater heating and steam latent heat. The feed water is assumed to exit the condenser at 160°F, which provides a standard 10 mm-Hg backpressure on the turbine. The water is heated to 445°F, which requires 296.6 Btu/lb (Ref A-3). The water undergoes a phase change to make saturated steam, which requires 780 Btu/lb. The steam is fed to a fuel-fired superheater and superheated to 530°F, which requires 60.1 Btu/lb. The storage system is required to supply all the required plant energy except the 60.1 Btu/lb for the superheater (94.7 percent of the required plant energy).

The storage system for the solar power plant system must be sized to produce 50 MWe for 10 hours. The conversion efficiency of the solar power plant proposed for Barstow is 30.4% (Ref A-1). The total energy, Q, that must be stored in the chemical storage system is

$$\begin{aligned}
 [A-1] \quad Q &= \frac{\text{Power requirement (watt)} \times 3.413 \frac{\text{Btu/hr}}{\text{watt}} \times \text{storage time (hr)} \times \text{storage \%}}{\text{Conversion efficiency}} \\
 &= 5.3 \times 10^9 \text{ Btu.}
 \end{aligned}$$

The energy storage units considered for satisfying these requirements were as follows:

- 1) Chemical Storage, fluidized bed and flow-through bed;
- 2) Sensible Heat Storage, oil.

C. DESCRIPTION OF THE CHEMICAL STORAGE SYSTEM

The pair of chemical reactions chosen for the chemical storage power application is

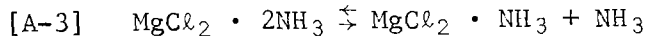
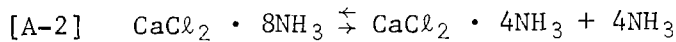


Figure A-1 presents a schematic representation of a chemical storage module in the heat storage mode (charge mode). Heat is extracted from the power plant boiler during the charge mode in the form of superheated steam (1465 psi, 950°F). The steam is condensed in a heat exchanger that is submerged in a 519°F fluidized bed of ammoniated MgCl_2 . Each module has four beds of ammoniated MgCl_2 . The number of modules is dictated by the molar balance shown in equations [A-2] and [A-3]. The heat from the condensing steam drives the ammonia off the ammoniated MgCl_2 . The ammonia flows to a CaCl_2 fluidized reactor at 100°F where it is absorbed to make ammoniated CaCl_2 . This absorption releases energy that is removed from the ambient temperature cooling water.

Figure A-2 presents a schematic representation of a chemical storage module in the discharge mode. During this mode, the storage system is supplying heat to the power plant. The heat is supplied to the plant in the form of saturated steam at 445°F, 400 psi. Low temperature energy from the power plant's heat rejection system is used to raise the ammoniated CaCl_2 bed temperature from 100°F to 105°F, which is its discharge state. The low-temperature energy added to the ammoniated CaCl_2 bed drives ammonia off the bed. The ammonia is transferred to the 519°F MgCl_2 bed where it combines with MgCl_2 and releases energy. The energy is removed from the bed by a water loop that brings in 160°F water and expels 445°F saturated steam that can be used for feedwater heating.

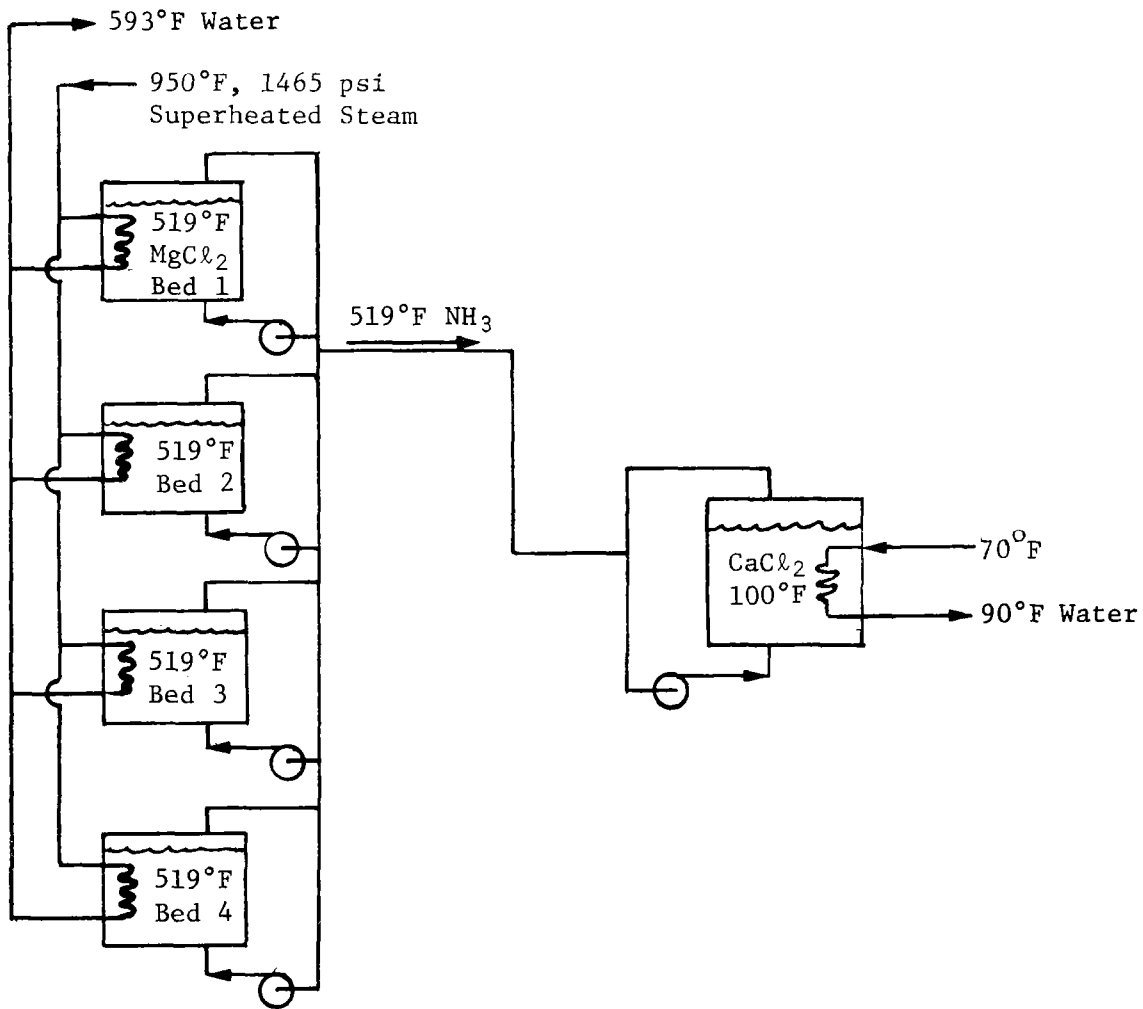


Figure A-1
 Schematic - Chemical Storage, Fluidized Bed Concept (Charging)

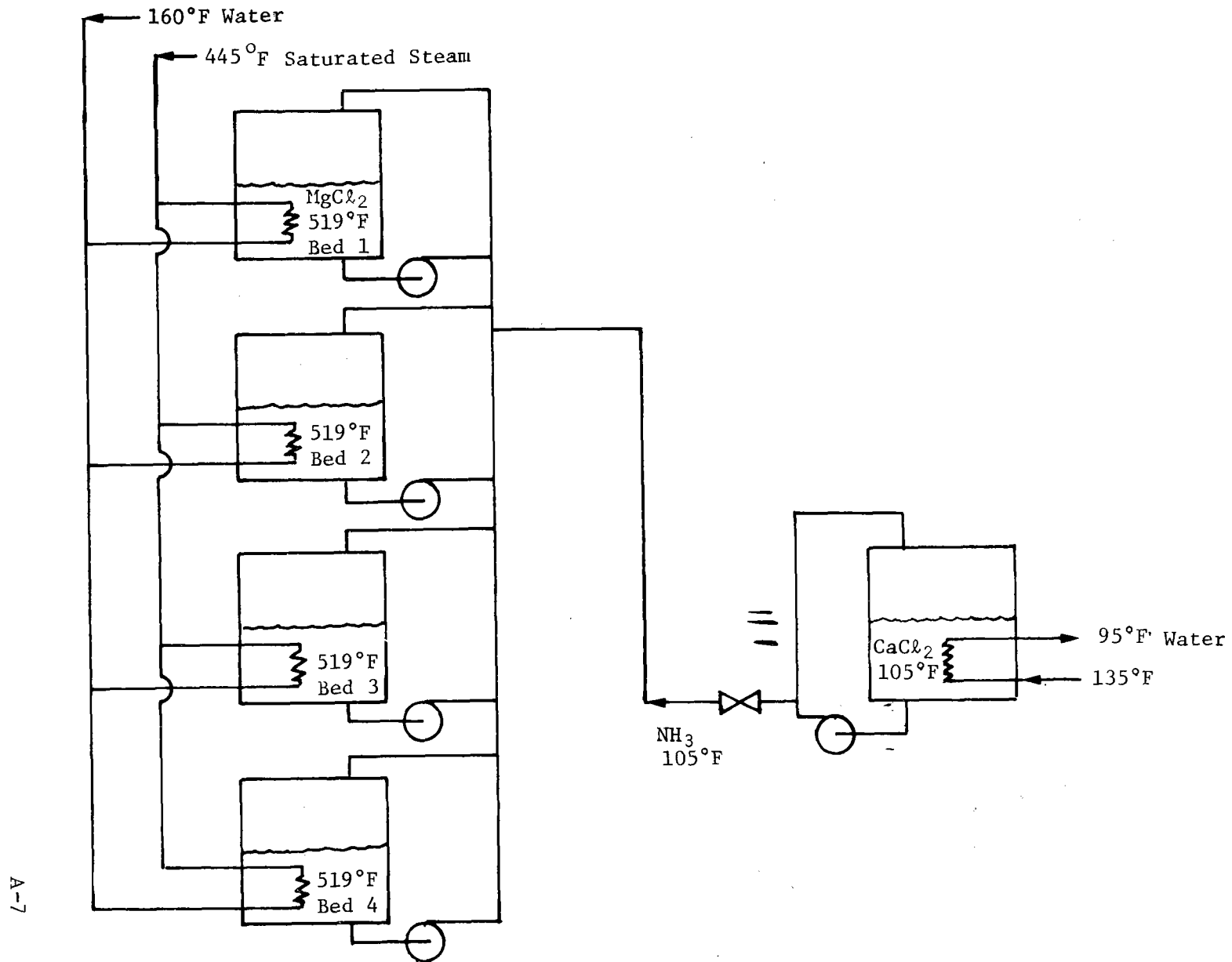


Figure A-2 Schematic - Chemical Storage, Fluidized Bed Concept (Discharging)

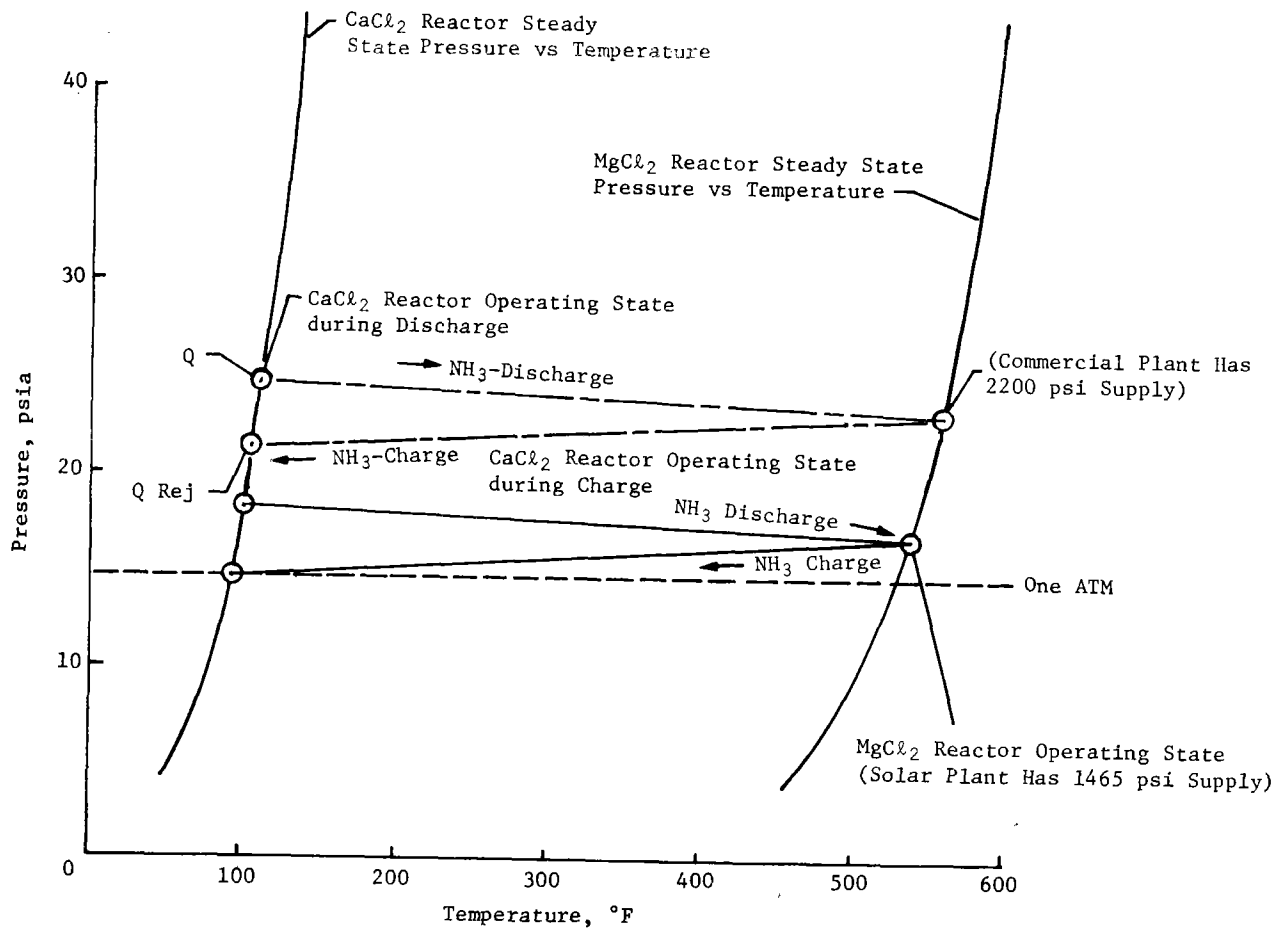


Figure A-3 Operating Characteristics of Salt Pair

The process just described is shown on a pressure-temperature diagram for ammoniated MgCl₂ and ammoniated CaCl₂ in Figure A-3. Figure A-3 shows the charge and discharge status of each reactor and direction of ammonia flow. The process for the commercial plant is shown in the same figure.

Figure A-4 illustrates a fixed bed concept for using the chemical energy in the ammoniated salt thermal storage system. Ammonia is pumped through the fixed bed in this system, but at velocities low enough that the bed is not fluidized.

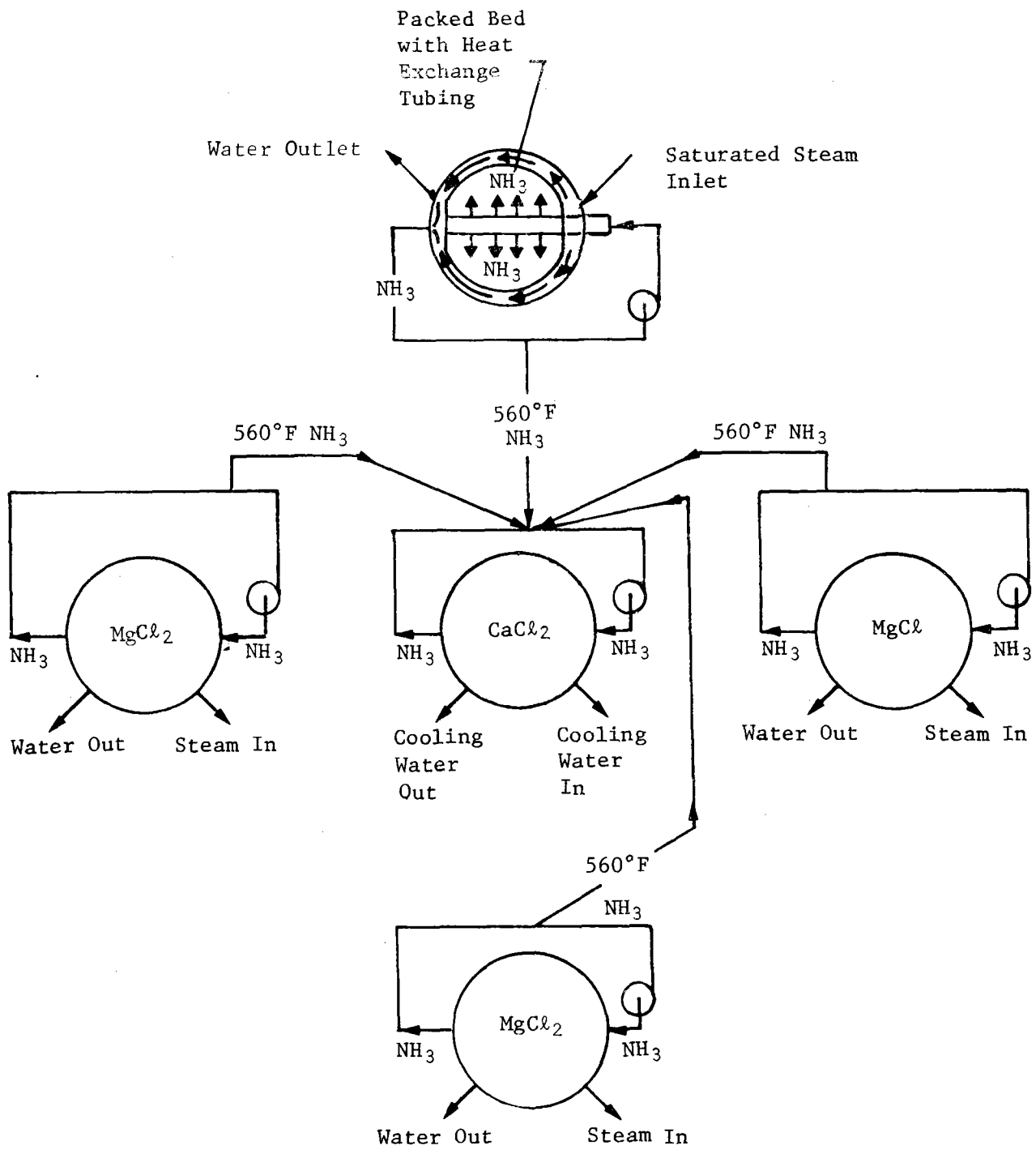


Figure A-4 Chemical Storage, Flow Through Bed-Charging Concept

D. SIZING THE CHEMICAL STORAGE SYSTEM WITH FLUIDIZED BEDS

The fluidized beds were sized in the following manner.

- 1) The quantity of $MgCl_2$ required was determined from the storage requirements.
- 2) The quantity of $MgCl_2$ that each reactor could hold was determined based on an assumed packing density for the $MgCl_2$.
- 3) The energy per module was determined.
- 4) The number of modules for the storage system was determined.
- 5) The quantity of $CaCl_2$ per module was determined.
- 6) The heat exchanger size for the $MgCl_2$ bed was determined.
- 7) The heat exchanger size for the $CaCl_2$ reactor was determined.
- 8) The lines were sized for the system.
- 9) The fluidizing compressor/motor was sized.

The details of the sizing analysis are presented in the following equation. The quantity of $MgCl_2$ (M_{MgCl_2}) is determined from

$$[A-4] \quad M_{MgCl_2} = \frac{Q}{q_{MgCl_2}}, \text{ lb}$$

where Q is the storage capacity of the system,

$$q_{MgCl_2} = \Delta hr_{MgCl_2} - q_{NH_3},$$

Δhr_{MgCl_2} is the heat of reaction for $MgCl_2 = 338 \text{ Btu/lb}$ (Table IV-6),

$$q_{NH_3} = \dot{m}_{NH_3} C_{P_{NH_3}} (T_2 - T_1), \text{ Btu/lb (MgCl}_2\text{)},$$

$$\dot{m}_{NH_3} = \frac{MW_{NH_3}}{MW_{MgCl_2}} M_{MgCl_2}, \text{ lb,}$$

MW is the molecular weight,

$$C_{P_{NH_3}} \text{ is the specific heat at constant pressure} \\ = 0.533 \text{ Btu/lb-}^\circ\text{F (Ref A-4),}$$

T_2 is the bed temperature of the $MgCl_2$ (519°F), and

T_1 is the bed temperature of the $CaCl_2$ (105°F).

Substituting the above values into equation [A-4], the quantity of $MgCl_2$ is determined:

$$M_{MgCl_2} = 17.8 \times 10^6 \text{ lb } MgCl_2.$$

The quantity of $MgCl_2$ that each reactor can hold is determined by assuming a packing density for the $MgCl_2$ and assuming a size for the bed. Assumptions are as follows:

- 1) The packing density of $MgCl_2$ is 30 lb/ft³ (Table IV-1);
- 2) The bed has a diameter equal to 30 ft and a depth equal to 30 ft (Ref A-5).

Therefore, the volume of the bed, a right circular cylinder, is 21,200 cubic feet. The $MgCl_2$ weight per reactor is the volume of the bed times the packing density of the $MgCl_2$. The resulting weight is 636,000 lb of $MgCl_2$ per reactor.

The molar balance from equations [A-2] and [A-3] dictate four $MgCl_2$ reactors for each $CaCl_2$ reactor in a module. The resulting $MgCl_2$ weight per module is 2,544,000 lb.

The quantity of $CaCl_2$ per module is determined by the $MgCl_2$ weight per reactor multiplied by the ratio of the molecular weights of $CaCl_2$ (111) and $MgCl_2$ (95). The resulting weight of $CaCl_2$ is 743,000 lb. The $CaCl_2$ reactor requires a packing density of 35 lb/ft³ (Table IV-2).

The energy storage per module is the $MgCl_2$ weight per module multiplied by the energy per pound of $MgCl_2$ (298.5 Btu/lb) or 759.38×10^6 Btu/module. The number of modules per storage system is determined by dividing the total storage requirement by the storage capacity per module. The resulting number of modules per storage system is seven.

The size of the heat exchangers for both the $MgCl_2$ bed and the $CaCl_2$ bed is calculated from equation [A-5]:

$$[A-5] \quad \dot{q} = UA\Delta T$$

where

\dot{q} is the heating rate in Btu/hr and is equal to the energy per module/duration

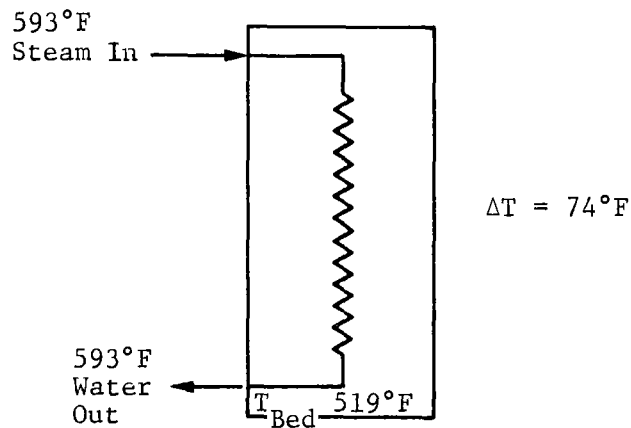
A is the heat exchanger area

U is the overall coefficient of heat transfer, and

ΔT is the temperature difference between the charging steam and the bed temperature.

For the charging mode, \dot{q} is equal to 18.9×10^6 Btu/hr/MgCl₂ bed.

The schematic for the charging heat exchanger follows.



The overall coefficient of heat transfer is

$$[A-6] \quad U = 1 / \left[(1/h_b) + f_t (1.2) + 1.2/h_t \right]$$

where

h_b is the bed side film coefficient,

f_t is the tube side fouling factor, and

h_t is the tube side film factor.

The inputs for equation A-6 are

$$h_b = 87 \text{ Btu/hr-}^\circ\text{F-ft}^2 \text{ (Ref A-6)}$$

$$f_t = 0.001 \text{ (Ref A-7)}$$

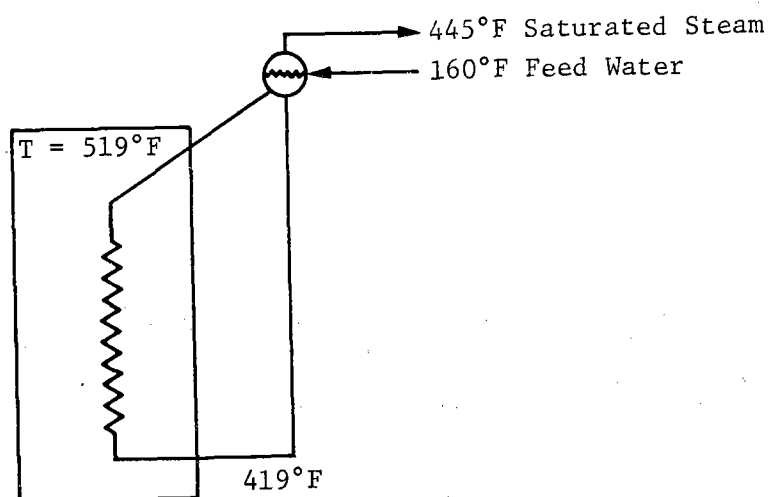
$$h_t = 900 \text{ Btu/hr-}^\circ\text{F-ft}^2 \text{ (Ref A-2).}$$

The bed side fouling was assumed to be zero because the abrasive action of the salt on the bed side of the tube is a fluidized bed should prevent scale buildup. The 1.2 factor in equation [A-6] is an approximate value for the outside-to-inside diameter of the tubes typically used in tubular shell and tube heat exchangers.

The overall coefficient of heat transfer is 70.6 Btu/hr-°F-ft². Substituting in equation [A-5] results in a heat exchanger area per MgCl₂ bed of 3618 ft².

The same bed heat exchanger is used for both charging and discharging. The larger of the areas for charging or discharging dictates the heat exchanger bed area.

A schematic of the heat exchanger for discharging, based on the assumption of a natural circulation boiler follows.

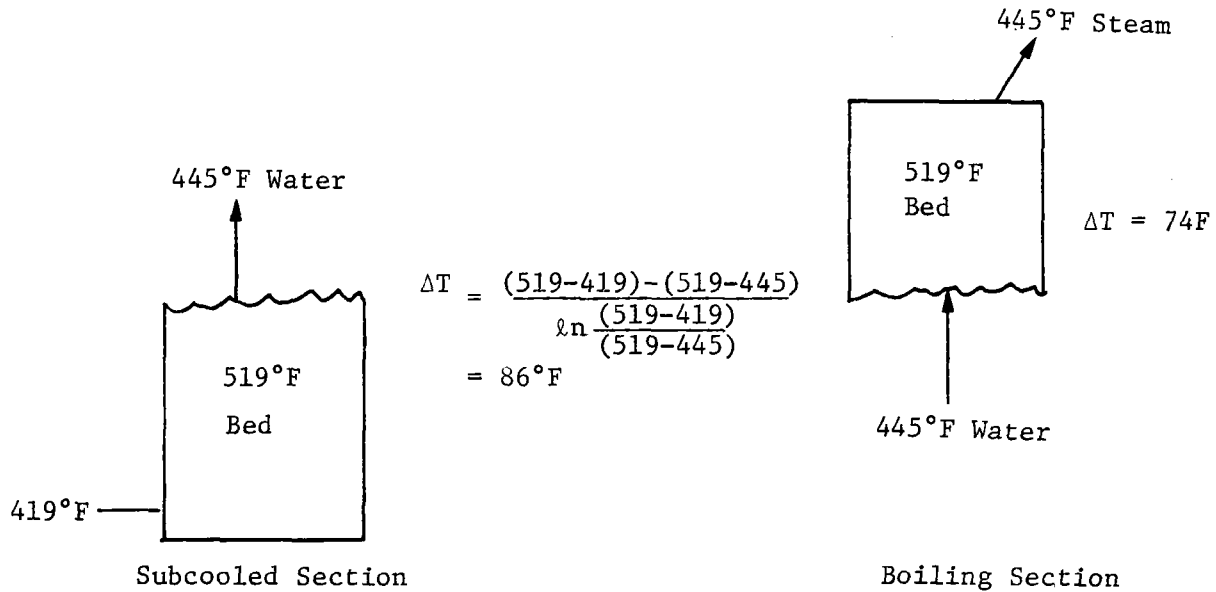


The natural circulation boiler is sized so the flow of steam and water in the boiler tubes is 11 times the steam outflow. The 11:1 circulation ratio is based on typical industrial practice (Ref A-8).

The water in the downcomer leg of the circulation system is 10 parts steam at 445°F and one part water at 160°F. The temperature entering the MgCl₂ bed is determined from

$$[A-7] \quad \Delta T = \frac{T_{\text{Water}} + \text{Recirculation Rate} (T_{\text{Steam}}), \text{ } ^\circ\text{F}}{\text{Total Rate}} = 419^\circ\text{F}$$

This means the water entering the $MgCl_2$ bed is subcooled $26^\circ F$. Therefore, the calculation of the area required for the cooler is divided in a subcooled section and a boiling section as shown in the following schematics.



The total change of enthalpy in the boiler is 1204.5 minus 129.4 Btu/lb or 1075.10 Btu/lb. The change in enthalpy for the subcooling is 424.5 minus 129.4 Btu/lb or 295.1 Btu/lb. The fraction of heat supplied to the subcooled water is 27.4%. The resulting subcooled heat load, q_{sc} , is

[A-8] $q_{sc} = 18.9 \times 10^6 \text{ Btu/hr} (0.274) = 5.18 \times 10^6 \text{ Btu/hr.}$

The overall coefficient of heat transfer determined from the following inputs is $33.4 \text{ Btu}/^\circ F\text{-hr-ft}^2$.

- 1) Bed side film coefficient = $87 \text{ Btu}/^\circ F\text{-hr-ft}^2$ (Ref A-6);
- 2) Tube side film coefficient = $70 \text{ Btu}/^\circ F\text{-hr-ft}^2$ (Ref A-2);
- 3) Tube side fouling factor = 0.001 (Ref A-7);
- 4) Bed side fouling factor = 0.

The area obtained for the subcooled section is calculated from equation [A-5] and is 1803 ft^2 .

The heat load for the boiling section is

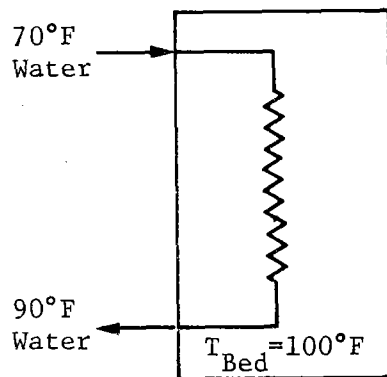
$$[A-9] \quad \dot{q}_{\text{Boiling}} = 18.9 \times 10^6 \text{ Btu/hr} (0.726) = 13.7 \times 10^6 \text{ Btu/hr.}$$

The overall coefficient of heat transfer is the same as that used for the analysis of the charging steam; $70.6 \text{ Btu/}^\circ\text{F-hr-ft}^2$. The resulting area for the heat exchanger of the boiling section is 2622 ft^2 .

The total heat exchanger area for discharging is 4425 ft^2 , which exceeds the requirement for charging; therefore, the total area required for the heat exchanger is the MgCl_2 reactor is 4425 ft^2 .

The rate of heat removal in the CaCl_2 reactor during the charging of the storage system is composed of (1) the chemical heat of reaction as the NH_3 is combined with the CaCl_2 , and (2) the sensible heat input to the system as the NH_3 is cooled from 519°F to 100°F . The total NH_3 transferred during a complete charge is $455,300 \text{ lb}$. The chemical reaction energy of the NH_3 is 1041 Btu/lb NH_3 ; therefore, the total chemical heat is $455,300 (1041)$ or $474 \times 10^6 \text{ Btu}$. The total sensible heat is $455,300 (0.533)$ ($519 - 100$) or $102 \times 10^6 \text{ Btu}$. The heat removal reate for a 10-hour charge time is $57.6 \times 10^6 \text{ Btu/hr}$.

The CaCl_2 reactor is assumed to be colled with 70°F river water. A schematic of the CaCl_2 reactor follows.



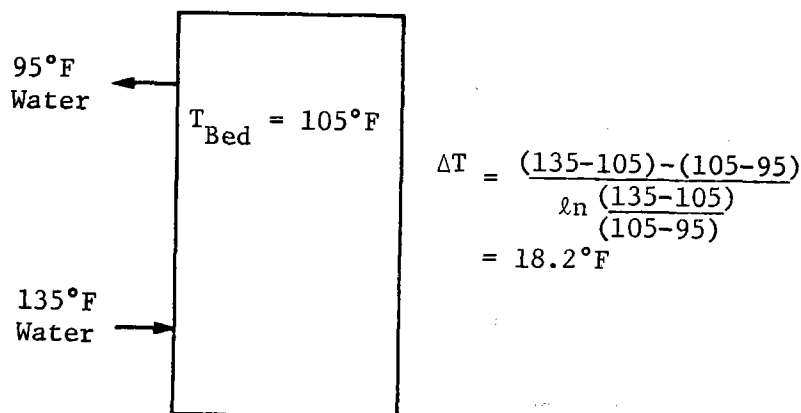
$$\Delta T_m = \frac{(100-70) - (100-90)}{\ln \frac{(100-70)}{(100-90)}} = 18.2^\circ\text{F}$$

The exit water temperature was chosen to provide a 10 F temperature difference for the heat exchanger. During the design of the actual system the exit water temperature will be based on an economic trade study that will consider pumping and heat exchanger costs.

The overall coefficient of heat transfer for the CaCl_2 reactor during charging is $45.4 \text{ Btu/hr-ft}^2\text{-}^\circ\text{F}$ based on the following inputs:

- 1) Bed side film coefficient, $87 \text{ Btu/hr-ft}^2\text{-}^\circ\text{F}$ (Ref A-6);
- 2) Tube side film coefficient, $150 \text{ Btu/hr-ft}^2\text{-}^\circ\text{F}$ (Ref A-2);
- 3) Tube side fouling factor = 0.002 (Ref A-7);
- 4) Bedside fouling factor = 0 .

The resulting area required for the heat exchanger during charging of the CaCl_2 reactor is $69,700 \text{ ft}^2$. As is the case with the MgCl_2 reactor, the CaCl_2 reactor uses the same heat exchanger during charging and discharging; therefore, an analysis similar to that performed for the MgCl_2 heat exchanger was conducted for the discharging case. In this analysis the heat necessary to raise the bed temperature from 100 to 105°F was neglected. Heat must be supplied at the rate of $47.4 \times 10^6 \text{ Btu/hr}$. An assumption is made that heat is supplied in the form of hot water available at 135°F with no penalty charged to the chemical storage system. The overall heat transfer coefficient is the same as for the charge cycle, $45.4 \text{ Btu/hr-ft}^2\text{-}^\circ\text{F}$. A schematic of the CaCl_2 reactor during discharge follows.



An area of $57,400 \text{ ft}^2$ of heat exchanger is necessary for discharging. The charging area is larger and, therefore, the CaCl_2 reactor requires $69,700 \text{ ft}^2$ of heat exchanger area.

The lines for carrying the NH_3 from the MgCl_2 reactors to the CaCl_2 reactor are sized using a continuity equation and the following assumptions:

- 1) The design velocity is 50 ft/sec;
- 2) The lines have circular cross section;
- 3) The density of ammonia at 32°F is 0.0482 lb/ft³ (Ref A-9).

The continuity equation states the mass flowrate, \dot{w} , is

$$[A-10] \quad \dot{w} = \rho AV$$

where

ρ is the density,

A is the area, and

V is the velocity.

The resulting area is 2.72 ft² for an ammonia flowrate of 11,384 lb/hr. The resulting diameter for the lines is 22.3 in but a 24-in. diameter will be assumed.

The fluidizing compressor/motor is sized in the following manner. A minimum fluidizing mass flux, G_{MIN} , is required to permit the bed to expand so the gas can flow without a pressure drop that exceeds the unit bed weight. The value of this minimum mass flux is estimated to be 4.8×10^{-4} lb/sec-ft² (Ref A-10). The area of the 30-ft diameter bed is 707 ft². The product of the bed area and the minimum mass flux results in a minimum fluidizing flowrate of 0.34 lb/sec. However, due to the irreversibility of the expansion of the bed, we will assume a fluidizing flowrate of 1 lb/sec (Ref A-11). The pressure drop through the bed is equal to the packing density of the bed multiplied by the depth of the bed or 900 lb/ft². The work required for fluidizing is represented by

$$\text{Work} = w (h_1 - h_2)$$

$$[A-11] \quad \dot{w}c_p = \frac{\dot{w}c_p}{R} (P_1V_1 - P_2V_2)$$

The fluidizing compressor/motor is sized for the minimum pressure, P_1 , of the ammonia or 2116.8 lb/ft² (Figure A-3). The upper pressure, P_2 , is equal to P_1 plus the delta pressure (900 lb/ft²) or 3016.8 lb/ft². The volume V_2 is found from the following equation of state:

$$[A-12] \quad pV^{\gamma} = \text{constant}$$

where

γ is the ratio of specific heats and equal to 1.3 for a triatomic gas (NH_3).

Substituting the above data in equation [A-11] results in theoretical work of 506 Btu/sec, which is 53 kilowatts or 71.6 horsepower. Therefore, a 100-horsepower motor will be used.

E. COST OF THE FLUIDIZED BED CHEMICAL STORAGE SYSTEM

The approach used to establish cost of the fluidized bed for the chemical storage system is based on the fixed capital cost estimation approach presented in Reference A-9 as well as individual quotes received from several manufacturers. The components costed were sized in Section II, paragraph B of Appendix A.

Costs were scaled up or down from the original estimates according to equation [A-13] which was obtained from Reference A-9.

$$[A-13] \quad C_n = r^n C$$

where

C_n is the cost of the new component,

C is the cost of the previous component,

r is the ratio of new to previous size (capacity), and

n is the cost exponential factor based on previous industrial experience and obtained from Reference A-9.

Table A-3 presents a summation of the costs for the equipment as well as the basis for the cost estimate.

The quantity of ammonia required was determined from equation [A-2] and the quantity of MgCl_2 required

$$[A-14] \quad (2,540,000((3)(17/95)) = 1,363,579 \text{ lb NH}_3$$

which is rounded off to 1,364,000 lb NH_3 .

Table A-3
Summary of Costs for the Chemical Storage System for the 50 MWe Solar Power Plant

Item	Qty/Module	Unit Cost, \$	Basis	Module Cost, \$	Cost per kWe-hr	\$/kWe
1. MgCl ₂	2,540,000 lb	0.20	Ref A-12	508,000	7.11	71.1
2. CaCl ₂	743,000 lb	0.05	Ref A-12	37,150	0.52	5.2
3. NH ₃	1,364,000 lb	0.10	Ref A-12	136,400	1.91	19.1
4. Fluidizing Compressors	5 ea	38,000	Ref A-13	190,000	2.66	26.6
5. Motors	5 ea	8,000	Ref A-1	40,000	0.56	5.6
6. MgCl ₂ Reactors	4 ea	325,000	Ref A-14	1,300,000	18.20	182.0
7. CaCl ₂ Reactor	1 ea	200,000	Ref A-14	200,000	2.80	28.0
8. MgCl ₂ Heat Exchanger	4 ea	8.26/ft ² x4425 ft ²	Ref A-1	146,280	2.05	20.5
9. CaCl ₂ Heat Exchanger	1 ea	8.26/ft ² x69,600	Ref A-1	575,200	8.05	80.5
10. Piping	840 ft, 24-in. dia	270/ft	Ref A-1, A-9	226,800	3.18	31.8
11. Valves, Control MgCl ₂ Reactor	4, 24-in. dia	6900	Ref A-1, A-9	27,600	0.39	3.9
Total				3,387,430	47.43	474.3
<p>System consists of seven modules or \$23,712,000 System storage capacity consists of 500,000 kWe-hr Total system cost, 47.43 \$/kWe-hr Storage related cost, 305.4 S/kWe Power related cost, 168.9 S/kWe</p> <p>Unit cost includes the drying of MgCl₂</p>						

The length of piping was determined in the following manner. The length of pipe from one $MgCl_2$ reactor to the $CaCl_2$ reactor was estimated to be 60 feet. This length was multiplied by two to account for expansion and then multiplied by four for each of the reactors resulting in 480 feet of pipe. The fluidizing line was assumed to be 45-ft long and multiplied by two for expansion and by four for the four loops resulting in 360 feet of pipe; therefore, the total length of 24-inch diameter pipe required was 840 feet.

F. SIZING THE CHEMICAL STORAGE SYSTEM WITH A FLOW-THROUGH BED

The chemical storage system using a flow-through bed is sized in the same manner as the system using the fluidized bed.

The amount of $MgCl_2$ required for the storage system for the 50 MWe solar plant is 17.8×10^6 lb, the same amount required for the fluidized bed. The same rationale used before dictates four $MgCl_2$ reactors per $CaCl_2$ reactor. Therefore, one-fourth the $MgCl_2$ is handled in each spherical tank or 4.45×10^6 lb. Assuming a packing density of 30 lb/ft^3 (Section II) for $MgCl_2$, the volume required for each tank is $148,333 \text{ ft}^3$. The necessary diameter of the spherical tank is 66 feet. Therefore, the 50 MWe system will consist of one module of five spherical tanks, each with a diameter of 66 ft. The energy per module is 5300×10^6 Btu or 1.55×10^6 kW-hr. The charge and discharge rate is 530×10^6 Btu/hr. The charge and discharge rate is 530×10^6 Btu/hr.

The size of the $MgCl_2$ heat exchanger for charging is determined from equation [A-5]. The inputs for this equation are

$$q \text{ is } 132.5 \times 10^6 \text{ Btu/hr,}$$

$$U \text{ is } 18.7 \text{ Btu/}^\circ\text{F-hr-ft}^2 \text{ from equation [A-6],}$$

$$h_b \text{ is } 20.0 \text{ Btu/}^\circ\text{F-hr-ft}^2 \text{ (Ref A-6),}$$

$$f_t = 0.001 \text{ (Ref A-7),}$$

$$f_b = 0.001 \text{ (Ref A-7),}$$

$$h_t = 900 \text{ Btu/}^\circ\text{F-hr-ft}^2 \text{ (Ref A-2), and}$$

$$T = 90^\circ\text{F.}$$

The resulting area for the heat exchanger is $78,730 \text{ ft}^2$.

The discharge case requires an area of 4183 ft² for the sub-cooled section and 11,358 ft² for the boiler section. Therefore, the required size for the heat exchanger for the MgCl₂ reactor is 78,730 ft².

The heat exchanger for the CaCl₂ reactor requires 19,400 ft² based on the charging mode of operation which governs in this case.

The diameter of the lines per equation [A-7] is 1.96 feet or 24 inches.

G. COST OF THE CHEMICAL STORAGE SYSTEM WITH A FLOW THROUGH BED

The cost of this system was determined in the same manner as shown in Section II, paragraph C of Appendix A. Table-A-4 presents a summation of the costs for the equipment as well as the basis for the cost estimate.

Table A-4

Summary of the Costs for the Chemical Storage System Using the Flow-Through Bed for a 50 MWe Solar Power Plant

A-22

Item	Qty/Module	Unit Cost, \$	Basis	Module Cost, \$	Cost per kWe-hr	\$/kWe
1. MgCl ₂	2,540,000 lb	0.20	Ref A-12	508,000	7.11	71.1
2. CaCl ₂	743,000 lb	0.05	Ref A-12	37,150	.52	5.2
3. NH ₃	1,364,000 lb	0.10	Ref a-12	136,400	1.91	19.1
4. Compressor/Motor	5 ea	300,000	Ref A-13	1,500,000	21.00	210.0
5. MgCl ₂ Tanks	4 ea	620,000	Ref A-14, A-9	2,480,000	34.72	347.2
6. CaCl ₂ Tank	1 ea	620,000	Ref A-14, A-9	620,000	8.68	86.8
7. MgCl ₂ Heat Exchanger	4 ea	8.26/ft ² x8730 ft ²	Ref A-1	288,600	4.04	40.4
8. CaCl ₂ Heat Exchanger	1 ea	8.26/ft ² x19400 ft ²	Ref A-1	160,350	2.24	22.4
9. Piping	840 ft/24-in.	270/ft	Ref A-1, A-9	226,800	3.18	31.8
10. Valves	8	27,200	Ref A-1	218,000	3.05	30.5
Total				6,175,300	86.56	846.5

System consists of seven modules or \$43,227,100
 System Storage Capacity consists of 500,000 kWe-hr
 Total System Cost, 86.45 \$/kWe-hr
 Storage Related Cost, 529.4 \$/kWe
 Power Related Cost, 317.1 \$/kWe

H. SIZING THE OIL STORAGE SYSTEM

The oil storage system, shown schematically in Figure A-5, was sized and preliminary cost numbers generated so the oil storage system cost and the chemical system cost could be compared.

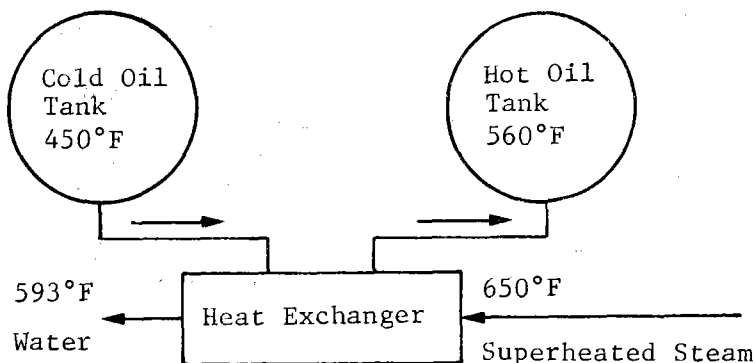


Figure A-5 Schematic of Oil Storage System-Charging

The oil storage system operates in the following manner. Heat is extracted from the power plant boiler during the charge mode in the form of saturated steam (650°F, 2200 psi). The steam is condensed in the heat exchanger that transfers the latent heat of the steam to the hydrocarbon oil storage fluid. The oil is heated from its cold reservoir temperature of 450°F to its hot reservoir temperature of 560°F.

During the discharge mode the oil flow is reversed bringing hot oil of 560°F into the heat exchanger and cooling it to 450°F. The heat that the oil gives up is transferred to feedwater, which enters the heat exchanger of 160°F and exits the exchanger as saturated steam at 450°F.

The Barstow studies (Ref A-1) state that the maximum oil storage temperature for this type of system is 570°F and the cold oil storage system is 460°F.

The oil storage system is sized in a manner similar to the chemical storage systems. The requirement for 5.3×10^9 Btu of stored energy translates to 71.9×10^6 pounds of oil, assuming the latent heat transferred to the oil is 73.7 Btu/lb ($0.67 \times (570-460)$). Reference A-1 indicates that the system is 96% effective with a hold-up in the system of 5%. Therefore, the amount of oil required increased to 78.6×10^6 pounds of oil.

Discussions with Pittsburg Des Moines Steel Company (Ref A-14) indicate that the maximum size spherical tanks that can be commercially built are 75-ft diameter. Therefore, the maximum volume per tank is 221,000 ft³. Assuming a density for oil of 45 lb/ft³ and 9% ullage in the tank, each tank holds 9,050,000 pounds of oil; therefore, nine spherical tanks are required to hold the oil. Also, the oil in a hot tank is required to transfer to a cold tank, which means one additional tank is required. As a hot tank is emptied, it becomes the cold tank for the next hot tank. Thus, a total of ten spherical oil tanks are required.

The heat exchanger is sized by the discharge mode of operation for this system. The rate of discharge required is 5.3×10^8 Btu/hr. The temperature of the oil at the saturated water point, T_{oil_SWP} , is 491°F. The temperature difference for the sub-cooled section of the heat exchanger is 39°F. The overall coefficient of heat transfer is 33 Btu/hr-ft²-°F based on the following film coefficients.

$$[A15] \quad h_{\text{water side}} = 70 \text{ Btu/hr-ft}^2\text{-}^\circ\text{F (Ref A-2)}$$

$$[A16] \quad h_{\text{oil side}} = 100 \text{ Btu/hr-ft}^2\text{-}^\circ\text{F (Ref A-2)}$$

The subcooled heat load is 148×10^6 Btu/hr. Therefore, using the preceding inputs and equation [A-5], the heat transfer area for the subcooled section is 115,000 ft². The heat transfer area for the boiler section, calculated in a similar manner, is 75,500 ft². Thus, the total area required for the heat exchanger is 190,600 ft².

I. COST OF THE OIL STORAGE SYSTEM

The cost of the oil storage system was determined in the same manner as shown in Section II, paragraph C of Appendix A. Table A-5 presents a summation of the costs for the equipment as well as the basis for the cost estimate.

Table A-5 Summary of Costs for the Oil Storage System for a 50 MWe Solar Power Plant

Item	Qty/Module	Unit Cost, \$	Basis	Module Cost, \$	Cost per kWe/hr	\$/kWe
1. Oil	78.6x10 ⁶ lb	0.13	Ref A-12	10,218,000	20.44	204.4
2. Tanks	10 ea	845,000	Ref A-14	8,450,000	16.90	169.0
3. Heat Exchanger	1 ea	$\frac{20}{2.42} \times 190,500$	Ref A-1	1,574,400	3.15	31.5
4. Piping	800 ft	277	Ref A-1, A-9	2,216,000	4.43	44.3
5. Pumps	2 ea (20,000 gpm)	82,000	Ref A-1, A-9	164,000	0.33	3.3
6. Valves	18 ea	13,699	Ref A-1, A-9	224,800	0.49	4.9
Total				22,863,200	45.74	457.4
System consists of one module or \$22,863,200 System Storage capacity consists of 500,000 kWe-hr Total system cost, 45.74 \$/kWe-hr Storage related cost, 37.34 \$/kWe-hr Power related cost, 84.0 \$/kWe						

III. CONVENTIONAL COMMERCIAL POWER PLANT

This section discusses the sizing and costing for a conventional power plant. The section is divided into the following areas:

- A. Requirements
- B. Quantity of Storage Required
- C. Description of the Chemical Storage System
- D. Sizing the Chemical Storage System with Fluidized Bed
- E. Cost of the Fluidized Bed Chemical Storage System
- F. Sizing the Chemical Storage System with a Flow Through Bed
- G. Cost of the Chemical Storage System with a Flow Through Bed
- H. Sizing the Oil Storage System
- I. Cost of the Oil Storage System

A. REQUIREMENTS

The energy storage systems considered here are for a steam-generated power plant providing electrical power. Superheating is used to bring the steam to the desired temperature. The requirements for this system are presented in Table A-6.

*Table A-6
Conventional Power Plant Requirements*

Power:	100 MWe
Duration:	24 hr
Storage Capacity:	21.9×10^9 Btu

The charge and discharge states for steam are similar to the states mentioned in Reference A-15 for a modern steam plant and are presented in Table A-7.

Table A-7 Charge and Discharge Steam States

	Pressure, psi	Temperature, °F	Saturation Temperature, °F
Charging Steam	2200	1000	650
Discharging Steam	423	560	450

B. QUANTITY OF STORAGE REQUIRED

The $MgCl_2$ bed temperature is maintained at a temperature midway between the saturation temperature of the charging steam ($650^\circ F$) and the saturation temperature of the discharging steam ($450^\circ F$). The saturation temperature of the charging steam represents the source temperature for the charging power. The superheat energy is assumed at the saturation temperature for heat exchanger sizing and calculations (Ref A-2). The $MgCl_2$ bed temperature is the source temperature for the discharging steam. An equally driving potential, the temperature difference, is available for charging and discharging, leading to a nearly equal charging and discharging rate capability with the preceding $MgCl_2$ bed temperature.

The discharge system from storage supplied saturated steam at $450^\circ F$. The additional energy required to supply superheat to get the steam to $560^\circ F$ is supplied from a fuel-fired, external source. The requirement is necessary because the bed temperature is $550^\circ F$ and cannot supply energy to $560^\circ F$ steam.

The storage system is sized to supply feedwater heating and steam latent heat. The feedwater is assumed to exit the condenser at $160^\circ F$, which provides a standard 10 mm-Hg back pressure on the turbine. The water is heated to $450^\circ F$, which requires 302.2 Btu/lb (Ref A-3). The water is boiled to make saturated steam, which requires 774.5 Btu/lb. The steam then exits the storage system heat exchangers and enters a fuel-fired superheater that superheats the steam to $560^\circ F$, which requires 76.3 Btu/lb. The storage system is required to supply all required plant energy except the 76.3 Btu/lb for the superheater or 93.4 percent of the required plant energy.

The storage system for the conventional power plant system must be sized for 100 MWe for 24 hours. The conversion efficiency of the conventional power plant is 35% (Ref A-1). The total energy that must be stored in the chemical storage system is determined from equation A-1 to be 21.9×10^9 Btu.

The energy storage units considered for satisfying these requirements were as follows:

- 1) Chemical Storage, fluidized bed and flow-through bed;
- 2) Sensible Heat Storage, oil

C. DESCRIPTION OF THE CHEMICAL STORAGE SYSTEM

The description of the chemical storage system given in Section II, paragraph C. of Appendix A is applicable except for the temperatures of the steam and the beds.

Figure A-1 presents a schematic representation of a chemical storage module in the heat storage mode (charge mode). Heat is extracted from the power plant boiler during the charge mode in the form of superheated steam (100°F, 2200 psi). The steam is condensed in a heat exchanger that is submerged in a 560°F fluidized bed of ammoniated $MgCl_2$. Each module has four beds of ammoniated $MgCl_2$. The ammonia flows to a $CaCl_2$ fluidized reactor at 105°F where it is absorbed to make ammoniated $CaCl_2$. This absorption releases energy that is removed from the ambient temperature cooling water.

Figure A-2 presents a schematic representation of a chemical storage module in the discharge mode. The storage system during the discharge mode is supplying heat to the power plant. The heat is supplied to the plant in the form of saturated steam at 450°F, 423 psi. Low-temperature energy from the power plant's heat rejection system is used to raise the ammoniated $CaCl_2$ bed temperature from 105°F to 110°F, its discharge state. The low-temperature energy added to the ammoniated $CaCl_2$ bed drives ammonia off this bed. The ammonia is transferred to the 560°F $MgCl_2$ bed where it combines with $MgCl_2$ and releases energy. The energy is removed from the bed by a water loop that brings in 160°F water and expels 450°F saturated steam that can be used for feedwater heating.

D. SIZING THE CHEMICAL STORAGE SYSTEM WITH FLUIDIZED BEDS

The fluidized beds were sized in the same manner as in Section II, paragraph D of Appendix A, namely:

- 1) The quantity of $MgCl_2$ required was determined from the storage requirements.

- 2) The quantity of $MgCl_2$ that each reactor could hold was determined based on an assumed packing density for the $MgCl_2$.
- 3) The energy per module was determined.
- 4) The number of modules for the storage system was determined.
- 5) The quantity of $CaCl_2$ per module was determined.
- 6) The heat exchanger size for the $MgCl_2$ bed was determined.
- 7) The heat exchanger size for the $CaCl_2$ reactor was determined.
- 8) The lines were sized for the system.
- 9) The fluidizing compressor/motor was sized.

The quantity of $MgCl_2$ required is 79.32×10^6 lb. Using the same assumptions made for the packing density of $MgCl_2$ and bed size, the weight of $MgCl_2$ per reactor is 636,000 lb and the energy per module is 759.38×10^6 Btu.

The number of modules for the storage system is the energy storage requirement divided by the storage capacity per module. This results in a requirement for 31 modules.

The quantity of $CaCl_2$ required per module is 743,000 lb.

The heat exchanger size for the $MgCl_2$ bed for the charging mode of operation is 4930 ft^2 . The heat exchanger size for the $CaCl_2$ reactor is calculated to be 69,000 ft^2 .

The lines for the 100 MWe system are 16-in. diameter. The fluidizing compressor/motor needs 100 hp.

E. COST OF THE FLUIDIZED BED CHEMICAL STORAGE SYSTEM

The cost of the system was determined in the same manner as that shown in Section II, paragraph C of Appendix A. Table A-8 presents a summation of the costs for the equipment as well as the basis for the cost estimate.

Table A-8 Summary of Costs for the Chemical Storage System for the 100 MWe Conventional Power Plant

A-30

Item	Qty/Module	Unit Cost, \$	Basis	Module Cost, \$	Cost per kWe-hr	\$/kWe
1. MgCl ₂ *	2,540,000 lb	0.20	Ref A-12	508,000	6.56	157.5
2. CaCl ₂	743,000 lb	0.05	Ref A-12	37,150	0.48	11.5
3. NH ₃	1,364,000 lb	0.10	Ref A-12	136,400	1.76	42.3
4. Fluidizing Compressors	5 ea	38,000	Ref A-13	190,000	2.45	58.9
5. Motors	5 ea	8,000	Ref A-1	40,000	0.52	12.4
6. MgCl ₂ Reactors	4 ea	325,000	Ref A-14	1,300,000	16.79	403.0
7. CaCl ₂ Reactor	1 ea	200,000	Ref A-14	200,000	2.58	62.0
8. MgCl ₂ Heat Exchanger	4 ea	8.26/ft ² x 4930	Ref A-1	163,000	2.11	50.5
9. CaCl ₂ Heat Exchanger	1 ea	8.26/ft ² x 69,600	Ref A-1	575,200	7.43	178.3
10. Piping	840 ft, 16-in. dia	170/ft	Ref A-1, A-9	142,800	1.84	44.3
11. Valves, Control MgCl ₂ Reactor	4, 16-in. dia	5400	Ref A-1, A-9	21,600	0.28	6.7
Total				3,314,150	42.80	1027.4
<p>System consists of 31 modules or \$102,738,650 System storage capacity consists of 2,400,000 kWe-hr Total system cost, 42.8 \$/kWe-hr Storage related cost, 676.3 \$/kWe Power related cost, 351.1 \$/kWe</p>						
* Unit Cost Includes Drying of MgCl ₂						

F. SIZING THE CHEMICAL STORAGE SYSTEM WITH A FLOW-THROUGH BED

The system is sized using previously described relationships. The 100 MWe storage system consists of three modules. Each module consists of four 75-ft diameter spherical tanks for MgCl_2 and one 75-ft diameter spherical tank for CaCl_2 . The heat exchanger for the MgCl_2 reactor requires 41,200 ft^2 of area and the heat exchanger for the CaCl_2 reactor requires 667,000 ft^2 of area. The diameter of the pipes is 30 inches.

G. COST OF THE CHEMICAL STORAGE SYSTEM WITH A FLOW-THROUGH BED

The cost of this system was determined in the same manner as that show in Section II, paragraph C of Appendix A. Table A-9 presents a summation of the costs.

H. SIZING THE OIL STORAGE SYSTEM

The oil storage system is sized using previously described methods. The system requires 347×10^6 lb of oil. Assuming a spherical tank diameter of 75 ft results in a requirement for 40 oil tanks. The area of the heat exchanger is 350,000 ft^2 .

I. COST OF THE OIL STORAGE SYSTEM

The cost of the oil storage system was determined in the same manner as those shown in Section II, paragraph C of Appendix A. Table A-10 presents a summation of the costs for the equipment as well as the basis for the cost estimate.

Table A-9

Summary of Costs for the Chemical Storage System Using the Flow-Through Bed for a Conventional 100 MWe Power Plant

A-32

Item	Qty/Module	Unit Cost, \$	Basis	Module Cost, \$	Cost per kWe-hr, \$	\$/kWe
1. MgCl ₂	26,520,000 lb	0.20	Ref A-12	5,304,000	6.63	159.1
2. CaCl ₂	5,680,000 lb	0.05	Ref A-12	284,000	0.36	8.5
3. NH ₃	6,840,000 lb	0.10	Ref A-12	684,000	0.86	20.5
4. Compressor Motor	5 ea	500,000	Ref A-13	2,500,000	3.13	75.0
5. MgCl ₂ Tanks	4 ea	845,000	Ref A-14, A-9	3,380,000	4.23	101.4
6. CaCl ₂ Tank	1 ea	845,000	Ref A-14, A-9	845,000	1.06	25.4
7. MgCl ₂ Heat Exchanger	4 ea	8.26/ft ² x 48,000	Ref A-1	1,600,000	2.00	48.0
8. CaCl ₂ Heat Exchanger	1 ea	8.26/ft ² x 667,000	Ref A-1	5,500,000	6.88	165.0
9. Piping	3600 ft/30 in.	326/ft 27,200	Ref A-1, A-9	1,170,000	1.46	35.1
10. Valves	12 ea		Ref A-1	326,000	0.41	9.8
Total				21,593,000	27.02	648.8

System consists of three modules or 64,779,000
 System storage capacity consists of 2,400,000 kWe-hr
 Total system cost, 27.02 \$/kWe-hr
 Storage related cost, 314.9 \$/kWe
 Power related cost, 333.9 \$/kWe

Table A-10 Summary of Costs for Oil Storage System for a 100 MWe Commercial Power Plant

Item	Qty/Module	Unit Cost, \$	Basis	Module Cost, \$	Cost per kWe-hr, \$	\$/kWe
1. Oil	347 x 10 ⁶	0.13	Ref A-12	45,100,000	18.79	451.0
2. Tanks	40 ea	845,000	Ref A-14	33,800,000	14.08	338.0
3. Heat Exchanger	350,000 ft ²	8.26	Ref A-1	2,893,000	1.21	28.9
4. Piping	32,000 ft	326/ft	Ref A-1, A-9	10,400,000	4.33	104.0
5. Pumps	2 (40,000 gpm)	160,000	Ref A-1, A-9	320,000	0.13	3.2
6. Valves	80 ea	27,200	Ref A-1, A-9	2,176,000	0.91	21.8
Total				94,689,000	39.45	946.90
<p>System consists of one module or \$94,689,000 System storage capacity consists of 2,400,000 kWe-hr Total system cost, 39.45 \$kWe/hr Storage related cost, 789.0 \$kWe Power related cost, 157.9 \$kWe</p>						

IV.

REFERENCES

-
- A-1. McDonnell Douglas: *Central Receiver Solar Thermal Power Systems*. Phase I, Volume V, Thermal Storage Subsystem. Report MDC G-6776, May 1977.
- A-2. Kreith, F.: *Principles of Heat Transfer*, 1959.
- A-3. Keenan, J. H. and Keyes, F. G.: *Thermodynamic Properties of Steam*. John Wiley and Sons, 1937.
- A-4. Weast, R. C.: *Handbook of Chemistry and Physics*. The Chemical Rubber Co., 1969.
- A-5. Telecommunication with HPD, Incorporated (Designers of Industrial Process Equipment), June 1977.
- A-6. Martin Marietta Corporation: *Phase I Initial Assessments, Final Report*. MCR-76-562, September 1976, p 17.
- A-7. *Standards of Tubular Exchanger Manufacturers Association (TEMA)*, Fourth Edition, Section 8, 1959, p 60.
- A-8. Telecommunication with Foster Wheeler (Commercial Boiler Manufacturer), June 1977.
- A-9. Perry, R. H. and Chilton, C. H.: *Chemical Engineers' Handbook, Fifth Edition*, McGraw-Hill Book Company, 1973.
- A-10. Martin Marietta Corporation: *Development of Ammoniated Salts from a Chemical Energy Storage System, Phase 1, Task 1 - Evaluation of Design and Uses*. MCR-76-323, June 1976.
- A-11. Zabrodsky, S. S.: *Hydrodynamics and Heat Transfer in Fluidized Beds*, The MIT Press, 1966.
- A-12. Chemical Marketing Reporter, June 1977.
- A-13. Telecommunication with Ingersoll-Rand, July 1977.
- A-14. Telecommunication with PDM, July 1977.

APPENDIX - ECONOMIC ANALYSIS OF ALTERNATIVE REACTOR DESIGNS

I. STORAGE CONTAINER COST

The amount of energy to be stored is

Stored Energy = Rate of Power Generation * Time of discharge

Stored Energy = 100 MWe * 10 hr = 1000 MWhe

$$= 10^6 \text{ kWhe} * 3413 \text{ B/kW-hr}/30\% = 10^{10} \text{ Btu}$$

The total volume of salt required is determined as follows:

$$\text{Volume of salt} = \frac{\text{Stored energy}}{\text{Heat of reaction} * \text{density}}$$

For $\text{MgCl}_2 \cdot 2\text{NH}_3$

$$\text{Volume} = \frac{10^{10} \text{ Btu lb ft}^3}{260 \text{ Btu } 18.7 \text{ lb}} = 2.055 \times 10^6 \text{ ft}^3$$

For $\text{CaCl}_2 \cdot 8\text{NH}_3$

$$\text{Volume} = \frac{10^{10} \text{ Btu lb ft}^3}{750 \text{ Btu } 31.2 \text{ lb}} = 0.428 \times 10^6 \text{ ft}^3$$

Number of Containers - For cylinders in fixed bed systems the maximum size was assumed to be $D = 20 \text{ ft}$, $L = 20 \text{ ft}$

$$\text{Volume} = \frac{\pi}{4} (20)^3 = 6823 \text{ ft}^3$$

$$\text{Area} = 1.5\pi (20)^2 = 1885 \text{ ft}^2$$

The number of containers for fixed bed system assuming a 20% void volume in each container is

$$\text{No} = \frac{\text{Volume of salt} * 1.2}{\text{Volume of container}}$$

$$\text{No} = \frac{(2.055 + 0.428) \times 10^6 \text{ ft}^3}{0.8 * 6823 \text{ ft}^3} = 494$$

For spherical containers a maximum diameter of 80 ft was assumed.

The volume of each container is $268,100 \text{ ft}^3$ and the area is $20,100 \text{ ft}^2$ per container and the number of containers required is 12.

For fluidized beds the void fraction was assumed to be 60% and the dimensions of the cylinder were taken as $L = 40 \text{ ft}$, $D = 20 \text{ ft}$.

The cost of the storage containers is calculated as follows:

- 1) Cost of 494 cylinders at $\$10/\text{ft}^2 = (494)(10)(1885) = \$9,311,900.$
- 2) Cost of 12 spheres at $\$10/\text{ft}^2 = (12)(10)(20,106) = \$2,412,720.$
- 3) Cost of 494 fluidized beds = $2(9,311,900) = \$18,623,800.$

II. SALT COST

The ammoniated salt cost is the sum of the cost of the anhydrous salt and the cost of ammonia. The unit prices assumed (Ref B-1) were as follows:

$$\text{MgCl}_2 = \$0.20/\text{lb}$$

$$\text{CaCl}_2 = \$0.05/\text{lb}$$

$$\text{NH}_3 = \$0.10/\text{lb}$$

The cost of $\text{MgCl}_2 \cdot 2\text{NH}_3$ is calculated using the following equation:

$$\text{Cost} = \text{Weight of } \text{MgCl}_2 \cdot 2\text{NH}_3 \left[\text{Cost of } \text{MgCl}_2 \left(\frac{\text{Mol wt of } \text{MgCl}_2}{\text{Mol wt of } \text{MgCl}_2 \cdot 2\text{NH}_3} \right) + \text{Cost of } \text{NH}_3 \left(\frac{\text{Mol wt of } \text{NH}_3}{\text{Mol wt of } \text{MgCl}_2 \cdot 2\text{NH}_3} \right) \right]$$

$$\text{Cost} = 2.055 \times 10^6 \text{ ft}^3 * 18.7 \text{ lb} \frac{0.2 * 95}{129} + \frac{0.1 * 34}{129} = \$6.68 \times 10^6$$

The cost of $\text{CaCl}_2 \cdot 8\text{NH}_3$ is $\$0.921 \times 10^6$

Total salt cost is 6.6×10^6 .

III. HEAT EXCHANGER COST

The heat transfer calculations are based on the following assumed values (Ref B-2 and B-3) for the coefficient of heat transfer.

- 1) Fixed bed without gas circulation = $5 \text{ Btu/hr-ft}^2.$
- 2) Spheres with gas circulation = $20 \text{ Btu/hr-ft}^2.$

3) Fluidized bed = 80 Btu/hr-ft².

The heat transfer rate used for discharging was 10 MWe or 10⁸ Btu/hr.

The required heat transfer area for the three approaches is shown in Table B-1.

Table B-1 Required Heat Transfer Area

	High-Temperature Area, ft ²	Low-Temperature Area, ft ²	Total, ft ²
Fixed Bed without Gas Circulation	20 x 10 ⁶	10 x 10 ⁶	30 x 10 ⁶
Spheres with Gas Circulation	5 x 10 ⁶	2.5 x 10 ⁶	7.5 x 10 ⁶
Fluidized Bed	1.25 x 10 ⁶	0.625 x 10 ⁶	0.875 x 10 ⁶

Note: Heat Transfer Rate in Low-Temperature Reactor is 1/2 that in High-Temperature Reactor.

The heat exchanger costs were calculated using a unit price of \$10/ft².

IV. SYSTEM COST

The system cost per kWe is determined using the equation:

$$C = C_s \cdot T + C_p$$

where

C = the system cost

C_s = the sum of the storage-related costs divided by the storage capacity

T = discharge time

C_p = Power-related costs

In this analysis the storage related costs are:

$$C_s = \frac{\text{Salt cost} + \text{container cost}}{\text{Storage Capacity}}$$

The power related costs were determined by

$$C_p = \frac{\text{Heat exchanger cost}}{\text{Power}}$$

For 494 fixed bed reactors without gas circulation, the storage cost is the salt cost plus containers. Therefore, the total storage cost is $6.6 \times 10^6 + 9.3 \times 10^6 = 15.9 \times 10^6$ and $C_s = \$15.9/\text{kWhe}$ for 10^6 kWhe storage capacity. The storage cost for 12 spherical containers with gas recirculation is $6.601 \times 10^6 + 2.413 \times 10^6 = \9.01×10^6 and $C_s = \$9.01/\text{kWhe}$. The storage cost for 494 fluidized reactor/containers is $6.601 \times 10^6 + 18,624 \times 10^6 = \25.23×10^6 and $C_s = \$25.23/\text{kWhe}$. The storage cost for 11 spherical storage containers plus 15 fluidized reactors* is:

$$6.6 \times 10^6 + (11/12)(2.413 \times 10^6) + (15/494)(18.624 \times 10^6) = \$9.38 \times 10^6 \text{ and } C_s = \$9.38/\text{kWhe}.$$

The results calculated above are summarized in Table B-2.

Table B-2 Economic Evaluation of Alternative Reactor Designs

	<u>Number</u>	<u>C_s, \$/kWe-hr</u>	<u>C_p, \$/kWe</u>	<u>C, \$/kWe</u>
Fixed Bed Cylinders without Gas Recirculation	494	15.9	3000	3159
Fixed Bed with Gas Recirculation	12	9.0	750	840
Fluidized Beds D = L/2 = 20 ft	494	25.2	187.5	439.5
Storage Spheres with Fluidized Bed Reactor with Solids Transport	11 15	9.38	187.5	281.3

*For cylinders, the maximum heat transfer area that can be installed in a reactor is about $20 \text{ ft}^2/\text{ft}^3$ (Ref. B-3). For fixed bed reactors without gas recirculation, the maximum area that can be installed is $(20)(6283) = 125,660 \text{ ft}^2/\text{reactor}$ and the minimum number of containers is $30 \times 10^6/125,660 = 239$. Therefore, the total number of 494 reactors required is satisfactory. For spheres, the maximum area that can be installed is $20(268,083) = 5.361 \times 10^6 \text{ ft}^2/\text{container}$ and the minimum number of containers with gas recirculation is $7.5 \times 10^6/5.361 \times 10^6 = 1.5$. Thus, the total number of 12 spheres required is also satisfactory. The minimum number of fluidized beds to contain the required area is $1.875 \times 10^6/125,660 = 15$.

REFERENCES

- B-1. Chemical Marketing Reporter, June 1977
- B-2. W. H. McAdams: Heat Transmission, 1954
- B-3. Martin Marietta Corporation: Phase I Initial Assessments, Final Report. MCR 76-562, Sept. 1976.